A potential LINC complex: The SUN-like protein TgSLP1 plays an essential role in cell division in the apicomplexan parasite *Toxoplasma gondii*

von Mirjam Wagner

Inaugural-Dissertation zur Erlangung der Doktorwürde
(Dr. rer. biol. vet.)
der Tierärztlichen Fakultät
der Ludwig-Maximilians-Universität München

A potential LINC complex: The SUN-like protein TgSLP1 plays an essential role in cell division in the apicomplexan parasite *Toxoplasma gondii*

von Mirjam Wagner
aus München

München 2023

Aus dem Veterinärwissenschaftlichen Department
der Tierärztlichen Fakultät
der Ludwig-Maximilians-Universität München

Lehrstuhl für Experimentelle Parasitologie

Arbeit angefertigt unter der Leitung von:

Univ.-Prof. Dr. Markus Meissner

Gedruckt mit Genehmigung der Tierärztlichen Fakultät

der Ludwig-Maximilians-Universität München

Dekan:	Univ.-Prof. Dr. Reinhard K. Straubinger, Ph.D.
Berichterstatter:	Univ.-Prof. Dr. Markus Meissner
Korreferent/en:	Univ.-Prof. Dr. Stefan Unterer

Tag der Promotion: 22. Juli 2023

Für meinen Ehemann Günni

und für unsere wundervollen Kinder

Magdalena und Antonia

Table of contents

Abbreviations

°C	**Degree Celsius**
µg	Microgram
µL	Microliter
µm	Micrometer
µM	Micromolar
A	Ampere
A	Adenin
***A. thaliana* or At**	*Arabidopsis thaliana*
Aa	Amino acid
AID	Auxin-inducible degron
Amp	Ampicillin
APS	Ammonium persulfate
BLAST	Basic local alignment search tool
bp	Base pair
BSA	Bovine serum albumin
C	Cytosin
C. elegans	*Caenorhabditis elegans*
$CaCl_2$ x $2H_2O$	Calcium chloride dihydrate
Cas9	CRISPR associated protein 9
Cb	Chromobody
CbEmerald	Chromobody Emerald
CCD	Coiled-coil domain
CenH3	Centromeric histone 3 variant
CH	Calponin homology
cKO	Conditional knockout
CO_2	Carbon dioxide
C-phase	Cytokinesis phase
Cre	Causes recombination
CRISPR	Clustered regularly interspaced short palindromic repeats
C-terminal	Carboxyl terminal
cytD	Cytochalasin D
D. melanogaster	*Drosophila melanogaster*
Da	Dalton
ddH_2O	Double destilled water
DHFR	Dihydrofolate reductase
DIC	Differential interference contrast
DiCre	Dimerisable Cre
DMEM	Dulbecco's modified eagle's medium
DMSO	Dimethyl sulfoxide
DNA	Deoxyribunucleic acid
dNTP	Deoxynucleodtide 5'-triphosphate
DTT	Dithiothreitol
E. coli	*Escherichia coli*
EDTA	Ethylene diamine tetraacetic acid
ER	Endoplasmic reticulum

ESCRT	Endosomal sorting complex required for transport
EtOH	Ethanol
EuPaGDT	Eukaryotic Pathogen gRNA Design Tool
FACS	Fluorescence-activated cell sorting
F-actin	Filamentous actin
Fig	Figure
Fw	Forward
g	Gravity
G	Guanin
G1-phase	Gap 1 phase
GAP	Glideosome associated protein
gDNA	Genomic deoxyribonucleic acid
GFP	Green fluorescent protein
GOI	Gene of interest
GRA	Dense granule antigen
GRASP	Golgi reassembly and stacking protein
gRNA	Guide RNA
h	Hour
H2B	Histone 2B
HA	Human influenza hemagglutinin
HCl	Hydrochloric acid
HFF	Human foreskin fibroblast
HU	Hydroxyurea
HXGPRT	Hypoxanthine-xanthine-guanine phosphoribosyl transferase
IFA	Immunofluorescence assay
IMC	Inner membrane complex
INM	Inner nuclear membrane
JACoP	Just another colocalisation Plugin
JAS	Jasplakinolide
KASH	Klarsicht, ANC-1, Syne Homology
kb	Kilobase
kDa	Kilo Dalton
KO	Knockout
LB	Lysogeny broth
LINC	Linker of nucleoskeleton and cytoskeleton
LOPIT	Localisation of organelle proteins by isotope tagging
LoxP	Locus of crossover (x)in P1
M	Molar
mAID	Mini-auxin-inducible-degron
Mb	Megabases
MDa	Mega Dalton
mg	Milligram
MIC	Micronemal protein
min	Minute
MJ	Moving junction
mL	Milliliter
MLC1	Myosin light chain 1
mM	Millimolar
mm	Millimeter

$MnCl_2$ x $4H_2O$	Mangan(II)-chloride tetrahydrate
MOPS	3-(N-morpholino)propanesulfonic acid
MORN1	Membrane occupation and recognition nexus protein 1
M-phase	Mitosis phase
mRNA	Messenger ribonucleic acid
MyoA	Myosin A
NaCl	Sodium chloride
NaOH	Sodium hydroxide
NCBI	National Center for Biotechnology Information
NE	Nuclear envelope
NEB	New England Biolabs
Nesprin	Nuclear envelope spectrin repeat
NHEJ	Non-homologous end joining
NLS	Nuclear localisation signal
NPC	Nuclear pore complex
nt	Nucleotides
N-terminal	Amino terminal
NUANCE	Nucleus and Actin connecting element
NUP	Nucleoporin
ONM	Outer nuclear membrane
OPT	Osteopotentia
ORF	Open reading frame
PAM	Protospacer adjacent motif
PBS	Phosphate buffered saline
PCR	Polymerase chain reaction
PDTC	Pyrrolidine dithiocarbamate
PFA	Paraformaldehyde
pH	Potential of hydrogen
PM	Plasma membrane
pmol	Picomol
PNS	Perinuclear space
PV	Parasitophorous vacuole
PVM	Parasitophorous vacuole membrane
R	Pearson's correlation coefficient
Rapa	Rapamycin
RbCl	Rubidium chloride
RFP	Red fluorescent protein
RNA	Ribonucleic acid
ROM	Rhomboid protease
RON	Rhoptry neck protein
ROP	Rhoptry bulb protein
rpm	Revolutions per minute
RT	Room temperature
Rv	Reverse
S. cerevisiae	*Saccharomyces cerevisiae*
S. pombe	*Schizosaccharomyces pombe*
SAG	Surface antigens
SD	Standard deviation
SDS-PAGE	Sodium dodecyl sulphate polyacrylamide gel elecrophoresis
sec	Second

sgRNA	Single-guide ribonucleic acid
SINE	SUN-interacting nuclear envelope proteins
snRNP	Small nuclear ribonucleoprotein
Spag	Sperm-associated antigen
S-phase	Synthesis phase
spp	Species pluralis
SUN	Sad1/ UNC-84
SYNE	Synaptic nuclear envelope protein
T	Tyrosin
***T. gondii* or Tg**	*Toxoplasma gondii*
TAE	Tris-acetate-EDTA
TBS	Tris-buffered saline
TEMED	Tetramethylethylendiamin
TfbI	Transformation buffer I
TfbII	Transformation buffer II
TgSLP1	*Toxoplasma gondii* SUN-like protein 1
TgSLP2	*Toxoplasma gondii* SUN-like protein 2
TMD	Transmembrane domain
TRIS	Tris(hydroxymethyl)aminomethane
TX-100	Triton X-100
UTR	Untranslated region
UV	ultraviolet
V	Volts
VPS	Vacuolar protein sorting-associated protein
w/v	Weight / volume
WHO	World health organisation
WIP	WPP domain interacting protein
wt	Wildtype
YFP	Yellow fluorescent protein

List of Figures

List of Tables

1 Introduction

1.1 Apicomplexan parasites

The phylum Apicomplexa comprises a large number of parasitic protists, with more than 6000 known and probably thousands more undescribed species. The term *Apicomplexa* is derived from the Latin words *apex* and *complexus,* referring to a characteristic cellular structure, the apical complex, that is needed to invade host cells, where the parasite survives and replicates inside a parasitophorous vacuole (Votýpka et al., 2016). Most apicomplexan parasites contain a unique organelle called the apicoplast, a nonphotosynthetic plastid, originally acquired by secondary endosymbiosis (Waller & McFadden, 2005). Apicomplexans are obligate intracellular parasites that are of medical and veterinary importance and are responsible for enormous economic losses in the livestock industries (Stelzer et al., 2019).

One of the most dangerous human parasite is *Plasmodium falciparum*, the causative agent of malaria that is transmitted through the bite of an infected female *Anopheles* mosquito. The World Health Organization estimated 247 million malaria cases and 619.000 death worldwide caused by the disease in the year 2021, with 95% of all cases occurred in African countries (World Health Organisation, 2022).

Cryptosporidiosis, a gastrointestinal illness caused by the apicomplexan parasite *Cryptosporidium* spp*.* is a significant threat to young children and immunocompromised patients especially in developing countries. Despite its relatively low notification rates in european countries, cryptosporidosis has the potential to cause large scale, waterborn endemic outbreaks in both developing as well as developed nations (O'Leary, 2021; European Centre for Disease Prevention and Control, 2021).

Babesia spp. are parasites of the phylum Apicomplexa that are transmitted to mammals by tick vectors and causing a disease named babesiosis, that can become severe and life-threatening in elderly and immunocompromised individuals (Renard & Mamoun, 2021).

While *Cryptosporidium* spp. and *Babesia* spp. are of both human and veterinary importance, other representatives of the phylum Apicomplexa have mostly veterinary and therewith economical significance, like *Neospora* spp., *Eimeria* spp. and *Theileria* spp. (Goodswen et al., 2013; McDonald & Shirley, 2009; Chakraborty et al., 2017).

This study is focussing on one of the most studied apicomplexan parasite, *Toxoplasma gondii*, a major cause of birth defects and death in immunocompromised patients. Different to most apicomplexan parasites, *T. gondii* has a very broad host range and can infect any nucleated cell from warm-blooded animals (Carruthers, 2002).

1.2 *Toxoplasma gondii*

1.2.1 History

More than one century ago, in 1908, the two French scientists Charles Nicolle and Louis Manceaux discovered a protozoan organism in tissues of a North African hamster-like rodent during their studies on leishmaniosis. They defined it as a new organism and named it *Toxoplasma gondii* that is referring to its bow-like shape (Greek: *toxo* = bow and *plasma* = creature) and to the host *Ctenodactylus gundi* in which it was initially found. In the same year, the researcher Alfonso Splendore identified the same organism in rabbit tissues (Nicolle & Manceaux, 1908; Weiss & Dubey, 2009).

Around 30 years after its discovery, in 1939, the medical importance of the parasite emerged, when it was identified in the tissue of a congenitally infected infant, that died one month postnatal. Parasite isolates from the brain of the infected child were isolated and the pathologists succeeded to infect rabbits and mice which developed encephalitis (Wolf et al., 1939).

Only a few years later, in 1948, a test to specifically recognise antibodies of patients with acute and latent *Toxoplasma* infection was developed (Sabin & Feldman, 1948). Multiple epidemicological studies with the Sabin-Feldman test were made and revealed the world-wide prevalence of infection with *T. gondii.* However the seroprevalence varies a lot among different countries, it has been estimated that up to one third of the world's population has been exposed to the parasite (Tenter et al., 2000).

In the 1950s and 1960s the hypothesis of *T. gondii* transmission via consumption of raw meat arised, but due to the high incidence also in herbivores and strict vegetarians, the transmission path remained obscure (Weinman & Chandler, 1954; Desmonts et al., 1965; Jacobs, 1963; Ferguson, 2009).

In 1965, researchers found isolated *T. gondii* parasites from cat faeces to be infectious for mice when orally transmitted (Hutchison, 1965). Work and Hutchison identified the isolated parasites as a new form of *Toxoplasma* and described it as the "new cyst" of *T. gondii* (Work & Hutchison, 1969). Several groups confirmed this new stage of *T. gondii* as coccidian oocysts with the typical asexual and sexual development of coccidians (Hutchison et al., 1969; Sheffield & Melton, 1970; Witte & Piekarski, 1970; Ferguson, 2009).

By then, the complete life cycle including felids as the definitive host transmitting the parasite was enlightened (Frenkel et al., 1970; Ferguson, 2009).

From the end of the 1970s on, the research on *T. gondii* moved from the basic parasitology and focused on molecular biology, immunology and genetics (Ferguson, 2009).

With the first studies that described cloning of individual genes by Burg and colleagues in 1988 and Cesbron-Delauw and colleagues in 1989, the ability to manipulate the genome of the parasite emerged and soon techniques to generate specific gene knockouts and complementations were developed (Burg et al., 1988; Cesbron-Delauw et al., 1989; Soldati & Boothroyd, 1993; Kim et al., 1993; Donald & Roos, 1994; Sibley et al., 1994; Soldati et al., 1995).

Since the breakthroughs in studying the genetics and another milestone in 2002, when Cohen and colleagues opened the field of studying proteomics in *T. gondii*, there are more than 22.000 papers published in the database PubMed on *Toxoplasma* (Cohen et al., 2002; pubmed.ncbi.nlm.nih.gov).

1.2.2 Pathogenesis

There are three ways of transmission of *Toxoplasma* parasites. The first is caused by a primary infection during pregnancy where the unborn foetus is exposed to tachyzoites that pass the placental barrier. Congenital toxoplasmosis can cause neurological, ocular and systemic damage with variable severity depending on the gestational age with the most serious outcome when the infection happens in the first trimester. More common are the other two possibilities of infection, which occur through oral transmission and are caused by different stages of the parasite. Transmission of bradyzoites in form of tissue cysts occur through ingestion of raw or undercooked meat from an infected intermediate host. Sporulated oocysts

from cat faeces can be transmitted via contaminated fruits, vegetables or water (Fig. 1.1; Cerutti, Blanchard & Besteiro, 2020).

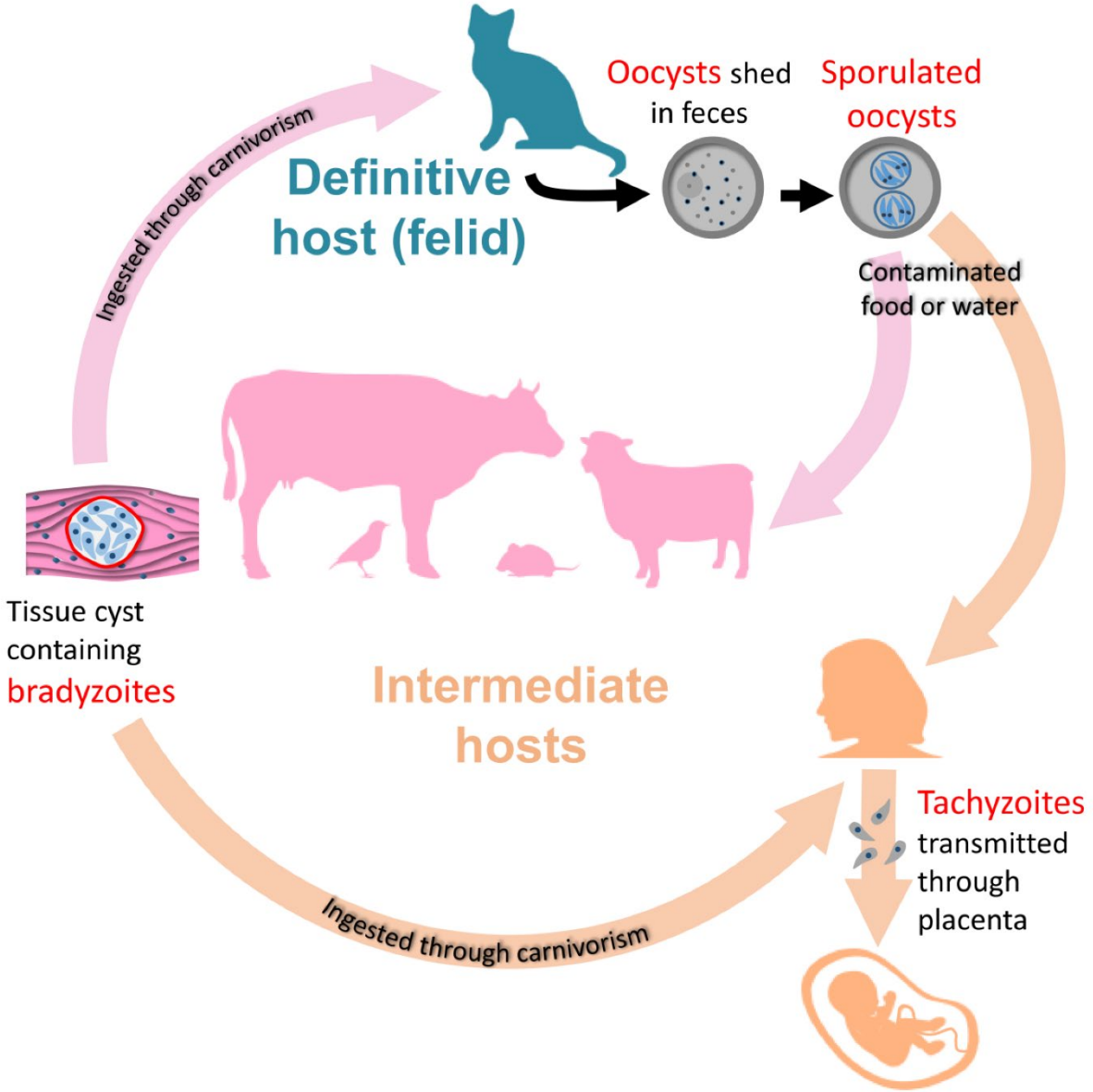

Fig. 1.1 Ways of transmission of *Toxoplasma* to humans
Schematic representation of how parasites can be transmitted to humans through a primary infection of the mother during pregnancy, through consumption of raw meat, or through food or water that is contaminated by faeces of infected felids (Cerutti, Blanchard & Besteiro, 2020).

In adults, most of the infections with *Toxoplasma* remain harmless and asymptomatic. However, in immunocompromised patients, the infection can lead to severe complications like ocular damage or encephalitis that can be life-threatening if not treated. Ingested tissue cysts or oocysts invade host cells, differentiate into tachyzoites that divide rapidly within the host and differentiate again into latent bradyzoites to hide from the immune system. These cysts persist for a lifetime in the host but can be reactivated in case of an immunosuppression, like for patients suffering AIDS or organ transplants (Weiss & Dubey, 2009; Sanchez & Besteiro, 2021).

There are three strains of *T. gondii* responsible for the majority of toxoplasmosis cases in animals and humans: type I, II and III. The type has high impact on the virulence and the pathogenicity. Based on experiments in mice, type II and III strains are less virulent, in contrast to the highly virulent type I strain that can kill a mouse within 7 days, upon infection with a single parasite (Saeij et al., 2005).

1.2.3 Lifecycle

Like in many Apicomplexans, the life cycle of *T. gondii* is completed within two different hosts and involves both sexual and asexual replication. While the sexual component is restricted to felids (definite host), the asexual cycle can take place in any warm-blooded animal (intermediate host). Different to closely related parasites, it is characteristic for *Toxoplasma* to circumvent the sexual reproduction in the definitive host – it can easily distribute by infecting intermediate hosts directly with tissue cysts (Su et al., 2003).

T. gondii exists in three different infectious stages. Tachyzoites, that are rapidly replicating during the acute infection in the intermediate host, bradyzoites that are persisting in tissue cysts during chronic infection of the intermediate host and sporozoites, developing in the oocysts that are shed by the definitive host (Fig. 1.2; Sanchez & Besteiro, 2021).

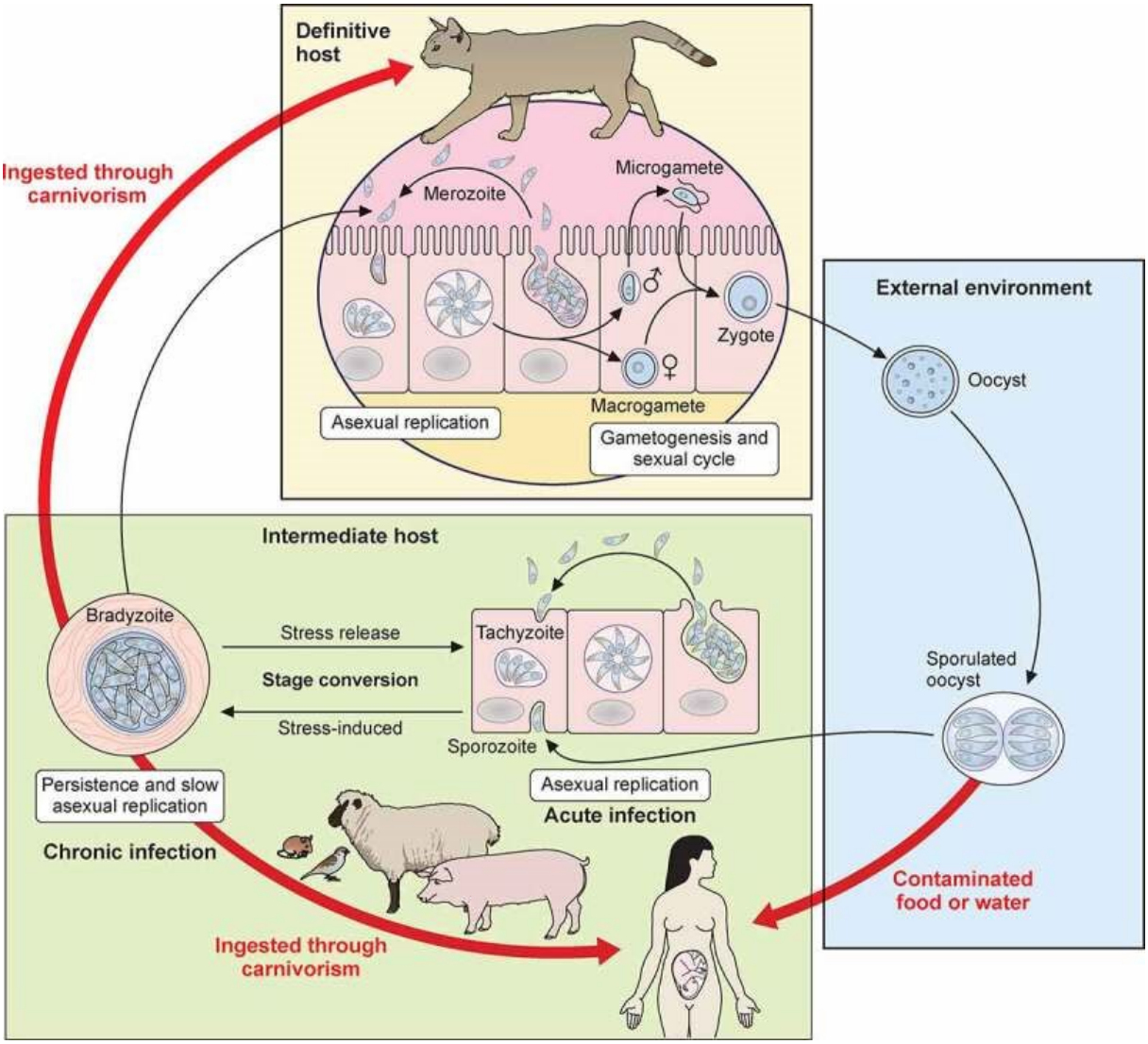

Fig. 1.2 The lifecycle of *T. gondii*
Parasites replicate sexually in the gut of felids (definitive host) and reach the environment as oocysts through the faeces. Sporulated oocysts can infect a variety of vertebrate hosts (intermediate host) where parasites replicate asexually. In this acute stage of infection, tachyzoites can pass the placenta causing congenital toxoplasmosis. Tachyzoites can infect tissue cells where they differentiate in slow growing bradyzoites. In this chronic infection stage, parasites can be ingested by felids through carnivorism (Sanchez & Besteiro, 2021).

1.2.3.1 Lifecycle in the definite host

The definite host for *T. gondii* are all members of the Felidae family. The usual way of infection is the ingestion of tissue cysts through predation of infected animals like mice, rats or birds. Inside the stomach and the small intestine of the cat, the wall of the tissue cyst is digested by

intestinal enzymes. Released bradyzoites invade epithelial cells of the small intestine and go through a few asexual multiplications to rise the schizont stage (Fig. 1.2). Five morphologically distinct types of schizonts are described, named A-E schizonts (Dubey & Frenkel, 1972). Merozoites are formed from type C-E schizonts via a process called endopolygeny, where several nuclei are divided before cytoplasmic segmentation takes place (Speer & Dubey, 2005). After a few rounds of asexual doublings, the merozoites differentiate into male microgametes and female macrogametes which fuse into diploid oocysts that are locked in a thick, impermeable wall and excreted with the cat faeces (Fig. 1.2; Ferguson et al., 1974; Ferguson et al., 1975). Due to temperature and oxygenation changings, the non-infectious oocysts from fresh cat faeces develop into infectious, sporulated oocysts within 48 hours (Fig. 1.2; Dubey et al., 1970a; Dubey et al., 1970b). These oocysts are extremely robust against many environmental influences (Dubey, 1998; Shapiro et al., 2019).

In contrast to the asexual life cycle in the intermediate host, the sexual stages are restricted to the feline intestines, however the molecular mechanism remains unknown. In a recent study it was speculated that felids are not expressing the delta-6-desaturase which is required for linoleic acid metabolism in their intestines. The lack of this enzyme results in a massive excess of linoleic acid which might be essential for the sexual reproduction of *T. gondii* (Martorelli Di Genova et al., 2019).

1.2.3.2 Lifecycle in the intermediate host

T. gondii can use any warm-blooded animal as intermediate host and replicate in any nucleated cell derived from a warm-blooded animal tested so far. Two stages of asexual development can occur in the intermediate host (Sibley, 2003; Tenter et al., 2000).

Highly proliferative and invasive tachyzoites (Greek: *tachos* = speed; Frenkel, 1973) spread within the host and are responsible for the symptoms of acute toxoplasmosis (Dubey et al., 1998; Blader et al., 2015). Some tachyzoites escape the destruction from the immune system and transform into slowly multiplying bradyzoites (Greek: *brady* = slow; Frenkel, 1973) that are structural quite similar to tachyzoites but they contain several amylopectin granules required for energy storage (Dubey et al., 1998). Protected within a tissue cyst and due to their decreased metabolic activity, bradyzoites are refractory to any current available drug

treatment (Fig. 1.2; Jeffers et al., 2019). Since they tend to reside within the brain, another complication for drug development is the crossing of the blood-brain-barrier (Pittman & Knoll, 2015).

The dissemination of tachyzoites is defined as the lytic cycle consisting of the main steps gliding and invasion, replication and egress (Fig. 1.3; Black & Boothroyd, 2000; Blader et al., 2015), that are described more detailed in the following sections.

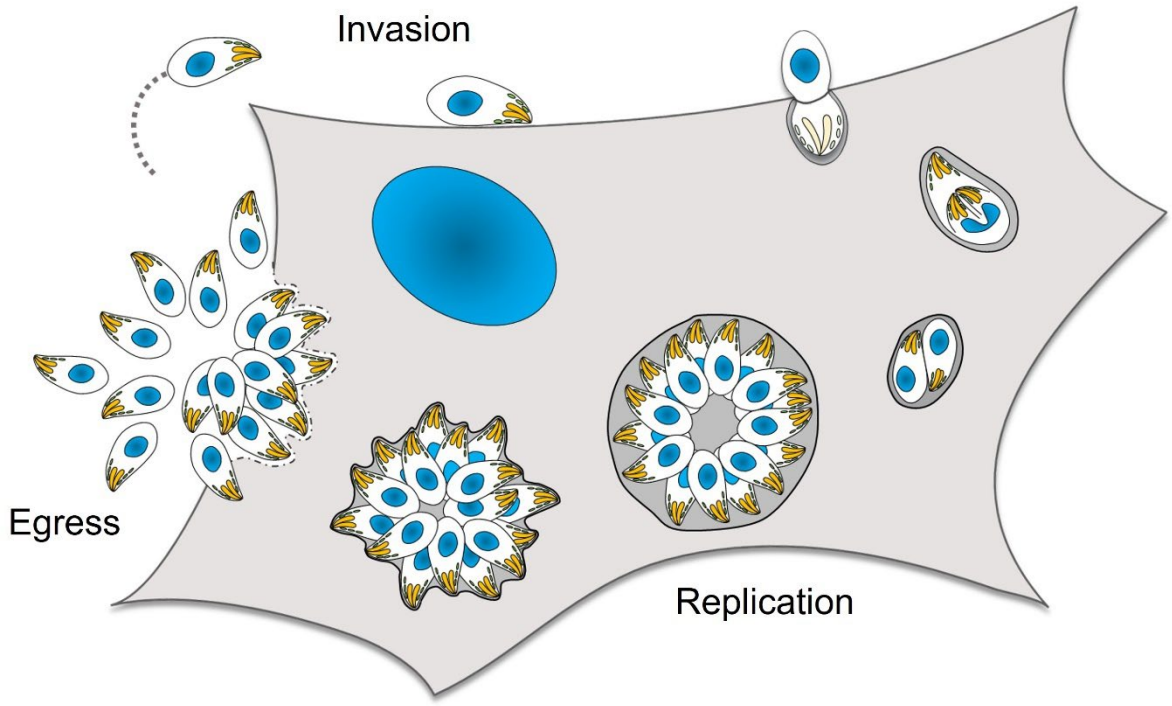

Fig. 1.3 The lytic cycle of *T. gondii*
Extracellular parasites glide and actively invade host cells, replicate by endodyogeny within a parasitophorous vacuole. After multiple rounds of replication, parasites egress to infect adjacent cells and start the cycle again. © Dr. Simon Gras

1.2.3.2.1 The ultrastructure of *T. gondii* tachyzoites

T. gondii tachyzoites are crescent-shaped and about 6 µm long and 2 µm wide with a pointed anterior and a rounded posterior pole (Fig. 1.4; Dubey et al., 1998). In addition to the conserved eukaryotic structures like the nucleus, a mitochondrion, ribosomes, the endoplasmic reticulum (ER) and a Golgi apparatus, the parasite possesses apicomplexan-

specific structures, such as the apical complex, the secretory organelles and the apicoplast as well as the surrounding layers, namely the inner membrane complex (IMC) and the plasma membrane (PM) (Fig. 1.4; Dubey et al., 1998).

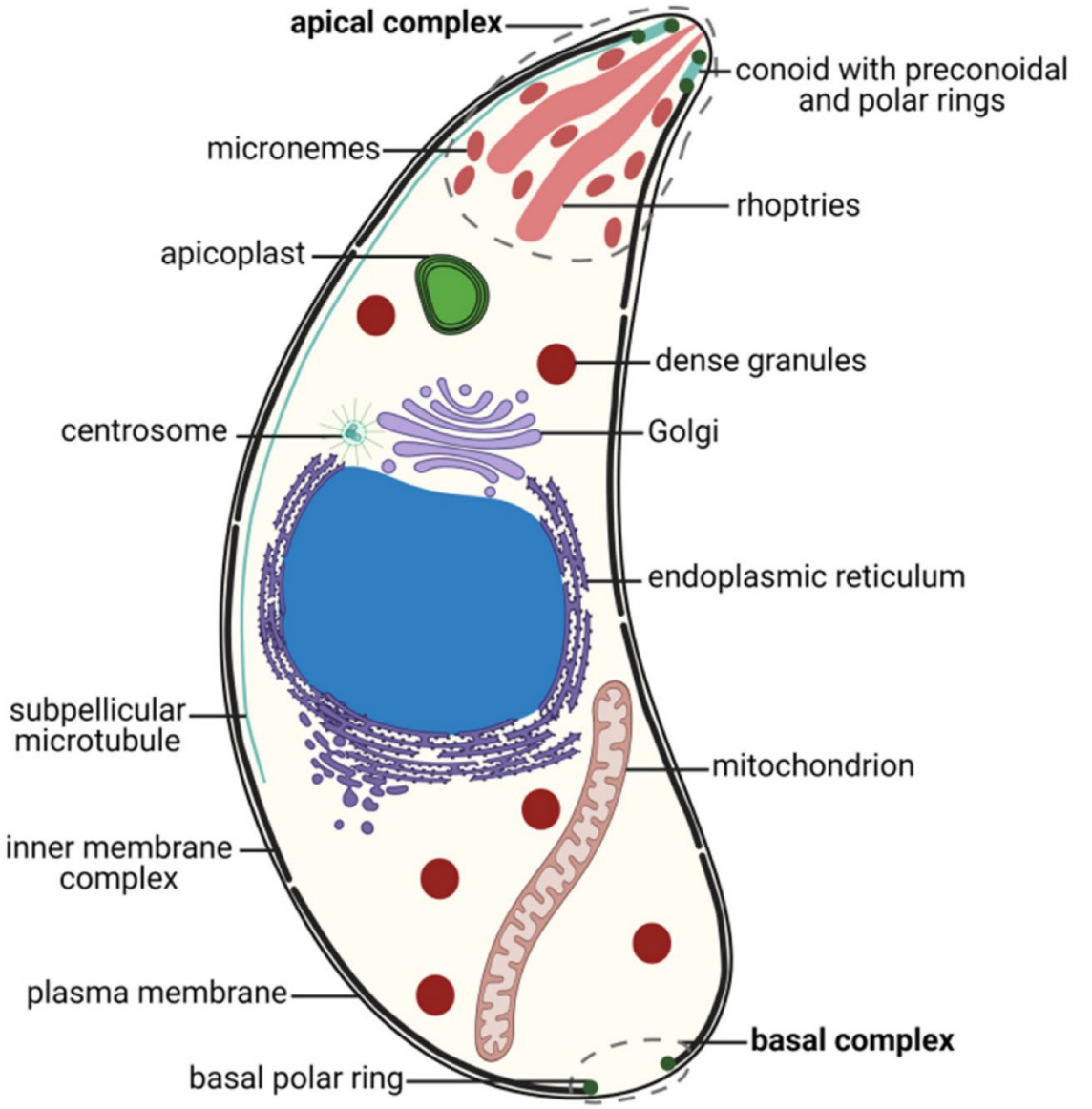

Fig. 1.4 The ultrastructure of *T. gondii*
Schematic overview of the ultrastructure of a *T. gondii* tachyzoite. Shown are the apical and basal complex, the surrounding plasma membrane and inner membrane complex, secretory organelles such as rhoptries, micronemes and dense granules and the main organelles such as the mitochondrion, the endoplasmic reticulum, the Golgi apparatus as well as the apicoplast (Delgado et al., 2022).

The apical complex, which gives the phylum its name, consists of the conoid, the apical polar ring, and secretory organelles such as the rhoptries and micronemes (Morrissette & Sibley, 2002). The conoid, a structure made of 14 tubulin fibres that are arranged in spirals around two microtubules, is enclosed by two preconoidal rings and the apical polar ring (Dubey et al., 1998; Hu et al., 2002b). Being a motile organelle, the conoid extrudes in a calcium-dependent manner and seems to be involved in secretion of micronemes and rhoptries during invasion of a host cell (Mondragon & Frixione, 1996; Hu et al., 2002b; Katris et al., 2014).

The apical polar ring forms a microtubule organisation center (MTOC) from which 22 sub-pellicular microtubules originate and extend two thirds of the parasite defining its shape (Russell & Burns, 1984; Hu et al., 2002b).

Micronemes, rhoptries and dense granules are part of the secretory system of *T. gondii.* While micronemes and rhoptries are located at the apical complex, dense granules are distributed throughout the parasite (Dubey et al., 1998). All three types of secretory organelles play essential roles during host cell invasion, in addition, dense granule proteins (GRA) are important for the maturation and maintenance of the parasitophorous vacuole (PV) in which tachyzoite replicate (Carruthers & Sibley, 1997; Carruthers et al., 1999; Mercier et al., 2005).

The apicoplast, a plastid-like organelle, was originally derived through secondary endosymbiosis and contains its own genome (Waller & McFadden, 2005). Since the apicoplast is essential for the parasite's survival, it participates in several processes such as biosynthesis of fatty acids and the synthesis of heme, isoprenoids and iron-sulfur clusters (Ramakrishnan et al., 2012; Seeber & Soldati-Favre, 2010).

The inner membrane complex surrounds the parasite between the plasma membrane and the subpellicular network with openings at the apical and basal poles. It is made up of flattened membrane vesicles called alveolis and is important for gliding and invasion by acting as an anchor for the actin-myosin motor complex (Harding & Meissner, 2014).

1.2.3.2.2 Gliding and invasion

At the beginning of the lytic cycle, highly motile tachyzoites reach host cells using a unique form of movement called gliding motility. Experiments on 2D slides revealed three distinct forms of movement: circular gliding, helical gliding and twirling (Hakansson et al., 1999). In a

3D gel matrix, parasites move in irregular corkscrew-like trajectories (Leung et al., 2014). Unlike most other eukaryotic cells, apicomplexan parasites do not crawl across a substrate, nor are their movements driven by flagella or cilia.

The current model of gliding motility involves secretion of micronemal (MIC) proteins and the structure proteins actin and myosin A (MyoA), forming the actomyosin motor complex (Meissner et al., 2013; Frénal et al., 2017; Whitelaw et al., 2017). The space between the inner membrane complex and the plasma membrane forms the glideosome that is composed of MyoA, myosin light chain 1 (MLC 1) and gliding associated proteins, such as GAP45, GAP50, GAP40 and several GAPM-proteins. While the tail domain of MyoA is linked to the IMC via MLC1, the MyoA head interacts with actin filaments that are located between the IMC and the plasma membrane of the parasite (Opitz & Soldati, 2002; Gaskins et al., 2004; Frénal et al., 2010).

When gliding is initiated, micronemes secrete adhesive transmembrane proteins (adhesins) at the apical pole of the parasite. Adhesins are then anchored into the plasma membrane of the parasite and interact with extracellular receptors of the host cell. The forward movement results from the MyoA mediated translocation of actin filaments along the parasite periphery towards its basal end (Frénal et al., 2017).

It was observed that parasites lacking components of the actomyosin motor complex were still able to survive which suggests an alternative mechanism of gliding and invasion (Egarter et al., 2014; Gras et al., 2017; Whitelaw et al., 2017). A different mode of motility was suggested by Gras et al. in 2019 and presented as the fountain flow model which is based on movement through the uptake and secretion of exogenous material (Gras et al., 2019).

Gliding is not only important for the migration through tissues and cells of the host, it also plays a crucial role in penetration and invasion of the host cell (Frénal et al., 2017).

While invading a host cell, *T. gondii* parasites perform multiple processes that are highly conserved among Apicomplexa. It requires the sequential protein secretion from parasite-specific organelles called micronemes, rhoptries and dense granules (Carruthers & Sibley, 1997). The first step of invasion is the attachment of the parasite to the host cell. Surface antigens (SAGs) recognise surface receptors of the host cell and the parasite attaches to the host cell by the discharge of micronemal proteins (Carruthers et al., 1999; Carruthers &

Boothroyd, 2007). The parasite forms a ring like structure called moving junction (MJ) within the host cell membrane by the secretion of rhoptry neck proteins (RONs). RON2, that serves as a receptor binds to the micronemal protein AMA1 that is anchored in the plasma membrane of the parasite (Alexander et al., 2005; Mital et al., 2005; Lamarque et al., 2011). Rhoptry bulb proteins (ROPs) and dense granule proteins are secreted and help to form the parasitophorous vacuole. The formation of the parasitophorous vacuole membrane (PVM) derives from invagination of the host cell membrane and depends on active penetration of the parasite (Carruthers & Sibley, 1997; Dubremetz, 2007). A rhomboid protease (ROMs) detach MIC proteins from the posterior end of the parasite (Carruthers & Boothroyd, 2007; Shen et al., 2014b). To finish the invasion process, the PV is pinched off via a fission pore and creates a niche for the parasite to replicate isolated from the lysosomal system of the host (Suss-Toby et al., 1996; Mordue et al., 1999). By acting as a molecular sieve, the PVM allows the diffusion of low molecular weight nutrients (Schwab et al., 1994; Clough & Frickel, 2017).

1.2.3.2.3 Replication

Toxoplasma parasites use a unique mode of cell division called endodyogeny where two daughter cells are formed within the mother parasite (Fig. 1.5; Goldman et al., 1958; Sheffield & Melton, 1968).

The cell cycle of *T. gondii* tachyzoites begins with a growth gap phase (G1), followed by the DNA synthesis phase (S) and mitosis (M). In contrast to the eukaryotic cell cycle, there is no or a very short G2-phase in *T. gondii* (Radke et al., 2001; Francia & Striepen, 2014). In the G1-phase, the Golgi elongates and the centrosome duplicates, initiating the S-phase (Hartmann et al., 2006). As DNA begins to replicate, daughter conoids, the apical complexes and early parts of the cytoskeleton, including IMC proteins form, acting as scaffolds in the assembly of daughter cells (Hu et al., 2002a; Hu et al., 2006). At the same time, the apicoplast elongates being associated with the centrosomes (Striepen et al., 2000). In the mitosis phase that is overlapping with cytokinesis, the nucleus and the apicoplast divide, followed by the ER and the mitochondrion (Nishi et al., 2008). Severed organelles are equally distributed among the newly formed daughter parasites. The secretory organelles such as the rhoptries and micronemes were thought to be fully synthesised de novo in each daughter cell (Sheffield & Melton, 1968; Nishi et al., 2008), however, a recent study showed that micronemes can also

be recycled from the mother to the developing daughter parasite (Periz et al., 2019). At the end of the budding process, MORN1 (membrane occupation and recognition nexus protein 1) forms a contractile ring at the basal complex and completes daughter cell segregation (Heaslip et al., 2010; Lorestani et al., 2010). The cytoskeleton of the mother cell is degraded and the plasma membrane incorporated into daughter cells along with newly synthesised plasma membrane (Sheffield & Melton, 1968; Anderson-White et al., 2012).

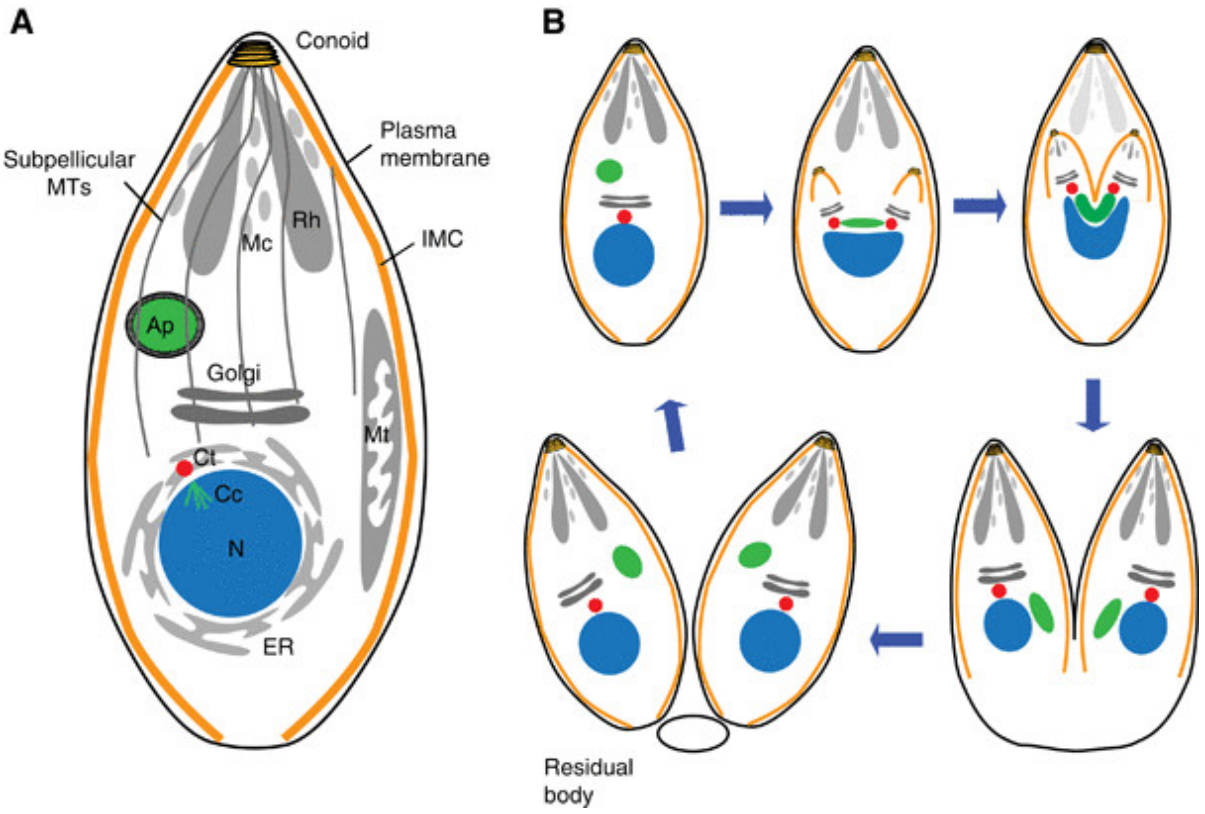

Fig. 1.5 Model of endodyogeny in *T. gondii*
(A) Schematic model of a *T. gondii* parasite and its organelles, Rh: rhoptries; Mc: micronemes; Ap: apicoplast; Mt: mitochondrion; MTs: microtubules; Ct: centrosome; Cc: centrocone; N: nucleus; ER: endoplasmic reticulum; IMC: inner membrane complex. (B) Schematic representation of the *T. gondii* tachyzoite division cycle (Jacot et al., 2013). © 2013, European Molecular Biology Organization

During the asexual replication cycle, *T. gondii* parasites are organised in rosette-like structures being attached to the intravacuolar network that also organises the residual body (Periz et al., 2019; Muniz-Hernández et al., 2011).

1.2.3.2.4 Nuclear division

Different to the nuclear division in mammalian cells, the nuclear envelope of *T. gondii* keeps its integrity during division, a process called closed mitosis (Francia & Striepen, 2014).

The nuclear division starts with the duplication of centrosomes. The centrosome has been proposed as master regulator of apicomplexan cell division and is the microtubule organisation center, which nucleates the microtubules of the mitotic spindle during division (Francia & Striepen, 2014). *T. gondii* centrosomes are constituted by an outer and an inner core (Suvorova et al., 2015). The outer core is more distal to the nucleus and most likely houses the centrioles, since TgCentrin1, a homologue of centrin1 that marks the centrioles in other species, has been shown to be localised to the outer core of the centrosome (Striepen et al., 2000; Suvorova et al., 2015; Tomasina et al., 2022). The inner core is localised proximal to the nucleus and harbours a protein, TgCep250L1, which has been shown to be involved in centriole cohesion and nuclear segregation (Suvorova et al., 2015; Chen & Gubbels, 2019; Tomasina et al., 2022). TgCep250 localises to the inner and outer core and has been shown to tether the inner and the outer core of the centrosome (Chen & Gubbels, 2019). The two cores seem to fulfil independent functions during parasite division. While the outer core is critical for daughter cell budding, the inner core is involved in nuclear division (Suvorova et al., 2015).

Recently it has been proposed that the centrosome is composed of another distinct structure, namely the “middle core”, shown with TgCep530 being located between the outer and the inner core (Courjol & Gissot, 2018; Tomasina et al., 2022). TgCep530 was shown to be crucial in the coordination of karyokinesis and cytokinesis and the centrosomal homeostasis (Courjol & Gissot, 2018). Figure 1.6 shows the dynamic development of the centrosome during cell division (Suvorova et al., 2015). Parasites in early G1-phase inherit a single centrosome being tightly associated with the nuclear envelope. While the outer core expands and duplicates in late G1-phase, the inner core separates and duplicates immediately afterwards in S-phase. Duplication of the centrosomal cores initiates the development of daughter buds, which occurs concurrently with mitosis (Hu et al., 2002a; Hartmann et al., 2006).

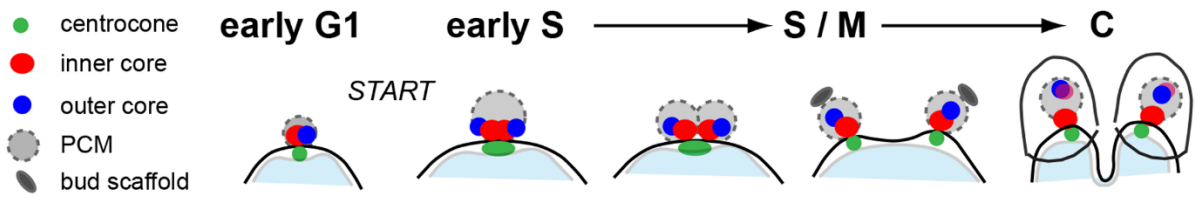

Fig. 1.6 Development of centrosome and centrocone during parasite cell division
Three duplication events can be recorded: first the duplication of the outer core of the centrosome, followed by the inner core and lastly the duplication of the centrocone (adapted from Suvorova et al., 2015). © 2015 Suvorova et al. CC BY license

During mitosis, each chromosome is attached to the microtubules via the kinetochore. The individual sites on chromosomes where the kinetochore binds are known as centromeres (Francia & Striepen, 2014). Chromosome segregation has been monitored by using CenH3 (centromeric histone 3 variant) as a molecular marker protein for the centromeres (Brooks et al., 2011). It has been shown that the centromeres of all chromosomes cluster and this cluster remains throughout the whole cell cycle at the nuclear periphery close to the centrosome (Brooks et al., 2011). It was hypothesised by Francia and Striepen that this physical attachment facilitates spindle microtubules access to the kinetochore in a crowded nucleus filled with uncondensed chromatin and therefore ensures proper chromosome segregation during division (Brooks et al., 2011; Francia & Striepen, 2014). Recently, it was proposed that the centromere cluster formation depends on its interaction with the nuclear envelope (Francia et al., 2020).

The mitotic spindle is embedded within the nuclear envelope in a specialised structure known as the centrocone (Dubremetz, 1973; Sheffield & Melton, 1968). It interacts with the cytoplasmic centrosome penetrating the nuclear envelope through pores and links the centrosome to the centromeres (Striepen et al., 2007). MORN1, a protein that was shown to have a conserved role in asexual and sexual development in *T. gondii*, localises at the apical and posterior end of the parasite and at the centrocone (Hu et al., 2006; Gubbels et al., 2006; Ferguson et al., 2008). Using MORN1 as a marker protein, it has been shown that the centrocone persists through the whole cell cycle, suggesting the chromosomes being permanently anchored to the spindle pole (Gubbels et al., 2006; Brooks et al., 2011). Brooks

et al. describe the centrocone as master organiser of chromosome location during mitosis and throughout the intracellular development of the parasite (Brooks et al., 2011).

In the last steps of mitosis, the centrocone duplicates and the centrosomes and chromosomes segregate into each daughter parasite creating a U-shaped nucleus (Radke et al., 2001; Suvorova et al., 2015). Finally, the nucleus separates by fission.

1.2.3.2.5 Egress

After several rounds of replication, the parasite induces egress to lyse the host cell and to continue proliferation. Egress is an active process triggered by the increase in intracellular calcium (Ca^{2+}) levels (Moudy et al., 2001; Arrizabalaga et al., 2004). Host cell damage or permeabilisation induces a calcium-dependent signalling pathway that is a response to changes in the environment of the PV, such as changing potassium levels. CDPK3, a calcium-dependent kinase, has been shown to be essential for microneme secretion and egress (McCoy et al., 2012; Lourido et al., 2012). The use of calcium ionophores makes it possible to promote synchronised egress in cell culture and has been used to study egress for the past 40 years (Endo et al., 1982; Caldas & de Souza, 2018). Successful egress requires the breakdown of two membrane barriers, the PVM and the host cell membrane (Schultz & Carruthers, 2018). The micronemal perforin-like protein PLP1 has been shown to play an essential role in egress by disrupting the PVM (Kafsack et al., 2009) and the phospholipase LCAT (lecithin-cholesterol acyltransferase) secreted by the dense granules contributes to the permeabilisation of the PVM and the host cell membrane (Schultz & Carruthers, 2018).

Finally, deletion of the actomyosin motor complex strongly affects egress, demonstrating that egress depends on gliding machinery activation and microneme secretion (Egarter et al., 2014; Gras et al., 2017; Frénal et al., 2017).

1.2.4 Characterisation of essential genes in *T. gondii*

The *T. gondii* genome comprises a set of 13 haploid chromosomes with a genome size of approximately 65 Mb. For a long time it was assumed that the genome consists of 14 chromosomes, which has recently been refuted by studies showing that chromosomes VIIb and VIII are physically linked (Bunnik et al., 2019; Xia et al., 2021).

With a single set of chromosomes, essential genes can only be studied with conditional knockout systems in *T. gondii*. Several methods at the genomic, transcriptional and protein level have been successfully adapted to *T. gondii* in the recent years (Jiménez-Ruiz et al., 2014). Most techniques using genetic modification are based on homologous recombination of exogenous DNA replacing the endogenous gene of interest. The efficiency of gene replacement has been dramatically increased by creating a strain that lacks the non-homologous end joining repair (NHEJ) pathway, which is achieved by deletion of the *ku80* locus (Fox et al., 2009; Huynh & Carruthers, 2009).

Methods controlling expression at the genomic level include the dimerisable Cre-mediated recombination system (DiCre, Andenmatten et al., 2013) and the CRISPR/ Cas9 system (Shen et al., 2014a; Sidik et al., 2014; Stortz et al., 2019).

Systems that function at the gene transcription level are, for example, the tetracyclin-inducible system (Meissner et al., 2001; Meissner et al., 2002; Van Poppel et al., 2006) or the U1-mediated gene silencing (Pieperhoff et al., 2015).

The auxin-inducible degron system (AID; Brown et al., 2018) and a system using a ligand-controlled destabilisation domain (ddFKBP; Herm-Götz et al., 2007) are based on the regulation of protein stability at the protein level.

Genome editing with CRISPR/ Cas9 was performed in this study to assess the subcellular localisation of uncharacterised proteins and to create conditional knockout mutants based on the DiCre system. Both the AID system and the U1 gene silencing system have been tried unsuccessfully to generate conditional knockout mutants.

1.2.4.1 Genome editing with CRISPR/ Cas9

Clustered regularly interspaced short palindromic repeats (CRISPR) were first described by Mojica et al. in 2005 and suggested as an adaptive immune system used by bacteria to defend themselves from viruses and exogenous DNA. In 2012, CRISPR/ Cas9 (Cas for CRISPR-associated protein) was suggested to serve as a potential method for programmable genome editing by the research group of Doudna and Charpentier (Jinek et al., 2012) and the system was successfully adapted to mammalian cells (Jinek et al., 2013; Mali et al., 2013; Cong et al.,

2013). In the recent years, the approach has been used in several model organisms including apicomplexan parasites.

In *T. gondii,* CRISPR/ Cas9 was established to generate mutants through targeted gene disruption or genome editing. The disruption of specific genes takes advantage of the NHEJ pathway used by the parasite to repair double strand breaks. Due to the high error rate, this mechanism often creates frame-shift mutations and insertions at the cleavage site. This was exploited in 2016 to perform a genome-wide screen, categorising the importance of each individual gene involved in the parasite fitness using a "phenotypic score" (Sidik et al., 2014; Sidik et al., 2016; Sidik et al., 2018). The phenotypic score can be used as an indicator of how important a gene is for the fitness of the parasite.

In combination with repair templates, the CRISPR/ Cas9 system can be used for the specific insertion of exogenous DNA, for example to label proteins with an epitope or a fluorescent tag (Fig. 1.7). The specific insertion of DNA (oligonucleotides or PCR products) can be supported by using parasite strains lacking the *ku80* locus due to their high rate of homologous recombination caused by the lack of NHEJ. Homology regions of approximately 40 bp ensure the correct integration of the repair templates. Using a fluorescently labelled Cas9 protein, the parasites can be selected by fluorescence-activated cell sorting (FACS) to increase the efficiency of this method (Sidik et al., 2014; Curt-Varesano et al., 2016; Di Cristina & Carruthers, 2018; Stortz et al., 2019).

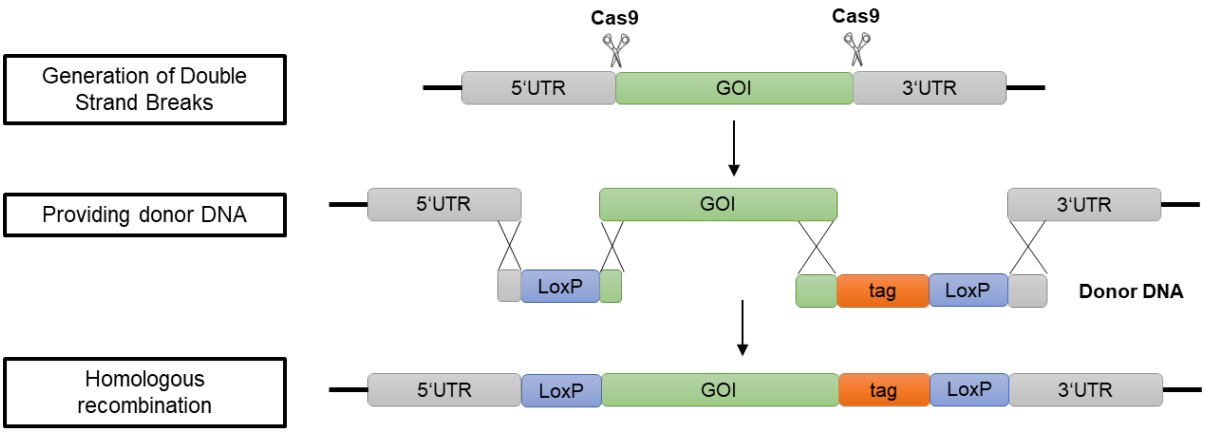

Fig. 1.7 Model of genome editing using CRISPR/ Cas9
Cas9 is generating double strand breaks at defined positions in the genome and insertion of exogenous DNA occurs via homologous recombination with provided donor DNA. GOI: gene of interest; UTR: untranslated region

1.2.4.2 The DiCre System

Cre recombinase (Cre for causes recombination) is an enzyme derived from the P1 bacteriophage that catalyses the site-specific recombination of DNA between two identical DNA sequences known as LoxP sites (LoxP for locus of crossover (x) in P1; Sternberg & Hamilton, 1981). Cre-mediated site-specific recombination has been suggested and demonstrated as a useful tool for genome modulation in eukaryotes (Sauer, 1987; Sauer & Henderson, 1988). To control activity of the Cre recombinase, the conditional Dimerisable Cre (DiCre) system was developed, in which the Cre enzyme is expressed as two separate, inactive subunits, both fused to the rapamycin-binding proteins FRB or FKBP. By adding the ligand, rapamycin, FRB and FKBP dimerise and the activity of Cre recombinase is restored (Jullien et al., 2003; Jullien et al., 2007). The conditional DiCre system was adapted to *T. gondii* and shown to be highly efficient (Andenmatten et al., 2013). However, there are disadvantages that need to be considered. The regulation is irreversible and depending on the protein stability, down-regulation can be very slow (Jiménez-Ruiz et al., 2014).

In this study, the system is used to conditionally knockout genes of interest by flanking the genomic locus with LoxP sites using genome editing via CRISPR/ Cas9 in a parasite stain that expresses DiCre (RH-Δ*ku80*-DiCre) (Andenmatten et al., 2013; Sidik et al., 2014; Stortz et al., 2019). After successful insertion of the LoxP sites, excision of the gene can be induced by adding rapamycin (Fig. 1.8). To assess the subcellular localisation of proteins and to test the knockout efficiency after rapamycin treatment, the genes examined in this study were additionally tagged with an epitope or a fluorescent tag.

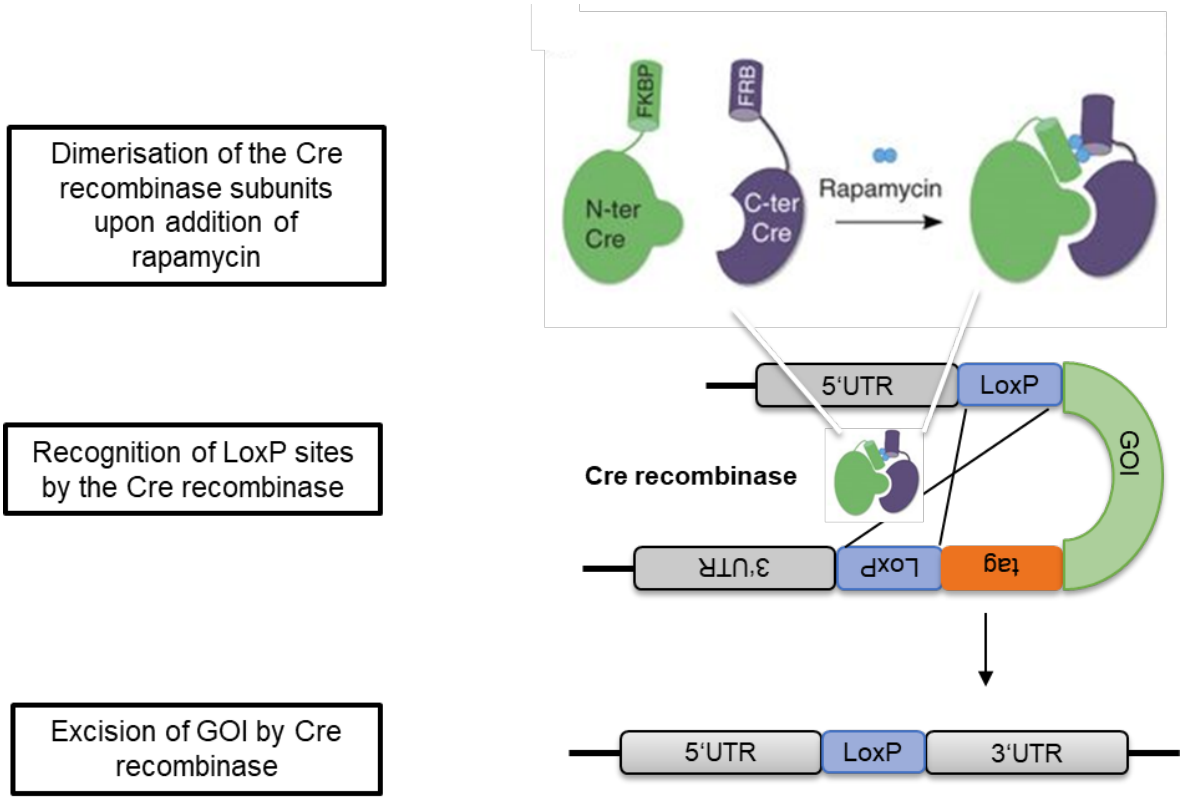

Fig. 1.8 Model of gene knockout using dimerisable Cre recombinase (DiCre)
The Cre recombinase is expressed as two separate, inactive subunits both linked to rapamycin binding proteins FKBP or FRB. By adding rapamycin as ligand, the subunits dimerise to an active Cre complex that recognises LoxP sites within the genome and excise genomic material between two LoxP sites. GOI: gene of interest; UTR: untranslated region (Figure adapted from Andenmatten et al., 2013).

1.3 The nuclear envelope in higher eukaryotes

One of the most important organelles of a eukaryotic cell is the nucleus, which contains most of the genetic material. The nucleus is surrounded by a double membrane called the nuclear envelope (NE), which acts as a barrier to separate nuclear contents from the cytoplasm (Kite, 1913). The nuclear envelope consists of an inner nuclear membrane (INM) and an outer nuclear membrane (ONM) associated with the ER. The area between the two membranes is termed the perinuclear space (PNS; Watson, 1955; Hetzer, 2010) and contains two large protein complexes that span the nuclear envelope and connect the interior of the nucleus to the cytoplasm (Fig. 1.9). The nuclear pore complexes (NPCs) appear as ring-like junctions between the two membranes, forming channels that navigate the transport of molecules between the nucleoplasm and the cytosol, e.g. RNA and ribosomal proteins (Watson, 1959;

Hetzer, 2010). With a molecular mass of 60 to 120 MDa in mammals, nuclear pore complexes are huge complexes composed of about 30 different proteins, collectively called nucleoporins (NUPs; Cronshaw et al., 2002).

The other protein complex forms bridge-like structures and physically couples the cytoskeleton to the nucleoskeleton to enable stability and correct positioning of the nucleus during a variety of cellular processes (Fig. 1.9; Gundersen & Worman, 2013). It is referred to as the linker of nucleoskeleton and cytoskeleton complex, short LINC complex (Crisp et al., 2006) and is described in detail in the following sections.

The nuclear envelope is mechanically supported by a protein meshwork that underlies the inner nuclear membrane and consists mainly of A-lamins (type A and C) and B-lamins (type B1 and B2) and lamin-associated proteins, hence termed the nuclear laminar (Gerace et al., 1978; Gruenbaum et al., 2015). Mutations in human lamin-encoding genes have been shown to cause human hereditary diseases known as laminopathies, indicating that the nuclear laminar plays an essential role in maintaining the integrity of the nuclear envelope (Burke & Stewart, 2002).

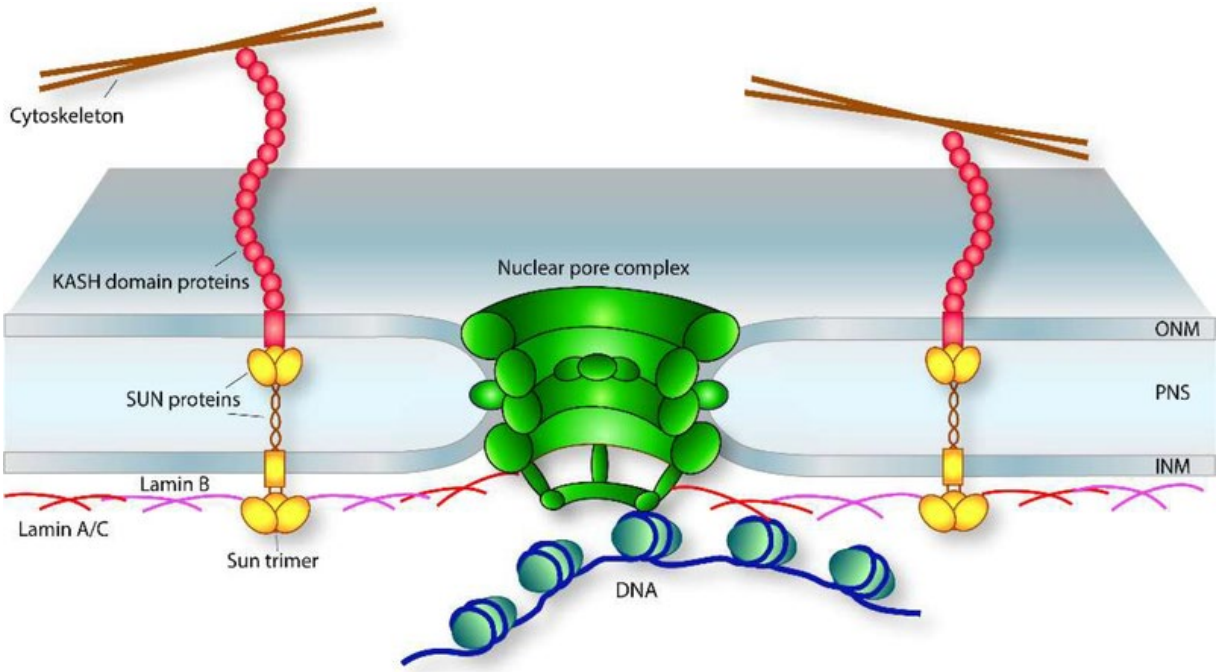

Fig. 1.9 Schematic cross-section of the nuclear envelope in mammalian cells
The model illustrates the two major protein complexes spanning the nuclear envelope: the LINC complex and the nuclear pore complex. The LINC complex connects the cytoskeleton to the nucleus through the interaction of KASH domain proteins and SUN domain proteins located in the inner or outer nuclear membrane, respectively. The nuclear pore complex spans the nuclear envelope and is the main transporter to allow exchange between nuclear and cytoplasmic compartments. ONM: outer nuclear membrane, INM: inner nuclear membrane, PNS: perinuclear space (Preston et al., 2018). CC BY 4.0 license

Cells of higher eukaryotes divide by “open” mitosis, meaning that the nuclear envelope disassembles prior to chromosome segregation (to allow the mitotic spindle access to the chromosomes) and reforms during late anaphase and telophase to restore the nucleocytoplasmic barrier (De Magistris & Antonin, 2018).

1.4 The linker of nucleoskeleton and cytoskeleton (LINC) complex

The LINC complex plays a critical role in the integration of nuclear and cytoplasmic functions by spanning the nuclear envelope and connecting the cytoskeleton to the nucleus. Hence, it

contributes to several important processes, from the transmission of mechanical forces across the nuclear envelope during nuclear positioning and migration to the control of centrosome positioning during DNA replication and repair (Oza et al., 2009; Sato et al., 2009; Katsumata et al., 2017; Horn, 2014; Wang et al., 2018). Its core components are Klarsicht, ANC-1 and Syne Homology (KASH) domain proteins, located at the outer nuclear membrane and Sad1 and UNC-84 (SUN) domain proteins, located at the inner nuclear membrane. Both SUN and KASH domain proteins contain transmembrane domains (TMD) and interact with each other in the perinuclear space (Fig. 1.10; Chang et al., 2015; Padmakumar et al., 2005; Crisp et al., 2006; Tapley & Starr, 2013). The N-terminus of SUN proteins extends into the nucleoplasm, where it interacts with lamins and other nuclear proteins, including chromatin and telomeric proteins (Fig. 1.10; Haque et al., 2006; Chi et al., 2007; Burke, 2018; Schmitt et al., 2007; Ding et al., 2007). On the other side of the nuclear envelope, KASH proteins cross the outer nuclear membrane and bind to cytoskeletal elements, such as actin filaments, microtubules and intermediate filaments in the cytoplasm (Fig. 1.10; Starr & Han, 2002; Starr & Fridolfsson, 2010).

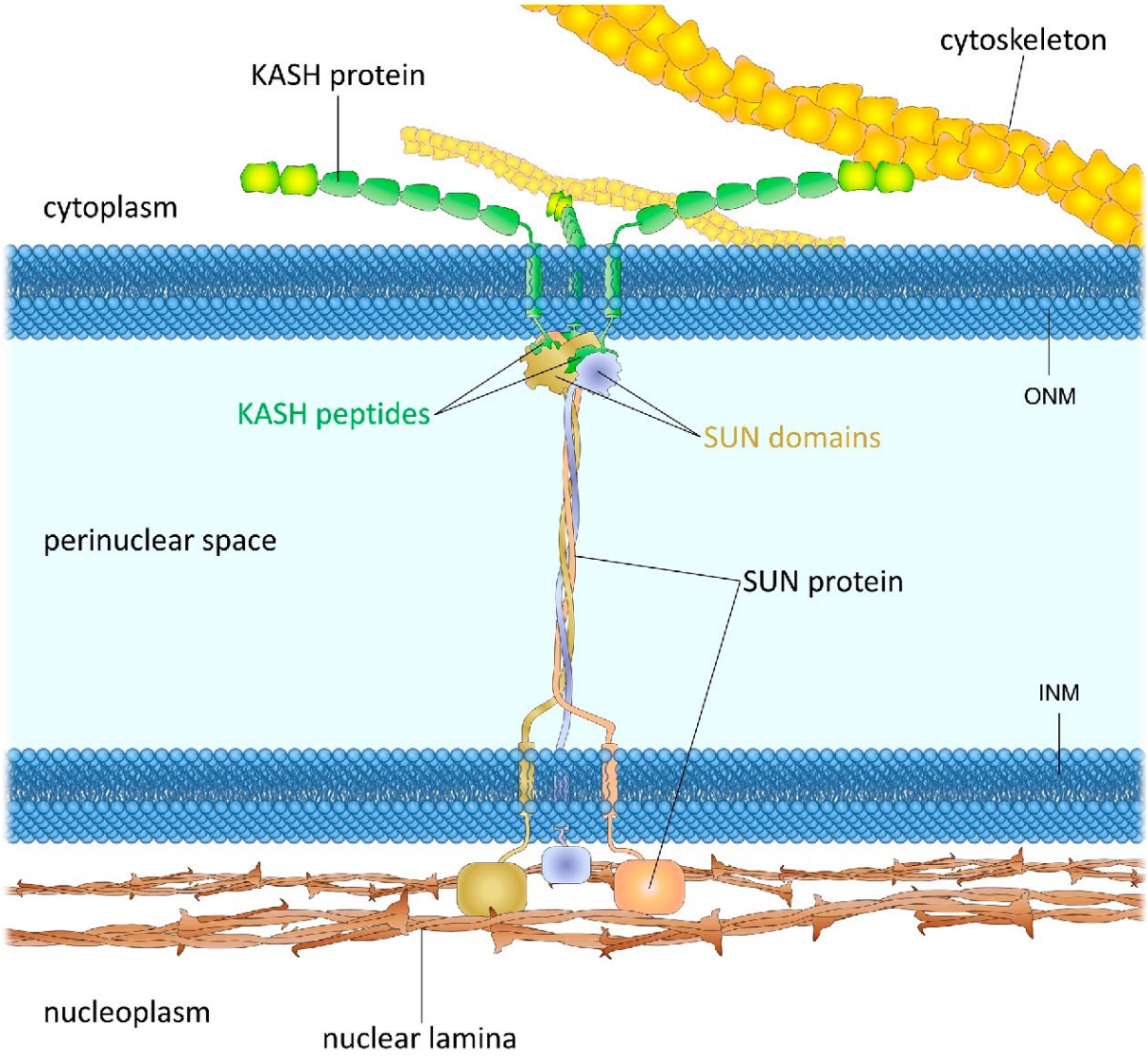

Fig. 1.10 Structure of the LINC complex in mammalian cells
The LINC complex consists of KASH and SUN domain proteins. While KASH domain proteins are embedded in the outer nuclear membrane (ONM) and interact with cytoskeletal components in the cytoplasm, SUN domain proteins are anchored in the inner nuclear membrane (INM) and interact with proteins of the nuclear laminar within the nucleoplasm. Both proteins interact in the perinuclear space with their SUN domains and their KASH domains (KASH peptides) (Chang et al., 2015). © 2015 Chang et al. CC BY 3.0 license

The first model of a complex bridging the nuclear laminar to the cytoskeleton was proposed by Lee et al. in 2002 and Starr and Han in 2003, in which the *Caenorhabditis elegans* lamin-binding protein UNC-84 and the cytoskeleton-binding protein ANC-1 interact in the perinuclear space (Lee et al., 2002; Starr & Han, 2003; Crispr et al., 2006).

This model was supported by demonstrating a conserved nuclear anchoring mechanism between *C. elegans* and mammalian cells by Padmakumar et al. in 2005 and Crisp et al. in 2006. The localisation of Nesprin-2, a giant actin-binding protein (Zhang et al., 2002), to the outer nuclear membrane has been shown to be dependent on the inner nuclear membrane protein SUN1 (Padmakumar et al., 2005). Hence, this protein assembly has been termed the linker of nucleoskeleton and cytoskeleton (LINC) complex (Crisp et al., 2006).

1.4.1 SUN domain proteins

The term "SUN domain" derives from the *Schizosaccharomyces pombe* protein Sad1 (Hagan & Yanagida, 1995) and the *C. elegans* protein UNC-84 (Malone et al., 1999). Fission yeast mutated in the *sad1* gene showed lethal deformation and malfunction of the spindle pole body, and it was suggested that Sad1 might anchor the spindle pole body to the nuclear envelope (Hagan & Yanagida, 1995). Malone et al. showed high sequence similarity of the C-termini of both yeast Sad1 and *C. elegans* UNC-84. Like Sad1, UNC-84 has been suggested to be involved in the interaction between the nucleus and the centrosome. Using the BLAST search, two mammalian proteins with high sequence homology in the C-terminus were identified and designated SUN1 and SUN2, for Sad1/UNC-84 domain protein (Malone et al., 1999). SUN1 and SUN2 have been shown to be type II membrane proteins localised to the inner nuclear membrane, with their N-termini exposed to the nucleoplasm and their C-terminal SUN domain reaching into the perinuclear space (Hodzic et al., 2004; Padmakumar et al., 2005; Haque et al., 2006; Tapley et al., 2011). The nucleoplasmic N-terminus of SUN1 was shown to interact with lamin A, demonstrating a direct interaction of SUN domain proteins with the nuclear laminar (Haque et al., 2006). First structural insights into the crystal structure of SUN2 revealed that conserved coiled-coil regions are required for trimerisation of SUN domains that bind three KASH peptides (Sosa et al., 2012).

Three other SUN proteins have been identified in mammals. While SUN1 and SUN2 were shown to be partially functionally redundant and were expressed in most cell types, the expression of SUN3, SUN4 (originally SPAG4 for sperm-associated antigen 4) and SUN5 (originally SPAG4L for SPAG4-like) is restricted to testis-specific cells (Crisp et al., 2006; Göb et al., 2010; Tarnasky et al., 1998; Shao et al., 1999; Jiang et al., 2011).

Besides UNC-84, which was one of the first described SUN domain proteins (Malone et al., 1999), another SUN protein, termed SUN-1 (or MTF-1), has been identified in the nematode *C. elegans* and was shown to be involved in chromosome movement during meiosis (Fridkin et al., 2004; Sato et al., 2009).

SUN domain proteins are highly conserved in eukaryotes and have been identified also in budding yeast (Mps3; Jaspersen et al., 2002), *Drosophila melanogaster* (Spag4 and Klaroid; Kracklauer et al., 2010; Patterson et al., 2004) and plants (*Arabidopsis thaliana* AtSUN1 and AtSUN2; Graumann et al., 2010).

Most of the SUN proteins share the typical domain organisation containing one transmembrane domain, coiled-coil regions and the conserved SUN domain exposed to the nuclear envelope or the ER (Fig. 1.11; Rothballer et al., 2013).

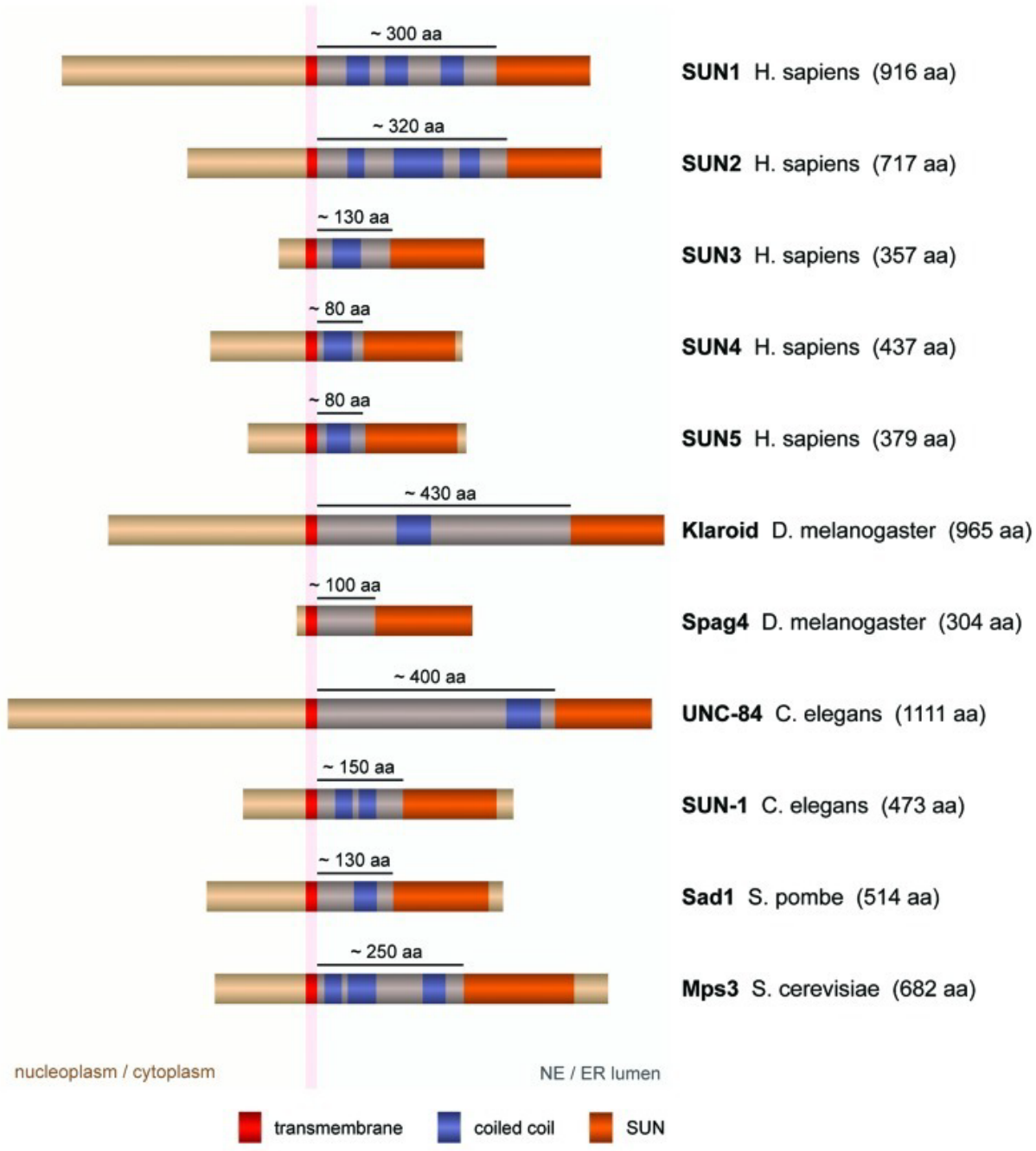

Fig. 1.11 Domain organisation of SUN domain proteins in different species
The typical domain organisation of SUN proteins is a transmembrane domain (red), coiled-coil regions (blue), and a conserved SUN domain (orange) that extends into the NE or the ER lumen. The length of the coiled-coil region differs between SUN proteins within different species. aa: amino acids; NE: nuclear envelope; ER: endoplasmic reticulum (Rothballer et al., 2013).

While the SUN domain of classic SUN proteins is located at the C-terminus, atypical SUN proteins have been identified that have their SUN domain in the middle. The mammalian mid-SUN protein osteopotentia (Opt) has been shown to be an integral membrane protein localised in the ER and could function as an adaptor protein connecting the rough ER to the cytoskeleton (Sohaskey et al., 2010). In *A. thaliana*, the mid-SUN proteins AtSUN3 and AtSUN4 localise to the nuclear envelope and the ER (Graumann et al., 2014).

1.4.2 KASH domain proteins

In 2002, Starr and Han showed that the nuclear envelope proteins ANC-1 (*C. elegans*), Klarsicht (*D. melanogaster*) and mammalian SYNE-1 and SYNE-2 share conserved regions of approximately 60 amino acids at their C-termini and named this homology region "KASH domain" for Klarsicht, ANC-1 and Syne Homology (Starr & Han, 2002). Mutations in *anc-1* were previously shown to cause nuclear anchoring defects in *C. elegans* (Hedgecock & Thomson, 1982) and Klarsicht was shown to be essential for the correct migration of nuclei during eye development in *D. melanogaster* (Welte et al., 1998; Mosley-Bishop et al., 1999). SYNE-1 and SYNE-2 (synaptic nuclear envelope protein) have been described by several different groups as containing multiple spectrin repeats and being involved in the migration of nuclei and maintenance of nuclear organisation by connecting the nucleus to the actin cytoskeleton and therefore alternatively referred to as Nesprin-1 and Nesprin-2 (nuclear envelope spectrin repeat) or NUANCE (nucleus and actin connecting element). Comprising transmembrane regions, KASH proteins are located at the outer nuclear membrane with the shorter, C-terminal KASH domain-containing part reaching into the perinuclear space and the larger, N-terminal part facing the cytoplasm (Apel et al., 2000; Zhang et al., 2001; Zhen et al., 2002; Mislow et al., 2002).

In addition to the highly conserved C-terminal KASH domain, mammalian Nesprin-1 and Nesprin-2 and a second KASH domain protein in *D. melanogaster,* MSP-300, share large central domains of multiple spectrin repeats that have been proposed to function similarly to the long coiled-coil domains of *C. elegans* ANC-1 (Fig. 1.12; Starr & Han, 2002; Rosenberg-Hasson et al., 1996). The number of spectrin repeats determines the length of a nesprin protein, making Nesprin-1 and Nesprin-2 to giant proteins of around 1 MDa and nearly 800

kDa, containing 74 and 56 spectrin repeats, respectively (Simpson et al., 2008). Not all KASH domain proteins contain spectrin repeats. For example, Klarsicht is only homologous in its C-terminal KASH region and contains no specific spectrin-repeat regions (Starr & Han, 2002).

The third structural feature of Nesprin-1, Nesprin-2, ANC-1 and MSP-300 are conserved N-terminal calponin homology (CH) domains that interact with actin (Fig. 1.12; Starr & Han, 2002; Zhen et al., 2002; Padmakumar et al., 2004).

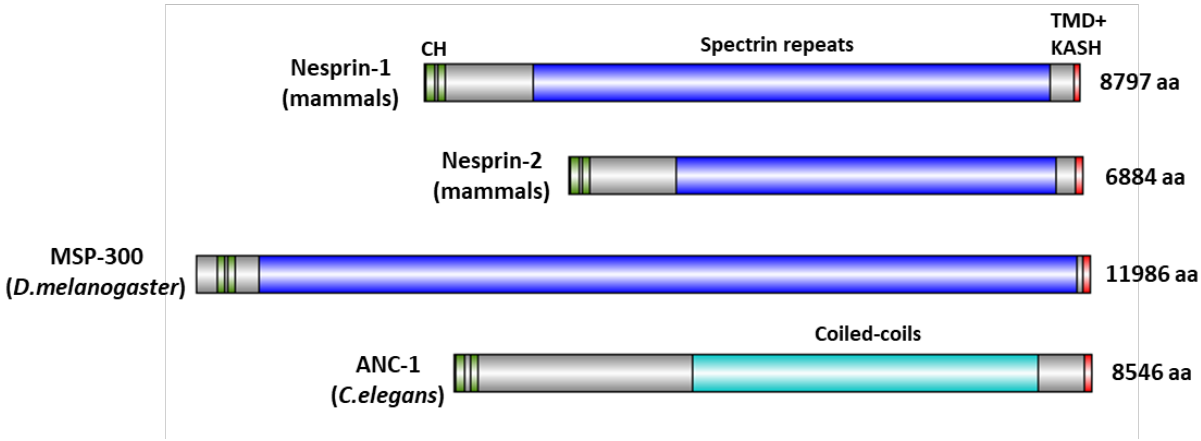

Fig. 1.12 Domain organisation of KASH domain proteins in different species
KASH domain proteins not only share the conserved KASH domain (red), but also calponin homology (CH) domain (green) and several spectrin repeats or coiled-coil regions (blue). Close to the KASH domain, the proteins also share transmembrane domains (TMD). The length of the proteins is given in amino acids (aa) on the right. The figure was created with the IBS Illustrator for biological sequences (Liu et al., 2015).

Additional mammalian nesprins and KASH domain proteins have been described: Nesprin-3 binds the cytoskeletal crosslinker protein plectin and therefore associates with intermediate filaments (Wilhelmsen et al., 2005). Nesprin-4 interacts with kinesin-1 and was suggested to contribute to microtubule-dependent nuclear positioning (Roux et al., 2009). The KASH domain protein KASH5 lacks spectrin repeats and its expression is restricted to germ cells (Morimoto et al., 2012). LRMP or Jaw1 is an atypical mammalian KASH protein localised to the outer nuclear membrane and the ER but is not associated with the cytoskeleton (Kozono et al., 2018).

While nesprins were originally described as nuclear envelope proteins that connect the nucleus to the cytoskeleton, several isoforms have been proposed and identified, differing in

size, expression, and subcellular localisation by cell type (Rajgor et al., 2012; Rajgor & Shanahan, 2013; Rey et al., 2021).

KASH-like proteins have been described in yeasts such as *S. cerevisiae* Mps2 and Csm4 (Munoz-Centeno et al., 1999; Chen et al., 2019; Conrad et al., 2008; Fan et al., 2020) and *S. pombe* Kms1 and Kms2 (Miki et al., 2004; Wälde & King, 2014).

Beside ANC-1, the first KASH domain protein described in *C. elegans,* three other KASH domain proteins exist in worms namely UNC-83, ZYG-12 and KDP-1 (Starr et al., 2001; Malone et al., 2003; McGee et al., 2009).

Intriguingly, while SUN domain proteins are highly conserved, KASH domain proteins are often species or phylum-specific and cannot be identified via standard bioinformatic approaches, for example the AtWIP proteins (WPP domain interacting proteins) in *A. thaliana* have been identified as functional analogues, but show little homology to known KASH proteins (Zhou et al., 2012; Zhou & Meier, 2013). Using a computational approach, five more KASH-like proteins, called SINE1-5 (SUN-interacting nuclear envelope proteins, due to their binding to AtSUN1 and AtSUN2) have been identified (Zhou et al., 2012).

1.4.3 SUN-KASH interaction and structure of the LINC complex

As described in the previous sections, two main components, SUN and KASH proteins, are required for the formation of a LINC complex.

The first crystal structures of mammalian LINC complexes revealed a detailed insight into the SUN-KASH interaction (Sosa et al., 2012; Zhou et al., 2012). SUN proteins form a trimer to bind to three KASH peptides forming a hexameric complex (Sosa et al., 2012). Several conserved residues have been reported to be important for the interaction between SUN and KASH: First, the three proline residues of a conserved motif (PPPX) at the C-terminus of KASH proteins bind within a pocket in the core of a SUN protomer. Second, the 7-tyrosine of the

KASH domain binds into a groove between two SUN protomers and third, a disulfide bond between cysteines of KASH and SUN (Fig. 1.13; Sosa et al., 2012; Hao & Starr, 2019).

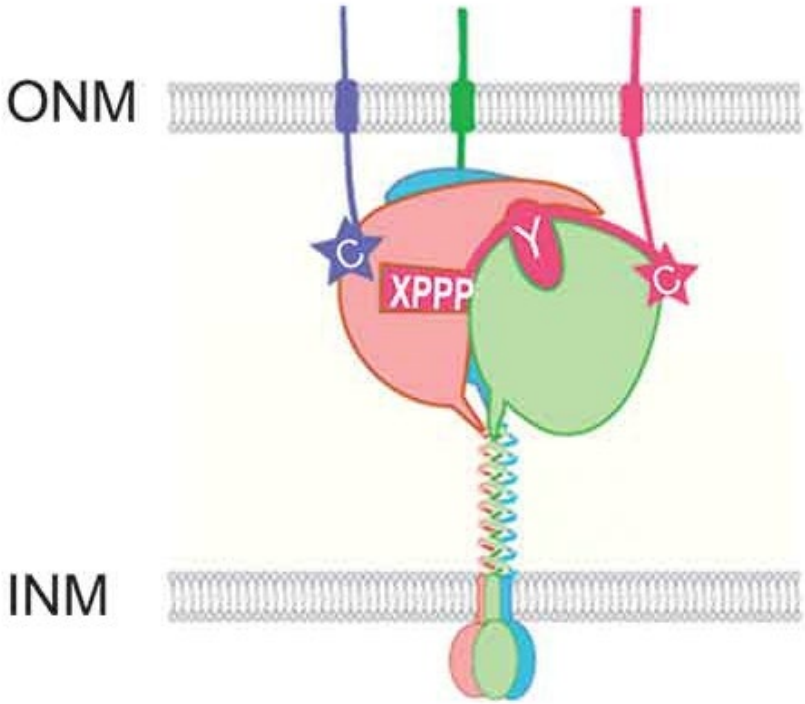

Fig. 1.13 Conserved residues that are essential for proper SUN-KASH interaction
SUN proteins form trimers at the inner nuclear membrane (INM) and extend to the outer nuclear membrane (ONM) where they bind to three KASH peptides to form a hexameric structure. Each KASH peptide is flanked by a SUN protomer at three residues: a conserved proline motif (PPPX), a tyrosine (Y) and a cysteine (C), Figure adapted from Hao & Starr, 2019).

1.4.4 Main functions of the LINC complex

The connection of the cytoskeleton to the nucleus is essential for transmitting forces from the surface of the cell to the nucleus. As described in the previous sections, at least five SUN domain proteins and six KASH domain proteins have been identified in mammalian cells, suggesting a diverse number of different LINC complex variants with different functions.

1.4.4.1 Nuclear anchorage, positioning and nucleokinesis

Disruption of the LINC complex formed by the SUN domain protein UNC-84 and the KASH domain protein ANC-1 in *C. elegans* leads to a strong nuclear anchoring defect (Malone et al., 1999; Starr & Han, 2002). Being conserved in mammals, it was suggested, that the mammalian LINC complex plays a similar role in nuclear anchorage and indeed, SUN1 and SUN2 were shown to interact with Nesprin-1 or Nesprin-2 to anchor myonuclei for proper motor neuron innervation in mice (Zhang et al., 2007).

The complex formed by SUN1 or SUN2 and Nesprin-3 helps to stabilise the anchorage and therefore maintains the structure and shape of the nucleus, caused by Nesprin-3 interaction with intermediate filaments through its ability to bind plectin (Ketema et al., 2007; Ketema et al., 2011).

Due to its binding to Kinesin-1, Nesprin-4 has been described to be required for microtubule-dependent nuclear positioning in secretory epithelial cells (Roux et al., 2009).

A role of the LINC complex in nucleokinesis was first observed in *C. elegans* where mutations in the respective genes of the SUN domain protein UNC-84 and the KASH domain protein UNC-83 interfered with nuclear migration (Starr et al., 2001).

1.4.4.2 Centrosome-associated LINC complexes

The centrosome and the spindle pole body, the equivalent organelle in yeast, play important roles in mitosis and nucleokinesis. To do this, they need to be tethered to the nucleus and it seems that the LINC complex is an important factor in this connection. Studies in mammals, *C. elegans* and yeast show LINC complexes connecting the centrosome to the nucleus.

For example, the LINC complex formed by SUN1 and SUN2 with Nesprin2 was shown to couple the nucleus to the centrosome during neurogenesis and neuronal migration in mice (Zhang et al., 2009).

In *C. elegans*, the centrosome is attached to the nucleus through the linkage of the SUN-KASH pair SUN1/ MTF-1 and ZYG-12. Additionally, it has been proposed that ZYG-12 recruits dynein to the nuclear envelope to bring the nucleus and the centrosome into proximity (Malone et al., 2003; Minn et al., 2009).

A recent study in budding yeast reveals a LINC complex formed by the SUN protein Mps3 and the KASH-like protein Mps2 during mitosis (Chen et al., 2019). Mps3, the only described SUN domain protein in

S. cerevisiae, has been shown to be concentrated at the spindle pole body and at the inner nuclear membrane (Jaspersen et al., 2002), and the KASH-like protein Mps2 was described to localise to the nuclear envelope and the spindle pole body (Munoz-Centeno et al., 1999). Although Mps2 lacks the canonical KASH domain, it forms an atypical centrosome-associated LINC complex with Mps3 (Chen et al., 2019).

In fission yeast, the complex formed by SUN domain protein Sad1 and the KASH domain protein Kms2 has been shown to play a role in spindle pole body remodelling required for mitosis (Wälde & King, 2014).

2 Aim of this study

Although LINC complexes can be found in many different species, no cytoskeletal-nuclear bridging complex has been identified in apicomplexan parasites. However, comparable processes exist in Apicomplexans, suggesting the existence of a LINC complex. For instance, the apicomplexan parasite *T. gondii* invades host cells through a tight junction that constricts the parasite during penetration. During this process, F-actin accumulates at the posterior pole of the parasite and around the nucleus, suggesting that there is distinct association between F-actin and the nucleus (Del Rosario et al., 2019). This leads to the hypothesis that F-actin and a potential apicomplexan LINC complex are involved in nuclear positioning, protection and deformation during invasion, as observed in other migratory cells (McGregor et al., 2016; Del Rosario et al., 2019). Similarly, the apicomplexan nucleus shows impressive deformation during replication in order to be distributed equally to the forming daughter cells, suggesting integration of cytoskeletal and nuclear functions (Suvorova et al., 2015).

The aim of this study is the identification and characterisation of possible components of an apicomplexan-specific LINC complex in *T. gondii.*

3 Materials

3.1 Equipment

Table 3.1 Equipment used in this study

Company	Description
BD Biosciences	FACSAria III Cell Sorter
BioRad	Mini Trans-Blot Electrophoretic Transfer Cell
	PowerPac Basic Power Supply
	Mini-Sub Cell GT Cell Horizontal electrophoresis system
Eppendorf	Centrifuge 5910 Ri
	Mastercycler EP Gradient (PCR thermocycler)
	Pipettes
Hartenstein	Pipettes
Leica	DMi8 wide-field microscope
LI-COR Biosciences	Odyssey CLx-1849
Lonza	Amaxa 4D-Nucleofector system
NIPPON Genetics	FastGene Blue/Green LED Transilluminator
Phoenix Instrument	Waterbath
Scientific industries	Vortex-Genie 2
Starlab	ErgoOne Single & Multi-channel pipettes
	Vortexer
Thermo Fisher Scientific	CO_2-Incubator
	Invitrogen DynaMag-2 Magnet
	NanoDrop Spectrophotometer
	Owl EasyCast minigel electrophoresis system
Zeiss	Axio Vert.A1 fluorescence microscope

3.2 Consumables, biological and chemical reagents

Table 3.2 Consumables and biological and chemical reagents used in this study

Company	Description	Ordering No.
Biochrom	Ultra pure water, sterile	L0015
BioRad	4-20% Mini-PROTEAN TGXP Precast Protein Gel	4561094
	Ammonium persulfate (APS) catalyst	1610700
	Tetramethylenediamine (TEMED)	1610800
BioSell	Fetal bovine serum (FBS)	FBS.US.0500
Biotium	GelRed Nucleic Acid Gel Stain	41003

Biozym	LE GeneticPure Agarose	850071
Braun	Injekt 5 mL Luer syringe	4606051V
	Sterican cannulas 0.45 mm	4657683
Faust	TPP Cell culture bottle 75 cm^2	TPP90076
	TPP Cell culture bottle 150 cm^2	TPP90151
	TPP Cryotubes	TPP89020
	TPP Tissue culture dishes 6 cm^2	TPP93060
	TPP Tissue culture test plate 6-well	TPP92406
	TPP Tissue culture test plate 24-well	TPP92424
	TPP Tissue culture test plate 96-well	TPP92496
Hartenstein	Agar Bacteriology grade	CA30
	Cell scratcher	ZS23
	Cover slips, high precision, 12 mm	DHR1
	Tryptone *BioChemica*	CT50
	Yeast extract *BioChemica*	CH15
Ibidi	µ-Dish 35 mm, high	81156
	µ-Slide 8 Well glass bottom	80827
Jülich Opische Systeme	Immersion Oil 518F 30°C Zeiss	444970-9000-000
LI-COR Biosciences	Chameleon Duo Pre-stained Protein Ladder	928-60000
	Intercept (TBS) blocking buffer	927-60001
	IRDye 800CW Streptavidin	926-32230
Merck	Amersham Protran western blotting membrane, nitrocellulose, pore size 0.45 µ	GE10600002
	Calcium chloride dihydrate ($CaCl_2$ x $2H_2O$)	1023820250
Millipore	Isopore membrane filter 3.0 µm/ 25 mm	TSTP02500
	Whatman Chromatography paper 3MM	WHA303072
New England Biolabs	1 kb Plus DNA Ladder	N3200S
	BsaI-HF v2	R3733S
	Deoxynucleotide (dNTP) solution mix	N0447S
	Gel Loading Dye, purple (6x), no SDS	B7025S
	One*Taq* DNA Polymerase	M0480S
	Q5 High-Fidelity DNA Polymerase	M0491S
	rCutSmart buffer	B6004S
	T4 DNA Ligase	M0202S
	T4 DNA Ligase Reaction buffer	B0202S
NIPPON Genetics	Midori Green Advance DNA/ RNA stain	MG04
Roche	DNA Molecular Weight Marker XVI (250 bp ladder)	11855638001
Roth	Acetic acid (100%)	6755.1
	Acetone ≥99.7%	CP40.1
	Dimethyl sulfoxide (DMSO)	4720.4
	Glycerol	6962.1
	Glycine	0079.3
	Giemsa stock solution 20x	T862.1

	Mangan(II)-chloride tetrahydrate ($MnCl_2$ x $4H_2O$)	0276.1
	Methanol Rotisolv ≥ 99.98%	HN41.1
	Microscope slides	H872.1
	Neubauer haemocytometer	T735.1
	Parafilm M	CNP8.1
	Ponceau S	5938.2
	Rotiphorese 50xTAE Buffer	CL86.2
	Rubidium chloride (RbCl)	4471.4
	Sodium chloride (NaCl)	3957.3
	Sodium dodecyl sulphate (SDS)	0183.3
	Sodium hydroxide (NaOH)	P031.1
Santa Cruz Biotechnology, Inc.	Jasplakinolide	SC202191
Science services	20% Paraformaldehyde (PFA)	E15713
Serva	Acrylamid/ Bis-Solution, 37.5:1	10688.03
Sigma	Ampicillin sodium crystallin	A9518
	Biotin ≥ 99% HPLC grade powder	B4501
	Bovine serum albumin (BSA)	A7030
	Cytochalasin D (cytD)	C8273
	DL-Dithiothreitol (DTT)	D0632
	Dulbecco's modified Eagle's medium, high glucose (DMEM)	D6546
	Ethylenediaminetetraacetic acid (EDTA)	EDS-100G
	Gentamycin solution 50 mg mL^{-1}	G1397
	Hydrochloric acid (HCl)	H1758
	Hydroxyurea (HU)	H8627
	L-glutamine solution 200 mM	G7513
	MOPS	M1254
	Orange G	O3756
	Phosphate-buffered saline 1x (PBS)	D8537
	Poly-L-lysine solution (0.1% w/v in H_2O)	P8920
	Potassium acetate	P1190
	Protease and phosphatase inhibitor cocktail	PPC1010
	Pyrrolidine dithiocarbamate (PDTC)	P8765
	Rapamycin powder	R0395
	Sodium deoxycholate	D6750
	Triton X-100 (TX-100)	T8787
	Trypsin-EDTA solution	T3924
SMS-Medipool	Braun Injekt Syringe 5 mL	300 020
	Braun Omnifix syringes 1 mL	300 130
	Sterican needle 26G x 1""/ Ø 0.45x12 mm	300 110
Thermo Fisher Scientific	Dynabeads MyOne Streptavidin T1	65601
	Hoechst 33342 Solution 20 mM	62249
	ProLong Gold Antifade Mountant	P36934

Thorlabs	Very low autofluorescence immersion oil, Leica Type F	MOIL-10LF
VWR	PCR tubes, flat caps	GREI683201_1000
	Petri dishes 90x14 mm	391-0560

3.3 Kits

Table 3.3 Kits used in this study

Company	Description	Ordering No.
Blirt	EXTRACTME DNA CLEAN-UP & GEL-OUT KIT	EM26.1
	EXTRACTME GENOMIC DNA KIT	EM013
	EXTRACTME PLASMID MINI KIT	EM01.1
Lonza	P3 Primary cell 4D nucleofector X Kit L	V4XP-3024

3.4 Buffers, solutions and media

Table 3.4 Protocols of buffers for molecular cloning used in this study

Description	Components
Annealing buffer	10 mM Tris pH 7.5 – 8.0 50 mM NaCl 1mM EDTA diluted in ddH_2O

Table 3.5 Protocols of buffers and media for cell and parasite culture used in this study

Description	Components
2x Freezing media	DMEM 25% FBS (v/v) 10% DMSO (v/v)
DMEM for cell culture	500 mL DMEM 10 % FBS 4 mM L-glutamine 25 µg mL^{-1} gentamycin
PFA fixing solution	4% PFA in PBS

Table 3.6 Protocols of buffers and media for bacterial cultures used in this study

Description	Components
LB-Agar	1.5 % (w/v) agar in LB-Medium
LB-Medium	10 g l^{-1} bacto-tryptone

	5 g l^{-1} yeast extract 10 g l^{-1} NaCl diluted in ddH_2O
Transformation buffer I	30 mM Potassium acetate 100 mM RbCl 10 mM $CaCl_2$ x $2H_2O$ 50 mM $MnCl_2$ x $4H_2O$ 15% (v/v) glycerol diluted in ddH_2O adjusted to pH 5.8 with acetic acid
Transformation buffer II	1 mM Mops 75 mM $CaCl_2$ x $2H_2O$ 10 mM RbCl 15% (v/v) glycerol diluted in ddH_2O adjusted to pH 6.5 with NaOH

Table 3.7 Protocols of buffers for protein biochemistry used in this study

Description	**Components**
10x Running buffer	35 mM SDS 250 mM Tris 192 mM Glycine diluted in ddH_2O
10x Transfer buffer	25 mM Tris 192 mM Glycine diluted in ddH_2O
1x Transfer buffer	100 mL 10x Transfer buffer 200 mL MeOH (100%) 700 mL ddH_2O kept at 4°C
10x Tris-Buffered saline (TBS)	200 mM Tris 1.5 M NaCl adjusted to pH 7.6 with HCl
Orange loading dye	125 mM Tris-HCl pH 6.5 50% glycerol 4% SDS 0.2% Orange G
Ponceau S	0.1% Ponceau S 5% acetic acid (100%) diluted in ddH_2O
RIPA buffer	0.5% sodium deoxycholate 150 mM NaCl 1 mM EDTA 0.1% SDS 50 mM Tris-HCl pH 8.0 1% Triton TX-100

3.5 Software

Table 3.8 Computer software used in this study

Software description	Reference
ApE - A plasmid editor v2.0.61	Davis & Jorgensen, 2022
Basic Local Alignment search tool (BLAST)	National Institute for Biotechnology Information (NCBI)
EuPaGDT – Eukaryotic Pathogen CRISPR gRNA design tool	Peng & Tarleton, 2015; University of Georgia
Fiji (is just ImageJ) v1.53c	Schindelin et al., 2012
IBS Illustrator for biological sequences	Liu et al., 2015
InterPro – Classification of protein families	Blum et al., 2021
JACoP (Just another colocalization plugin) LGPLv3	Bolte & Cordelières, 2006
Las X software (v.3.4.2.183668)	Leica Application Suite X (Las X)
LI-COR Biosciences	LI-COR Image Studio Software
Tm Calculator version 1.13.1	New England Biolabs
ToxoDB	Gajria et al., 2008
toxoLOPIT explore	Barylyuk et al., 2020

3.6 Oligonucleotides

Primers up to 100 bp were synthesised by the company Thermo Fisher Scientific, Longmers (more than 100 bp) were synthesised by the company Integrated DNA Technologies (IDT).

Table 3.9 Oligonucleotides to generate the endogenous tagged line and the conditional knockout mutant of TgUNC1

Name	Sequence	Purpose
TgUNC1_sgRNA-Cterm-tag-fw	**AAGTT**GACTTGCCAGCCGGTGATTCC**G**	integration into Cas9YFP-sgRNA vector
TgUNC1_sgRNA-Cterm-tag-rv	**AAAAC**GGAATCACCGGCTGGCAAGTC**A**	integration into Cas9YFP-sgRNA vector
TgUNC1_Cterm-tag-donor-fw	CGCCAGGTGTCCCTGAGGTGTCAGTGC ACCTGGAGAGCCCCGCAGGGAAA**GCTA AAATTGGAAGTGGAGG**	PCR amplification of the repair template
TgUNC1_Cterm-tag-donor-rv	AAGCCACCGTTCCCTCAATTCGTACTACT CGTCACGGCTTCCTCAACTCA**ATAACTT CGTATAATGTATGCTATACG**	PCR amplification of the repair template
TgUNC1_sgRNA-Upstr-LoxP-fw	**AAGTT**GAAGACAAAGATTGCAAAAC**G**	integration into Cas9YFP-sgRNA vector
TgUNC1_sgRNA-Upstr-LoxP-rv	**AAAAC**GTTTTGCAATCTTTGTCTTC**A**	integration into Cas9YFP-sgRNA vector

TgUNC1_Upstr-LoxP-donor	CTCGCGTCCTTTCTTTTTCGCTTCCGGTTTTGCAA**ATAACTTCGTATAGCATACATTATACGAAGTTAT**TCTTTGTCTTCACAATGCTGCCGACGTATCA	repair template
TgUNC1_5UTR-fw	CTTATTCGCCGTGGAGTTCTG	genotyping
TgUNC1_internal-fw	GCAGGTAATTGGTGTCCAAGAG	genotyping
TgUNC1_3UTR-rv	GTCTCATGTTTGCCTCCGTG	genotyping
TgUNC1_Upstr-LoxP-contr-rv	GAAGACAAAGAATAACTTCGTATAATGTATGC	genotyping

Table 3.10 Oligonucleotides to generate the endogenous tagged line of TgSLP2

Name	Sequence	Purpose
TgSLP2_sgRNA-Cterm-tag-fw	**AAGTT**GTATTCGAACTCTAGTTAGC**G**	integration into Cas9YFP-sgRNA vector
TgSLP2_sgRNA-Cterm-tag-rv	**AAAAC**GCTAACTAGAGTTCGAATAC**A**	integration into Cas9YFP-sgRNA vector
TgSLP2_Cterm-tag-donor-fw	AGCGAGGAGCCCCACGGGTGGAAGAGGCAGCTGGAATGCTCCCAGCAAACG**CTAAAATTGGAAGTGGAGG**	PCR amplification of the repair template
TgSLP2_Cterm-tag-donor-rv	AGGACCCGAAGCTGACTGTTCTCCGTTTCTGTTGCTCTATTCGAACTCTA**ATAACTTCGTATAATGTATGCTATACG**	PCR amplification, repair template
TgSLP2_internal-fw	ACCTGTGAAGGACGCAAGAG	genotyping
TgSLP2_3UTR-rv	CTCTCGGTTTCCTCGTTCTGTC	genotyping

Table 3.11 Oligonucleotides to generate a conditional knockout of TgSLP2 (not successful)

Name	Sequence	Purpose
TgSLP2_sgRNA-Upstr-LoxP-fw (1)	**AAGTT**GCAGGCATCCCGCCCCCTCT**G**	integration into Cas9YFP-sgRNA vector
TgSLP2_sgRNA-Upstr-LoxP-rv (1)	**AAAAC**AGAGGGGGCGGGATGCCTGC**A**	integration into Cas9YFP-sgRNA vector
TgSLP2_Upstr-LoxP-donor (1)	AGCTCAAGCTCTGTCTCCTTTCTTGGAGCCCA**ATAACTTCGTATAGCATACATTATACGAAGTTAT**GAGGGGGCGGGATGCCTGCGTCCGCTCCGACCGC	repair template
TgSLP2_5UTR-fw (1)	TCTCCTGTCTCTTCTTTGCCTG	genotyping
TgSLP2_Upstr-LoxP-contr-rv (1)	CCCCTCATAACTTCGTATAATGTATGC	genotyping
TgSLP2_sgRNA-Upstr-LoxP-fw (2)	**AAGTT**GCCGCTTCTTCCTTATCTTCT**G**	integration into Cas9YFP-sgRNA vector
TgSLP2_sgRNA-Upstr-LoxP-rv (2)	**AAAAC**AGAAGATAAGGAAGAAGCGGC**A**	integration into Cas9YFP-sgRNA vector
TgSLP2_Upstr-LoxP-donor (2)	GTGTCCGGCTCTGCCGCTTCTTCCTTATCTATAACTTCGTATAGCATACATTATACG	repair template

	AAGTTATTCTCGGTCGTTTTCGTCTTCGTCGTTCGTC	
TgSLP2_outside-5UTR-fw (2)	ATGTCCAAGTTCGTTCGTCG	genotyping
TgSLP2_Upstr-LoxP-contr-rv (2)	ACGACCGAGAATAACTTCGTATAA	genotyping
TgSLP2_sgRNA-Internal-LoxP-fw	**AAGTT**AGAGAGGGATCGAAAAGTGG**G**	integration into Cas9YFP-sgRNA vector
TgSLP2_sgRNA-Internal-LoxP-rv	**AAAAC**CCACTTTTCGATCCCTCTCT**A**	integration into Cas9YFP-sgRNA vector
TgSLP2_Internal-LoxP-donor	TCGGGGAAGGTACCGAGAGAGAGGGATCGAAA**ATAACTTCGTATAGCATACATTATACGAAGTTAT**CCAGTGGAGGGGAAGAGAGCGAGACAGATGCTCA	repair template
TgSLP2_5UTR-fw (1)	TCTCCTGTCTCTTCTTTGCCTG	genotyping
TgSLP2_Internal-LoxP-contr-rv	CCCCTCCACTGGATAACTTCGTATAATGTATGC	genotyping
TgSLP2_sgRNA-U1-silencing-fw	**AAGTT**TTTCTATTGCCCGCTAGTAC**G**	integration into Cas9YFP-sgRNA vector
TgSLP2_sgRNA-U1-silencing-rv	**AAAAC**GTACTAGCGGGCAATAGAAA**A**	integration into Cas9YFP-sgRNA vector
TgSLP2_U1-silencing-donor	AAATACAGAACGCAATTAACTCTAACAGAACGATTTCTATTGCCCGCTAGATAACTTCGTATAGCATACATTATACGAAGTTATCAGGTAAGTTGGGAACAGGTAAGTTGGGAACAGGTAAGTTGGGAACAGGTAAGTTTACAGGCCAGTGTACGAACAAATCAGAAGCAGATGGCTGAGAAACCATTC	repair template
TgSLP2_U1-silencing-contr-fw	CATTACCTGCACACGTTCGG	genotyping
TgSLP2_U1-silencing-contr-rv	CAGGGAATGGTTTCTCAGCC	genotyping

Table 3.12 Oligonucleotides to generate the endogenous tagged line and the conditional knockout mutant of TgSLP1

Name	Sequence	Purpose
TgSLP1_sgRNA-Cterm-tag-fw	**AAGTT**GTTTCTGGGCATGCCTAGTTG**G**	integration into Cas9YFP-sgRNA vector
TgSLP1_sgRNA-Cterm-tag-rv	**AAAAC**CAACTAGGCATGCCCAGAAAC**A**	integration into Cas9YFP-sgRNA vector
TgSLP1_Cterm-tag-donor-fw	GCCTGAGAGTCCACGGCGAGAAGGCGGTGCTGAAGTCCACCACCCTCAAC**GCTAAAATTGGAAGTGGAGG**	PCR amplification of the repair template
TgSLP1_Cterm-tag-donor-rv	AGCATGTGCGACTGCTTTGCTTTCTTTGCCTACGTTTCTGGGCATGCCTA**ATAACTTCGTATAATGTATGCTATACG**	PCR amplification of the repair template
TgSLP1_sgRNA-Upstr-LoxP-fw	**AAGTT**GTTTCTGGCTGCTCTGAGCA**G**	integration into Cas9YFP-sgRNA vector
TgSLP1_sgRNA-Upstr-LoxP-rv	**AAAAC**TGCTCAGAGCAGCCAGAAAC**A**	integration into Cas9YFP-sgRNA vector

TgSLP1_Upstr-LoxP-donor	GCCGCTGCTTCTCCTTCGCCGTGCTCAG AGCAGC**ATAACTTCGTATAGCATACATT ATACGAAGTTAT**CAGAAACATCCTGCG ATGGACTCCTTCGAGCG	repair template
TgSLP1_5UTR-fw	CAGCGGGCTTCTGTATTTGC	genotyping
TgSLP1_internal-fw	CTGAAGGAGAAGCCGGTACG	genotyping
TgSLP1_3UTR-rv	GCAGTTGGGCATTCCATTTCG	genotyping
TgSLP1_Upstr-LoxP-contr-rv	GATGTTTCTGATAACTTCGTATAATGTAT GC	genotyping

Table 3.13 Oligonucleotides to generate the endogenous tagged line of TLAP4

Name	Sequence	Purpose
TLAP4_sgRNA-Nterm-tag-fw	**AAGTT**GTTTCCCGAAATTGCTCTGTT**G**	integration into Cas9YFP-sgRNA vector
TLAP4_sgRNA-Nterm-tag-rv	**AAAAC**AACAGAGCAATTTCGGGAAAC**A**	integration into Cas9YFP-sgRNA vector
TLAP4_Nterm-tag-donor-fw	CGGGACTTCTCCCTGTGTCTCTCGCGAA AAAACCCTGGGTTCCAAACAGAAATTTT TT**ATGGTGAGCAAGGGCG**	PCR amplification of the repair template
TLAP4_Nterm-tag-donor-rv	CATTTTGCAGAGATGTCCACTGCGTTCC ATAAAAAATTTCCCGAAATTG**CCCTTGT ACAGCTCGTCCATGC**	PCR amplification of the repair template
TLAP4_5UTR-fw	GGTTTCAACGCTTCTTCTTCG	genotyping
TLAP4_internal-rv	CTACATCGAAGAATGCCACCT	genotyping

Table 3.14 Oligonucleotides to generate the endogenous tagged line of VPS31

Name	Sequence	Purpose
VPS31_sgRNA-Cterm-tag-fw	**AAGTT**GCGAGACTAAGCGAGAGACC**G**	integration into Cas9YFP-sgRNA vector
VPS31_sgRNA-Cterm-tag-rv	**AAAAC**GGTCTCTCGCTTAGTCTCGC**A**	integration into Cas9YFP-sgRNA vector
VPS31_Cterm-tag-donor-fw	CCACTGCTGCCGGATTGCCTTTCGAAGA CGAAGGAGAGCAGGAGCGAGAC**GCTA AAATTGGAAGTGGAGG**	PCR amplification of the repair template
VPS31_Cterm-tag-donor-rv	TTGTTTTCCTTCGCGTTCTGTTTCTTTTCC TCTCCCGGGTCTCTCGCTTA**ATAACTTC GTATAATGTATGCTATACG**	PCR amplification of the repair template
VPS31_3UTR-fw	AACTCTTCGACTCTGTTCTCCTTCG	genotyping
VPS31_HA-tag-rv	GGATAGCCAGCGTAGTCCGGG	genotyping

Table 3.15 Oligonucleotides to generate the endogenous tagged line of TGGT1_279360

Name	Sequence	Purpose
TGGT1_279360_sgRNA-Cterm-tag-fw	**AAGTT**GCCGGTTCGCTGTGCGTGCTC**G**	integration into Cas9YFP-sgRNA vector
TGGT1_279360_sgRNA-Cterm-tag-rv	**AAAAC**GAGCACGCACAGCGAACCGGC**A**	integration into Cas9YFP-sgRNA vector
TGGT1_279360_Cterm-tag-donor-fw	TGCTGTTCTGGCTCCACGGCGAGTCGCC ACCGCCTGCTCCTCCAGTAGCC**GCTAAA ATTGGAAGTGGAGG**	PCR amplification of the repair template
TGGT1_279360_Cterm-tag-donor-rv	TGTTGTCAACCTCAGAATGAGCTTGCTG GTTTCCCGGTTCGCTGTGCGTG**ATAACT TCGTATAATGTATGCTATACG**	PCR amplification of the repair template
TGGT1_279360_internal-fw	CACTCCTTGATGATGCTCGG	genotyping
TGGT1_279360_3UTR-rv	GTAGTTATTGCCCGAGTTGC	genotyping

Table 3.16 Oligonucleotides to generate the endogenous tagged line of TGGT1_321410

Name	Sequence	Purpose
TGGT1_321410_sgRNA-Cterm-tag-fw	**AAGTT**GTCATCTCAGGGAAAGCAGCT**G**	integration into Cas9YFP-sgRNA vector
TGGT1_321410_sgRNA-Cterm-tag-rv	**AAAAC**AGCTGCTTTCCCTGAGATGAC**A**	integration into Cas9YFP-sgRNA vector
TGGT1_321410_Cterm-tag-donor-fw	TTGCATCTTTTGGCGCAGTCCCGACTCT ACACCCTCCCTCCCCGCCGTCT**GCTAAA ATTGGAAGTGGAGG**	PCR amplification of the repair template
TGGT1_321410_Cterm-tag-donor-rv	CAGACGCAGAGGCGACGGAGAGACCC AAGCAGCGACGAAAACATCCCAGC**ATA ACTTCGTATAATGTATGCTATACG**	PCR amplification of the repair template
TGGT1_321410_internal-fw	CTCGGCCCTGCCGCACCATG	genotyping
TGGT1_321410_3UTR-rv	CATGCGTAGCTCTGCGACTTC	genotyping

Table 3.17 Sequencing primer for Cas9YFP-sgRNA vectors

Name	Sequence	Purpose
Sequencing_Cas9YFP-pU6-sgRNA-tracrRNA-vector	CCTTCGAACTCTCGAATGTC	Sequencing of Cas9YFP-sgRNA vectors

3.7 sgRNAs

Table 3.18 Sequences and binding positions within the genome of all sgRNAs generated in this study

Name	start position within genome	Sequence	PAM
TgUNC1_sgRNA-Cterm-tag	2 bp upstream of STOP (revcom)	ACTTGCCAGCCGGTGATTCC	AGG
TgUNC1_sgRNA-Upstr-LoxP	3 bp upstream of START (revcom)	GAAGACAAAGATTGCAAAAC	CGG
TgSLP2_sgRNA-Cterm-tag	11 bp downstream of STOP (revcom)	CTATTCGAACTCTAGTTAGC	TGG
TgSLP2_sgRNA-Upstr-LoxP(1)	8 bp downstream of START (revcom)	GCAGGCATCCCGCCCCCTCT	GGG
TgSLP2_sgRNA-Upstr-LoxP(2)	681 bp upstream of START, outside of 5UTR	CCGCTTCTTCCTTATCTTCT	CGG
TgSLP2_sgRNA-Upstr-LoxP(3)	1825 bp upstream of START, upstream of TGGT1_207110 (revcom)	GTTCAGCTGTGAATGTCAGC	TGG
TgSLP2_sgRNA-internal-LoxP	174 bp downstream of START	AGAGAGGGATCGAAAAGTGG	AGG
TgSLP2_sgRNA-Cterm-U1-silencing	1978 bp downstream of STOP	TTTCTATTGCCCGCTAGTAC	AGG
TgSLP1_sgRNA-Cterm-tag	14 bp downstream of STOP (revcom)	TTTCTGGGCATGCCTAGTTG	AGG
TgSLP1_sgRNA-UpstrLoxP	8 bp upstream of START (revcom)	GTTTCTGGCTGCTCTGAGCA	CGG
VPS31_sgRNA-Cterm-tag	10 bp upstream of STOP	GCGAGACTAAGCGAGAGACC	CGG
TLAP4_sgRNA-Nterm-tag	6 bp upstream of START	TTTCCCGAAATTGCTCTGTT	TGG
TGGT1_279360_sgRNA-Cterm-tag	14 bp downstream of STOP	CCGGTTCGCTGTGCGTGCTC	GAA
TGGT1_321410_sgRNA-Cterm-tag	75 bp downstream of STOP	TCATCTCAGGGAAAGCAGCT	GGG

3.8 Antibodies

Table 3.19 Antibodies used in this study

Antibody	Species	Dilution	Reference
Aldolase	Rabbit	1:2000	Sibley, L. D.
Centrin1	Mouse	1:1000	Sigma 04-1624
GAP45	Rabbit	1:5000	Soldati, D.
GFP	Mouse	1:1000	Roche 11814460001
GRA1	Mouse	1:500	Biotem Bio.018.4
HA	Rat	1:1000	Roche 11867423001

IMC1	Mouse	1:1000	Ward, G.
MIC2	Mouse	1:500	Carruthers, V.
MIC8	Rabbit	1:500	Soldati, D.
ROP2,4	Mouse	1:500	Dubremetz, J. F.
TOM40	Rabbit	1:2000	van Dorreen, G.
AlexaFluor 350 goat-anti-rabbit	Goat	1:5000	Invitrogen A-11046
AlexaFluor 488 goat-anti-mouse	Goat	1:5000	Invitrogen A-11001
AlexaFluor 594 goat-anti-mouse	Goat	1:5000	Invitrogen A-11005
AlexaFluor 488 goat-anti-rabbit	Goat	1:5000	Invitrogen A-11008
AlexaFluor 594 goat-anti-rabbit	Goat	1:5000	Invitrogen A-11012
AlexaFluor 488 goat-anti-rat	Goat	1:5000	Invitrogen A-11006
IRDye680RD goat-anti-rabbit	Goat	1:1000	LI-COR 026-68071
IDRye800CW goat-anti-rat	Goat	1:1000	LI-COR 926-32219
IDRye800CW goat-anti-mouse	Goat	1:1000	LI-COR 926-32210
Streptavidin AlexaFluor 488 conjugate		1:1000	Invitrogen S11223
Streptavidin AlexaFluor 594 conjugate		1:1000	Invitrogen S11227

3.9 Plasmids

Table 3.20 Plasmids used in this study

Plasmid	Purpose	Reference
GRASP-RFP	Transient expression, marks cis-Golgi	Pfluger et al., 2005
GalNac-YFP	Transient expression, marks trans-Golgi	Nishi M., 2008 (unpublished)
H2B-mRFP	Transient expression, marks nucleus	Gubbels et al., 2006
ptubmCherryFR-TgTubA1	Transient expression, marks α-tubulin	Hu et al., 2002b
Pmorn1YFP-MORN1	Transient expression, marks MORN1	Gubbels et al., 2006
Tub-Cas9YFP-pU6-ccdB-tracrRNA	sgRNA cloning for CRISPR/ Cas9	Meissner M., Jiménez-Ruiz, E. (unpublished)
puC19-3xHA_LoxP_ddmyCGFP	PCR amplification of the template DNA for stable tagged lines	Meissner M., Singer M. (unpublished)
puC19-mCherry-LoxP	PCR amplification of the template DNA for stable tagged lines	Meissner M., Singer M. (unpublished)
puC19-sYFP2-LoxP	PCR amplification of the template DNA for stable tagged lines	Meissner M., Singer M. (unpublished)
pGEM-LIC-TurboID-stop-LoxP	PCR amplification of the template DNA for stable tagged lines	Meissner M., Singer M. (unpublished)
pGEM-mAID-3HA-T2A-HX	PCR amplification of the template DNA for stable tagged lines	Meissner M., Gow M. (unpublished)
pDHFR-Chromobody-GreenemeraldFP-NoseI	Transient expression, marks F-actin	Periz et al., 2017

3.10 Cells

3.10.1 Mammalian cells

Human Foreskin Fibroblasts (HFF, SCRC-1041) were purchased from LGC/ ATCC and used as monolayers to maintain and for experiments with *T. gondii* tachyzoites.

3.10.2 Bacteria strains

For generation and replication of plasmids, DH5α Competent *Escherichia coli* (High Efficiency) bacteria were purchased from New England Biolabs (NEB; C2987I) and multiplied by using a protocol based on rubidium chloride (Green & Rogers, 2013; section 4.1.12).

3.10.3 *Toxoplasma gondii* strains

Table 3.21 *T. gondii* strains used and generated in this study

***T. gondii* strain**	**Reference**
RH-Δ*ku80*-DiCre	Andenmatten et al., 2013
RH-Δ*ku80*-CbEmerald	Periz et al., 2017
RH-Δ*ku80*-DiCre-LoxP-*TgUNC1*-3xHA-LoxP	This study
RH-Δ*ku80*-DiCre-Δ*TgUNC1*	This study
RH-Δ*ku80*-DiCre-LoxP-*TgSLP2*-3xHA-LoxP	This study
RH-Δ*ku80*-DiCre-LoxP-*TgSLP1*-sYFP2-LoxP	This study
RH-Δ*ku80*-DiCre-LoxP-*TgSLP1*-sYFP2-LoxP-mCherry-*TLAP4*	This study
RH-Δ*ku80*-DiCre-LoxP-*TgSLP1*-sYFP2-LoxP-*VPS31*-3xHA	This study
RH-Δ*ku80*-CbEmerald-*TgSLP1*-mCherry	This study
RH-Δ*ku80*-DiCre-LoxP-*TgSLP1*-TurboID	This study
RH-Δ*ku80*-DiCre-*TGGT1_279360*-mCherry	This study
RH-Δ*ku80*-DiCre-*TGGT1_279360*-3xHA	This study
RH-Δ*ku80*-DiCre-LoxP-*TgSLP1*-sYFP2-LoxP-*TGGT1_279360*-3xHA	This study
RH-Δ*ku80*-DiCre-*TGGT1_321410*-mCherry	This study
RH-Δ*ku80*-DiCre-LoxP-*TgSLP1*-sYFP2-LoxP-*TGGT1_321410*-mCherry	This study

4 Methods

4.1 Molecular biology

4.1.1 Cloning of Cas9YFP-sgRNA-tracrRNA constructs

To endogenously tag genes in *T. gondii,* genome editing via CRISPR/ Cas9 described by Stortz et al. in 2019 was used. To generate sgRNA plasmids for specific cleavage of DNA, sgRNAs were designed using the EuPaGDT software (Peng & Tarleton, 2015) and cloned into a pU6-DHFR vector coding for nuclear Cas9YFP expression (Fig. 4.1; Cas9YFP-pU6-ccdB-tracrRNA) via endonuclease digestion with BsaI, primer annealing and standard ligation as previously described (Curt-Varesano et al., 2016). Both the undigested backbone vector and the final vector with inserted sgRNA are shown in Figure 4.1.

The sgRNAs should meet certain requirements (20nt length, PAM on 3'end, NGG as PAM sequence), which can be set automatically using the software parameter SpCas9. To minimise potential off-target cutting, a BLAST search of the chosen sgRNA was performed. All experiments were made using the *Toxoplasma gondii* GT1 genome (Gajria et al., 2008) and only sgRNAs with the less potential off-targets were selected. To ensure proper integration of the sgRNA into the Cas9YFP plasmid, the following sequences were added to the previously designed sgRNA.

Forward primer: **AAGTT**-sgRNAsequence-**G**

Reverse primer: **AAAAC**-reverse-complement-sgRNAsequence-**A**

Both sgRNA sequences must not contain the PAM. If the respective sgRNA does not have a **G** or **A** at the beginning, an additional **G** must be added to the forward primer and consequently a **C** to the reverse primer. Sequences of all sgRNAs used in this study are listed in section 3.7.

A

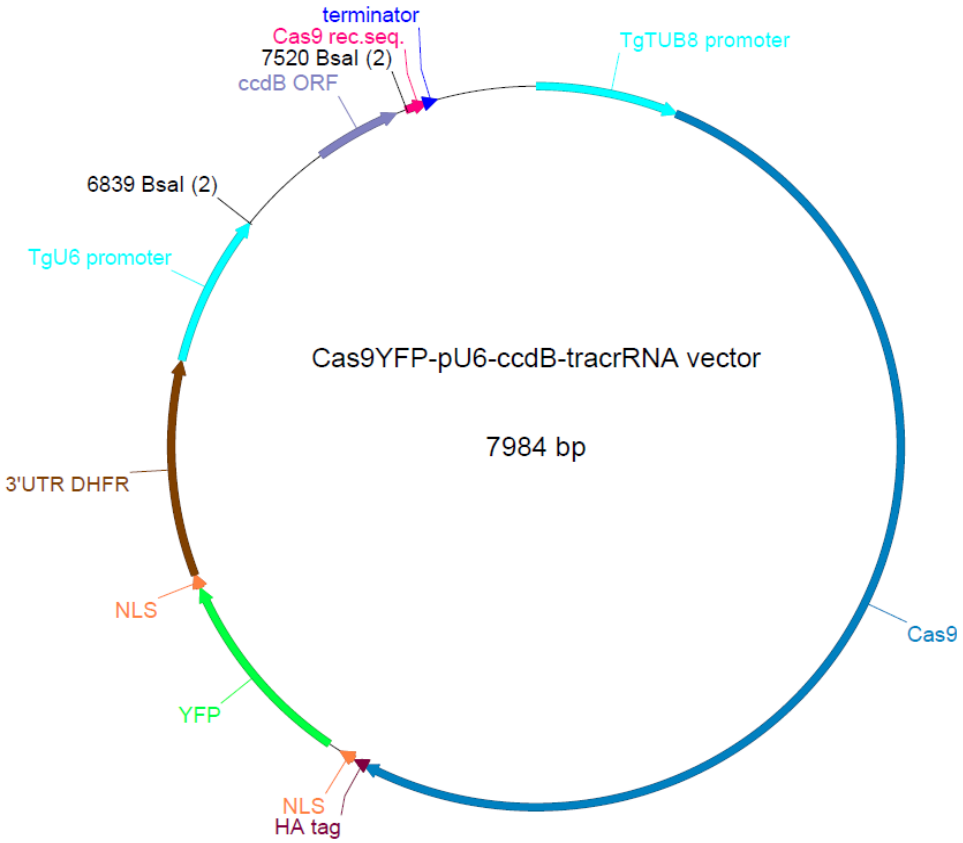
terminator
Cas9 rec.seq.
7520 BsaI (2)
ccdB ORF
TgTUB8 promoter
6839 BsaI (2)
TgU6 promoter
Cas9YFP-pU6-ccdB-tracrRNA vector
7984 bp
3'UTR DHFR
NLS
Cas9
YFP
NLS
HA tag

B

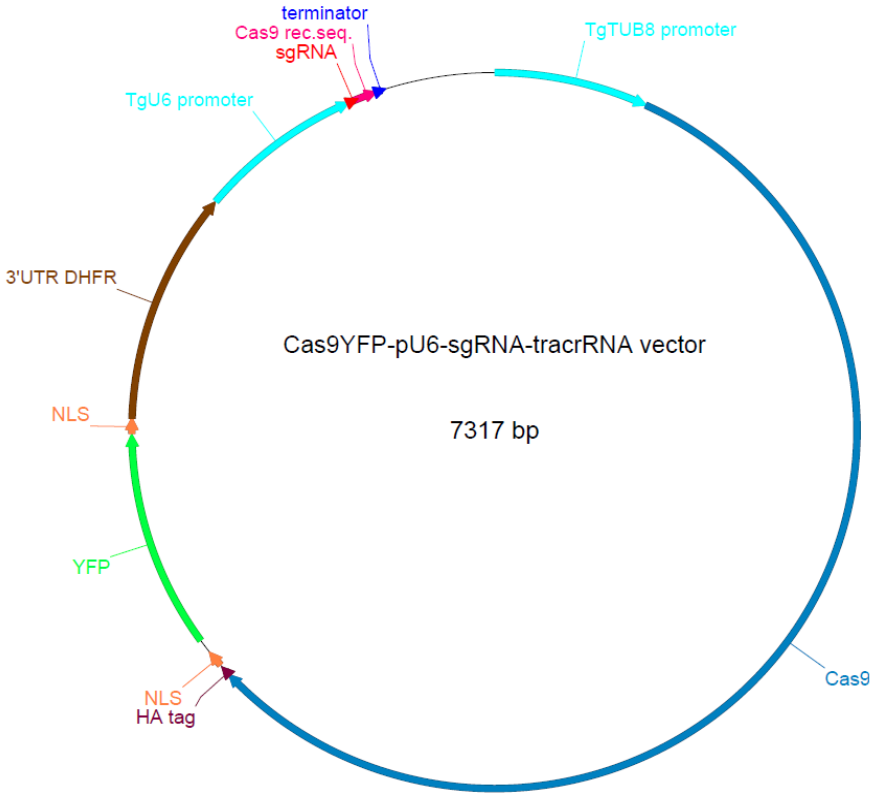
terminator
Cas9 rec.seq.
sgRNA
TgTUB8 promoter
TgU6 promoter
3'UTR DHFR
Cas9YFP-pU6-sgRNA-tracrRNA vector
7317 bp
NLS
YFP
Cas9
NLS
HA tag

Fig. 4.1 Plasmid maps of Cas9YFP-sgRNA-tracrRNA constructs
(A) The Cas9YFP-pU6-ccdB-tracrRNA vector was used as backbone for all sgRNA constructs created in this study to endogenously tag genes using CRISPR/ Cas9. The C-terminal HA-NLS-YFP-NLS tagged Cas9 expression unit is under the control of the *Toxoplasma* TUB8 promoter and the single guide RNA (sgRNA) cloning site is fused to the Cas9 recognition sequence, controlled by the *Toxoplasma* U6 promoter. The restriction sites BsaI was used to linearise the plasmid for cloning. (B) Map of the final vector including the sgRNA for genome editing using CRISPR/ Cas9. Plasmid maps were created using ApE- A plasmid Editor (Davis & Jorgensen, 2022).

4.1.2 Polymerase chain reaction

A polymerase chain reaction (PCR) was performed to amplify DNA fragments for molecular cloning and to test genetically modified *T. gondii* parasite strains for correct DNA integration. Reactions to generate repair templates for genetic manipulation were performed with a Q5 High-Fidelity DNA Polymerase (NEB) due to its ultra-low error rates. To test clones for correct tag integration, One*Taq* polymerase (NEB) was used. All oligonucleotides were synthesised by Thermo Fisher Scientific (listed in section 3.6). Mixture preparation and thermal profiles are shown in Tables 4.1 and 4.2. Reactions were performed with an Eppendorf EP Gradient Mastercycler. For molecular cloning and sequencing, PCR samples were cleaned using the EXTRACTME DNA CLEAN-UP & GEL-OUT KIT (Blirt).

Table 4.1 Preparation of the PCR mix using Q5 polymerase or One*Taq* polymerase

Q5 polymerase			**One*Taq* polymerase**	
Component	**Volume [µL]**		**Component**	**Volume [µL]**
5x Q5 reaction buffer	5		5x One*Taq* Standard buffer	5
10 mM dNTP mix (NEB)	0.5		10 mM dNTP mix (NEB)	0.5
25 ng template DNA	0.5		template DNA	0.5
10 µM primer fw	1.25		10 µM primer fw	1.25
10 µM primer rv	1.25		10 µM primer rv	1.25
Q5 DNA polymerase (NEB)	0.25		One*Taq* DNA polymerase (NEB)	0.125
ddH_2O	up to 25		ddH_2O	up to 25

Table 4.2 Thermic profile of the PCR reactions using Q5 polymerase or OneTaq polymerase

Q5 polymerase			**One*Taq* polymerase**	
Temperature [°C]	**Time [sec]**		**Temperature [°C]**	**Time [sec]**
98	120		95	30
98	15		95	30
50-72*	30	35x	50-68*	30	30x
72	30/kb**		68	30/kb**
72	120		68	300
4	∞		4	∞

*calculated based on the respective melting temperature of the primer using the TmCalculator from NEB (version 1.13.1)

** calculated based on the size of the amplified DNA fragment

4.1.3 Restriction digest

To integrate DNA fragments into a plasmid, it must be digested with restriction endonucleases. In this study, this method was used to integrate sgRNAs into the Cas9YFP-pU6-ccdB-tracrRNA vector. 5 µg of Cas9YFP vector were mixed with 5 µL of rCutSmart buffer (NEB), 1 µL of BsaI-HFv2 (NEB) and made up to 50 µL reaction with ultrapure water. The digest was incubated at 37°C for 2 hours and purified by agarose gel electrophoresis.

4.1.4 Agarose gel electrophoresis

Agarose gel electrophoresis was used to verify the correct size of the amplified DNA fragments or to separate and purify digested plasmid fragments. To prepare agarose gels, 0.8% agarose (Biozym) was mixed with 1x TAE (Roth) buffer and boiled in the microwave until the agarose powder was completely dissolved. As a reference, 3 µL of 250 bp DNA ladder (Roche) or 1 kb plus DNA ladder (NEB) were loaded next to the samples.

To verify the correct size of PCR reactions for molecular cloning or to test genetically modified parasite clones, 1 µL of PCR reaction was mixed with 6x purple loading dye (NEB), pipetted into the wells of a 0.8% agarose gel and separated with an electrophoresis chamber (Thermo Fisher Scientific), filled with 1x TAE buffer at 120 V for 20-40 minutes. To analyse the DNA with UV light, 1-2 µL of GelRed (Biotium) were added to the gel and visualised with a UV transilluminator.

To purify the digested plasmid fragments, 50 µL of the digestion reaction were pipetted onto a 0.8% agarose gel supplemented with 4-6 µL Midori Green DNA stain (NIPPON Genetics), separated by electrophoresis at 120 V for around 30 minutes and visualised with a blue light transilluminator (NIPPON Genetics). The fragment with expected size was cut from the gel with a scalpel and purified using the EXTRACTME DNA CLEAN-UP & GEL-OUT KIT (Blirt).

4.1.5 Annealing of Oligonucleotides

For the construction of Cas9YFP-pU6-sgRNA-tracrRNA plasmids, 1 µM of each forward and reverse primer was mixed with annealing buffer (Table 3.4) to a volume of 20 µL, heated to 95°C for 5 minutes and slowly allowed to cool to room temperature.

4.1.6 Ligation

A ligation reaction was performed to integrate the sgRNA sequences into the Cas9YFP vector. 25-50 ng of the digested vector was mixed with 1 µL annealed primers, 1 µL T4 DNA ligase buffer, 1 µL T4 DNA ligase (NEB) and ultrapure water to a total volume of 10 µL and incubated for 1 hour at room temperature or overnight at 16°C.

4.1.7 Transformation into DH5α *Escherichia coli*

Ligation reactions or plasmids from an existing stock were transformed into chemically competent DH5α *Escherichia coli* bacteria (NEB). Chemically competent bacteria (stored at -80°C) were thawed on ice, mixed with 10 µL ligation reaction or 25-50 µg plasmid and incubated on ice for 30 minutes. After a heat shock at 42°C for 30 seconds, followed by incubation on ice for 2 minutes, 400 µL of LB-medium (Table 3.6) were added and the sample was incubated on a shaker for 1-2 hours at 37°C. To reduce the volume, bacterial cells transformed with ligation reactions were centrifuged at 1500 g for 2 minutes, plated onto LB-agar plates (Table 3.6) supplemented with 100 µg mL^{-1} ampicillin (Sigma) and incubated overnight at 37°C. Single bacterial colonies plated on LB-agar after transformation were picked

up with a sterile pipette tip and incubated with shaking overnight at 37°C in 3 mL liquid LB-medium supplemented with 100 µg mL^{-1} ampicillin.

4.1.8 Isolation of plasmid DNA from *E. coli*

To isolate plasmid DNA from *E. coli* bacteria, a plasmid miniprep was prepared using the EXTRACTME PLASMID MINI KIT (Blirt) according to the manufacturer's manual.

4.1.9 Measuring of nucleic acid concentration

Concentrations of plasmid DNA were determined using the nanodrop (Thermo Fisher Scientific) according to the instructions of the manufacturer.

4.1.10 DNA sequencing

All newly generated plasmids and parasite strains were sequenced by Eurofins Genomics. For this purpose, 20-50 ng of plasmid or 30 µL of purified PCR product of the respective genomic locus in the newly generated parasite strain were sent to the company. 10 µL of 10 µM sequencing primers were sent separately. All primers used for sequencing are listed in section 3.6.

4.1.11 Isolation of genomic DNA from *T. gondii*

Two different methods were used to isolate genomic DNA from *T. gondii*.

To screen multiple clones for correct genomic integration, 50 µL of parasites (that naturally lysed the host cells) were pelleted at high speed for 5 minutes, the pellet was resuspended in 18 µL elution buffer and 2 µL proteinase K from the EXTRACTME GENOMIC DNA KIT (Blirt), incubated at 50°C for 1 hour, boiled at 95°C for 10 minutes and used as template for PCR (1 µL).

For proper verification of clones, genomic DNA was isolated from 300 µL parasites (that naturally lysed the host cells) using the EXTRACTME GENOMIC DNA KIT (Blirt) according to the manufacturer's instructions.

4.1.12 Preparation of chemically competent DH5α *E. coli*

To generate chemically competent *E. coli* bacteria, a previously described protocol was used (Green & Rogers, 2013). DH5α competent *E. coli* bacteria (NEB) were spread onto LB-agar plates (Table 3.6) and grown overnight. A single colony was picked the next day and grown overnight in 5-10 mL LB-medium (Table 3.6). 400 mL of LB-medium were inoculated with 1 mL of the overnight culture and grown for several hours at 37°C to a density of 0.5 OD_{595} with constant shaking. The culture was chilled on ice for 15 minutes, divided into 200 mL aliquots and centrifuged at 4500 g for 10 minutes at 4°C. After removing the supernatant, the bacterial pellets were resuspended in each 160 mL of chilled transformation buffer I (TfbI, Table 3.6) and kept on ice for 15 minutes. After centrifugation for 5 minutes at 2000 g at 4°C, the pellets were resuspended in each 16 mL of chilled transformation buffer II (TfbII, Table 3.6) and aliquoted (100 µL) on dry ice and immediately frozen in liquid nitrogen and stored at -80°C until use.

4.2 Cell biology

4.2.1 Culturing of mammalian cells

Human foreskin fibroblasts (HFFs, ATCC) were cultured at 37°C and 5% CO_2 in a humidified incubator (Thermo Fisher Scientific). Cells were maintained and cultured in Dulbecco's modified Eagle's medium (DMEM, Sigma) supplemented with 10% fetal bovine serum (FBS, BioSell), 4 mM L-glutamine (Sigma) and 25 µg mL^{-1} gentamycin (Sigma) in 6 cm TPP tissue culture dishes (Faust). The cells were split weekly at a ratio of 1:3 to 1:4 using trypsin-EDTA solution (Sigma) to detach cells from the culture flasks into new flasks, dishes or well plates, depending on the experiment.

4.2.2 Culturing of *T. gondii* parasites

To maintain RH *T. gondii* parasites (type I), recently lysed extracellular tachyzoites were passed to confluent HFF monolayers. To pass intracellular parasites, HFFs infected with parasites were separated from the bottom of the culture dish using a cell scraper, and parasites were released from the host cells by syringing the solution 2-3 times through a 26G needle gauge. The volume of the parasites transferred was adjusted according to the experiment.

4.2.3 Transfection of *T. gondii*

4.2.3.1 Preparation of DNA

In order to generate tagged or floxed parasite strains using CRISPR/ Cas9, the respective sgRNA-Cas9YFP plasmid for each targeted gene must be transfected together with a repair template. 10-20 µg of plasmid DNA were mixed with 5 µL oligonucleotide (100 µM, for LoxP integration) or with a PCR product (purified with the EXTRACTME DNA CLEAN-UP & GEL-OUT KIT, Blirt) for tagging. To precipitate the DNA, 300 mM sodium acetate and 3 volumes of 100% ethanol were added and after freezing the sample at -80°C for at least 20 minutes, it was pelleted at 0°C at maximum speed for 1 hour. The pellet was washed twice with 70% ice-cold ethanol, centrifuged for 20 minutes and dried in a sterile hood for 10 minutes.

4.2.3.2 Stable transfection

To generate stable parasite lines, parasites were transfected in an Amaxa 4D-Nucleofector system (Lonza) with a P3 Primary cells 4D-Nucleofector X kit L (Lonza). Freshly lysed parasites or mechanically released (as described in 4.2.2) intracellular parasites of the respective strains were used for transfections. $1x10^6$ - $1x10^7$ parasites of each strain were centrifuged for 5 minutes at 1500 g and the pellet was resuspended in 100 µL P3 buffer and mixed with previously prepared DNA. The programme FI-158 was used for electroporation. Transfected parasites were resuspended in fresh DMEM and added onto confluent HFF cells.

4.2.3.3 Transient transfection

To transiently transfect parasites, $1x10^6$ - $1x10^7$ freshly lysed or manually released parasites of the respective strain were pelleted for 5 minutes at 1500 g, resuspended in 100 µL P3 buffer and mixed with 5-10 µg of ethanol-precipitated plasmid DNA. Parasites were electroporated as described in 4.2.3.2 and transferred to HFF cells grown on coverslips in 24-well plates. When indicated, parasites were induced directly by the addition of 50 nM rapamycin (Sigma). An equal amount of dimethyl sulfoxide (DMSO, Roth) was added to all controls (not induced). After 24-48 hours, transiently transfected parasites were fixed with 4% paraformaldehyde (PFA, Science services) at room temperature for 30 minutes and prepared for microscopy (see section 4.3.2).

4.2.4 Isolation of *T. gondii* clones with FACS sorting

The transfected parasites to generate stable lines were enriched using fluorescence-activated cell sorting (FACS) based on their nuclear Cas9YFP signal. 24 to 48 hours after transfection (described in section 4.2.3.2), parasites were checked for nuclear Cas9YFP expression using a fluorescence microscope and mechanically released from the host cells. Therefore, the host cell layer was detached from the dish with a cell scraper, parasites were released from the host cells by syringing the suspension twice through a 26G needle gauge, and the parasites were separated from host cell debris by filtering the suspension through a 3 µm filter. Transiently Cas9YFP-expressing parasites were sorted into 96-well plates containing confluent layers of HFFs using a FACSAria III Cell Sorter (BD Biosciences). 5-10 fluorescent events were sorted per well. After at least 5 days of incubation, the 96-well plates were screened for single plaques and checked for genomic integration of the respective tag using PCR.

4.2.5 Cryopreservation of *T. gondii* strains

For long-term storge of generated *T. gondii* parasite lines, HFF cells were infected with 300 µL of freshly egressed parasites and incubated for 24 to 48 hours to generate large intracellular vacuoles. Media was removed and 500 µL of fresh DMEM were added to the infected host cell monolayer. The cells were carefully removed from the culture dish with a cell scraper, mixed

gently with 500 µL of 2x freezing media containing DMEM supplemented with 30% FBS and 20% DMSO and transferred to a 1.5 mL cryotube and immediately frozen at -80°C. Samples were transferred to liquid nitrogen tanks for long-term storage.

Cryopreserved parasites were thawed at 37°C for 5 minutes and immediately transferred to fresh confluent HFF cells. After 24 hours incubation, the medium was changed and the parasites were maintained as previously described.

4.3 Phenotypic characterisation

4.3.1 Plaque assay

Growth assays were performed using a 6-well plate; HFF cells were infected with $1x10^3$ parasites per well and incubated for 7 days either with 50 nM rapamycin (induced) or DMSO (not induced). After removal of the medium, the cells were gently washed with PBS, fixed with 1 mL ice-cold methanol for 20 minutes, washed with PBS and stained with Giemsa solution (Roth, diluted 1:20 in ddH_2O) for 1 hour with shaking. After washing once with PBS, the plates were allowed to dry and photographed with a standard digital camera.

4.3.2 Immunofluorescence assay (IFA)

Immunofluorescence analysis was performed to determine the subcellular localisation of proteins. For this purpose, infected HFF monolayers grown on coverslips were fixed with 4% PFA at room temperature for 30 minutes. Samples were washed with PBS, blocked and permeabilised for 30 minutes using 2% bovine serum albumin (BSA, Sigma) and 0.2% Triton X-100 (Sigma) in PBS. Antibody labelling was performed using the indicated combinations of primary antibodies for 1 hour, followed by incubation with secondary antibodies for 1 hour. All antibodies and concentrations used in this study are listed in section 3.8. Antibody incubations were performed in a wet chamber (a petri dish containing a wet paper towel) and protected from light. Insight the wet chamber, each coverslip was placed upside down on top of 20 µL of antibody diluted in PBS containing 2% BSA and 0.2% TX-100 solution on parafilm. Three washes in PBS were performed between antibody incubations. When indicated, the nucleus was stained with 1 µg mL^{-1} Hoechst 33342 (Thermo Fisher Scientific) in PBS for 10

minutes. Coverslips were mounted on microscope slides with ProLong Gold Antifade Mountant (Thermo Fisher Scientific) and allowed to dry at room temperature prior to microscopy. Slides were stored at 4°C without light.

To image extracellular parasites, glass bottom dishes were coated with 0.1% poly-L-lysine (Sigma) for 30 minutes, washed twice with ultrapure water and allowed to dry in a sterile hood. Intracellular parasites were mechanically released from the host cells by removing the host cell layer from the culture plate, syringing the solution twice through a 26G needle gauge, and filtering the parasites though a 3 µm filter to remove the host cell debris. The released parasites were added on the prepared glass bottom dish and left for 30 minutes to settle. After this time, the extracellular parasites were fixed with 4% PFA for 30 minutes and immunofluorescence assay was performed as described previously.

4.3.3 Microscopy

All microscopy images and movies were acquired on a Leica DMi8 widefield microscope with Leica Application Suite X (Las X, v.3.4.2.183668) and processed with Fiji software (v.1.53c; Schindelin et al., 2012). Time-laps video microscopy was performed using glass bottom dishes in a closed chamber to maintain culture conditions (37°C and 5% CO_2). The Pearson correlation coefficient R was calculated using the ImageJ plugin JACoP (LGPLv3; Bolte & Cordelières, 2006).

4.3.4 Cell cycle arresting drugs

Parasites were arrested in G1-phase using 80 µM pyrrolidine dithiocarbamate (PDTC, Sigma) or in S-phase using 300 µM hydroxyurea (HU, Sigma). Parasites were preincubated on coverslips in 24-well plates for 24 hours and treated with PDTC, HU or DMSO as control. After 6 hours, cells were fixed with 4% PFA followed by immunofluorescence assay (section 4.3.2). 100 vacuoles per condition were counted for TgSLP1 expression. The experiment was carried out in biological and technical triplicates.

4.3.5 Actin remodelling compounds

Parasites were incubated with either 0.1 µM or 0.2 µM jasplakinolide (Jas, Santa Cruz Biotechnology, Inc.) or 0.5 µM cytochalasin D (cytD, Sigma) for 1 hour at 37°C. Afterwards, the parasites were fixed using 4% PFA followed by immunofluorescence assay (section 4.3.2).

4.4 Protein biochemistry

4.4.1 Preparation of *T. gondii* cell lysates

For protein detection by immunoblot analysis, parasites were cultured for 72 hours on HFFs and induced with 50 nM rapamycin 24 hours post infection when indicated. $1x10^6$ parasites per line and condition were pelleted at 4°C and 1500 g for 5 minutes, washed in cold PBS, briefly frozen at -80°C, mixed with 10 µL of orange loading dye (Table 3.7) and 0.1 M DTT (Sigma), boiled at 100°C for 10 minutes and briefly centrifuged.

4.4.2 Sodium dodecyl sulphate polyacrylamide gel electrophoresis (SDS PAGE)

Proteins from the prepared samples were separated according to their size using sodium dodecyl sulfate polyacrylamide gel electrophoresis (SDS PAGE; Laemmli, 1970). Either 4-20% precast polyacrylamide minigels (BioRad) or home-made gels consisting of 12% resolving gel and 5% stacking gel (see table 4.3) were used for SDS PAGE. Tetramethylenediamine (TEMED; BioRad) and ammonium persulfate (APS; BioRad) were used to catalyse the gel polymerisation and added to the mix just prior to casting the gels.

Table 4.3 Preparation of polyacrylamide gels

	resolving gel	**stacking gel**
30% Acrylamide/ Bis solution (37.5:1) (Serva)	12%	5%
Tris-HCl pH 8.8	375 mM	-
Tris-HCl pH 6.8	-	63 mM
10% SDS	0.1%	0.1%
10% APS	0.1%	0.1%
TEMED	0.04%	0.1%

The gel was clamped into an electrophoresis chamber, filled with 1x running buffer (Table 3.7) and the prepared samples were loaded onto the gel along with 3 µL Chameleon Duo pre-stained protein ladder (LI-COR Biosciences). Voltage was applied (120 V) for about 2 hours until the samples had completely passed through the gel.

4.4.3 Western blotting

The separated proteins were transferred from the polyacrylamide gel to a nitrocellulose membrane (Amersham Protran, pore size 0.45 µm) using a wet transfer. For this purpose, the gel and the membrane were stretched in transfer buffer (Table 3.7) between two sponges and two sets of three whatman filter papers (Millipore) in a blotting chamber (BioRad) filled with ice-cold, 1x transfer buffer (Table 3.7) and a current of 400 mA was applied for 1 hour. To avoid overheating, the blotting chamber was placed on ice.

To examine the transfer efficiency, the proteins on the membrane were stained with Ponceau S solution (Roth) for 5-10 minutes with shaking and washed once with tap water.

4.4.4 Immunostaining and visualisation

After Ponceau staining, the membrane was blocked with Intercept blocking buffer (LI-COR Biosciences) diluted 1:2 with 1x TBS (Table 3.7) with shaking at room temperature for 1 hour or at 4°C overnight. To detect specific proteins with antibodies, the membranes were incubated in a wet chamber with the respective primary antibody diluted in 500 µL of 1:2 blocking buffer for 1 hour at room temperature. The membranes were then washed three times with 1x TBS and incubated for another 1 hour in a wet chamber with the secondary antibody (IRDye, LI-COR Biosciences) diluted in 500 µL of 1:2 blocking buffer at room temperature. The membranes were again washed three times with 1x TBS and imaged using Odyssey CLx-1849 (LI-COR Biosciences) with LI-COR Image Studio Software. All antibodies used in this study are listed in section 3.8.

4.4.5 Proximity-based labelling of proteins using TurboID

To identify potential interactor proteins of TgSLP1, proximity-dependent labelling with biotin followed by streptavidin pulldown was performed. TgSLP1 was C-terminally tagged with TurboID in RH-Δ*ku80*-DiCre parasites using CRISPR/ Cas9. RH-Δ*ku80*-DiCre parasites were used as wildtype control.

4.4.5.1 Detection of biotinylated proteins via immunofluorescence assay

The biotinylation of proteins was tested by immunofluorescence assay using streptavidin AlexaFluor 488 conjugate. Therefor parasites were incubated without (control) or with 150 µM biotin (Sigma) for 10 minutes, 30 minutes or 4 hours. After the time points, the samples were fixed, stained with the streptavidin conjugate (Invitrogen) and imaged.

4.4.5.2 Parasite collection for western blot analysis and pulldown experiments

To generate late intracellular *T. gondii* vacuoles, HFF cells were heavily infected with tachyzoites of the respective strains and incubated for 24-30 hours at 37°C with 5% CO_2. Intracellular parasites were labelled with 150 µM biotin diluted in DMEM or, as a control, incubated in DMEM without biotin for 4 hours. After incubation, the cell dishes were placed on ice for 5 minutes and thus the following steps were all performed on ice. Parasites were gently washed 2 times with PBS and released from the host cells by scratching the host cell layer from the cell dish bottom and syringing the suspension twice through a 26G needle gauge. The parasites were separated from the host cell remains by filtration through a 3 µm filter, counted and pelleted at 1500 g for 5 minutes at 0°C. The parasite pellet was resuspended in ice-cold PBS and aliquoted to $1x10^6$ parasites for western blot analysis or $3.5x10^7$ for the pulldown experiment.

The samples for pulldown experiments were diluted in 20 µL of RIPA buffer (Table 3.7) supplemented with 1:10 protease and phosphatase inhibitor (Sigma), incubated on ice for 30 minutes, frozen in liquid nitrogen and stored at -80°C until they were used for the pulldown.

4.4.5.3 Pulldown of biotinylated proteins using magnetic streptavidin beads

The frozen parasites were lysed in 1 mL RIPA buffer supplemented with 1:100 protease and phosphatase inhibitor (Sigma) and incubated on ice for 30 minutes. 5% of the sample were collected as an input control. To pull down biotinylated proteins, 100 µL of MyOne Streptavidin Dynabeads T1 (Invitrogen) per sample were placed in 1.5 mL Eppendorf tubes and washed three times in 1 mL PBS using the DynaMag-2 Magnet magnetic rack (Thermo Fisher Scientific). After the final wash, the supernatant was removed from the beads and the parasite samples (digested in RIPA buffer) were added onto the beads. The samples were incubated with the beads at 4°C with shaking for 2.5 hours. Next, the supernatant was removed using the magnetic rack, 5% were collected as flow-through and the beads were washed five times with RIPA buffer without Triton, collecting 5% of the supernatant from the first wash. After the final wash, the beads were stored in 50 µL of RIPA buffer without Triton (5% were separated as eluate for western blot control) and frozen at -80°C until sending them for on-bead digest mass spectrometry. Mass spectrometry was performed by the Glasgow Polyomics facility.

Acetone precipitation of the input, flow-through and first wash was performed by adding 200 µL of ice-cold 100% acetone. Samples were pelleted at 16000 g for 1 hour at 0°C, acetone was removed and 20 µL of 1x orange loading dye supplemented with 0.1 M DTT were added before boiling the samples at 100°C for 10 minutes with shaking. The eluate sample was mixed directly with 10 µL of 1x orange loading dye supplemented with 0.1 M DTT and boiled at 100°C for 10 minutes. The samples were loaded onto an SDS gel and western blot analysis was performed. The samples to observe the levels of biotinylation on the western blot were treated as described in 4.4.1. Protein bands were visualised using IRDye 800CW streptavidin conjugate (LI-COR Biosciences) to detect biotinylated proteins.

5 Results

5.1 Sad1/ UNC family proteins in *T. gondii*

5.1.1 Identification of Sad1/ UNC family proteins in *T. gondii*

The LINC complex connects the nucleus to the cytoskeleton and performs several functions including the movement of the nucleus and maintenance of the centrosome-nucleus connection. In opisthokonts, it is composed of KASH domain proteins and SUN domain proteins (Tapley & Starr, 2013; Padmakumar et al., 2005; Crisp et al., 2006).

Two proteins that contain a SUN domain and one hypothetical protein containing an UNC-50 domain were identified in the genome of *T. gondii* using the ToxoDB.org database (Gajria et al., 2008), making them good candidates for being components of an apicomplexan LINC complex. Based on their domain architecture, they are referred to as TgUNC1 (TGGT1_255270), TgSLP1 for SUN-like protein 1 (TGGT1_250010) and TgSLP2 for SUN-like protein 2 (TGGT1_207120). Based on data resulting from a genome-wide screen of *T. gondii* using CRISPR/ Cas9, disruption of *sad1/ unc* genes causes loss of parasite fitness, indicating that they fulfil crucial roles during the parasite's asexual life cycle (Sidik et al., 2016; Sidik et al., 2018; Fig. 5.1A). Data from a recently published study map the subcellular localisation of thousands of proteins in *T. gondii* using a method called hyperplexed localisation of organelle proteins by isotope tagging (hyperLOPIT). The study localises TgUNC1 with a high probability to the Golgi, whereas TgSLP1 and TgSLP2 most likely localise to the ER (Fig. 5.1A; Barylyuk et al., 2020).

5.1.2 Domain organisation

The two SUN domain proteins show different domain organisations. The SUN domain of TgSLP1 is at the C-terminus whereas in TgSLP2 is located in the middle part of the protein (Fig. 5.1). Both proteins have one predicted transmembrane domain, whereas TgUNC1 possesses multiple predicted transmembrane domains. Similar to SUN domain proteins described in other organisms, TgSLP1 has regions with coiled-coil domains (CCD) (Fig. 5.1B; Jones et al., 2014).

A

Gene ID			Localisation of SUN domain in the gene	Phenotypic score	LOPIT
TGGT1_255270	TgUNC1	hypothetical protein	-	-2.26	Golgi
TGGT1_250010	TgSLP1	Sad1/UNC family protein	C-terminus	-4.52	ER
TGGT1_207120	TgSLP2	Sad1/UNC family protein	middle	-3.86	ER

B

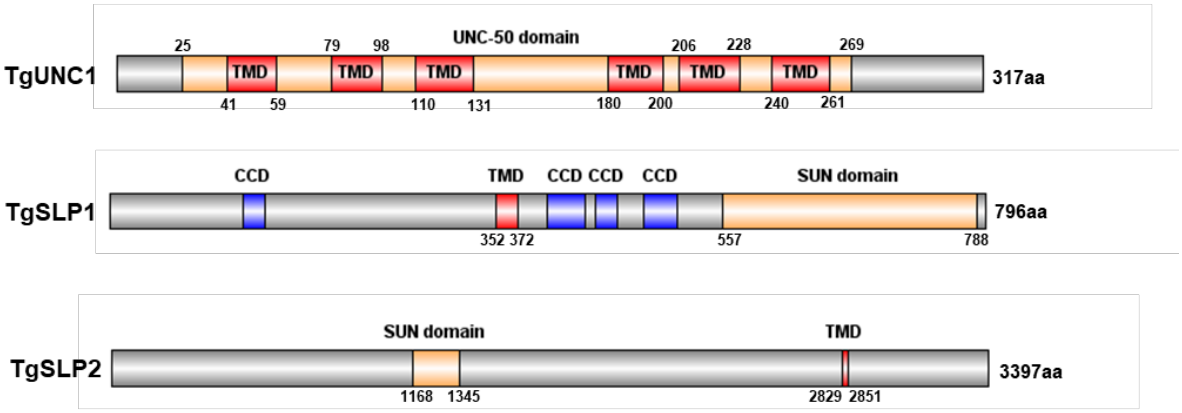

Fig. 5.1 Overview of Sad1/ UNC family proteins in *T. gondii*
(A) Table of Gene IDs, domain organisation, phenotypic score and prediction of subcellular localisation (LOPIT) of Sad1/ UNC family proteins in *T. gondii*. (B) Schematic overview of UNC-50 domain, SUN domain, coiled-coil domain (CCD) and transmembrane domain (TMD) organisation in Sad1/ UNC family proteins in *T. gondii*. Numbers indicate the domain positions in amino acids (aa). The figure was created with the IBS Illustrator for biological sequences (Liu et al., 2015).

5.2 Characterisation of TgUNC1

5.2.1 Generation and analysis of transgenic parasites for TgUNC1

To assess the subcellular localisation of TgUNC1, the gene was C-terminally tagged with an epitope tag (3xHA) using CRISPR/ Cas9 (Stortz et al., 2019) as detailed in the section 4.1. Simultaneously with the endogenous labelling, two LoxP sites, one upstream of the start codon of *unc1* and another downstream of the coding region, were inserted into the genome to create a conditional knockout (cKO) line in parasites expressing dimerisable Cre (DiCre; Andenmatten et al., 2013; Fig. 5.2A). Correct integration of the tag and LoxP sites was confirmed by PCR and sequencing. Efficient Cre-mediated recombination upon addition of

rapamycin was also confirmed by PCR and western blot analysis demonstrated that the protein is undetectable 48 hours post induction (Fig. 5.2).

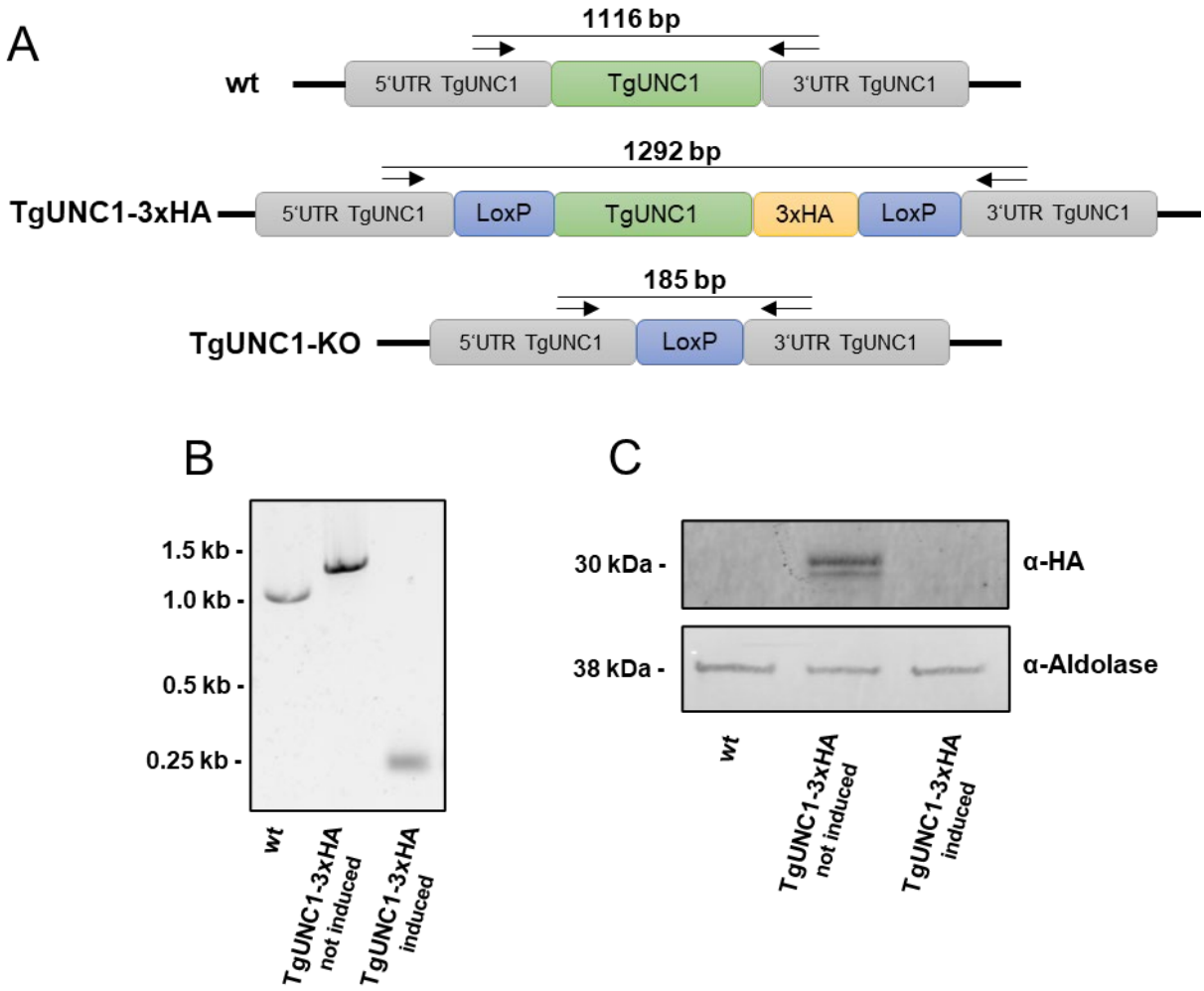

Fig. 5.2 Generation and confirmation of the tagged line and the conditional knockout of TgUNC1
(A) Schematic overview of the TgUNC1 locus before genetic manipulation (endogenous), after C-terminal tagging and integration of LoxP-sites (TgUNC1-3xHA) and upon excision of the gene using DiCre induction (TgUNC1-KO) (B) PCR analysis confirms the correct integration of tags and excision of *unc1* after 48 hours of rapamycin treatment. Primer positions and length of PCR products are indicated in (A). (C) Western blot analysis using α-HA antibody on the wildtype (wt) and not induced or induced TgUNC1-3xHA lines verifies the expected protein size of around 35 kDa and protein depletion under induced conditions. α-Aldolase is used as loading control.

5.2.2 TgUNC1 localises to the Golgi

Immunofluorescence analysis was performed to determine the subcellular localisation of TgUNC1 in *T. gondii* tachyzoites. TgUNC1 localises as a defined structure apical to the nucleus (Fig. 5.3A). Further colocalisation analysis demonstrates that TgUNC1 localises at the Golgi apparatus. To this end, a marker protein of the trans-Golgi network, GalNac (Nishi M., 2008, unpublished; Fig. 5.3B) or the cis-Golgi network, GRASP (Pfluger et al., 2005; Fig. 5.3B) were transiently expressed in the TgUNC1 tagged parasite lines and an IFA was performed. To quantify the degree of colocalisation between the fluorophores, the Pearson correlation coefficient (R) of 20-25 parasites was determined using the ImageJ plugin JACoP (Bolte & Cordelières, 2006). Being close to 1, the Pearson correlation coefficient confirms a good colocalisation of TgUNC1 with the Golgi apparatus of *T. gondii* (Fig. 5.3B).

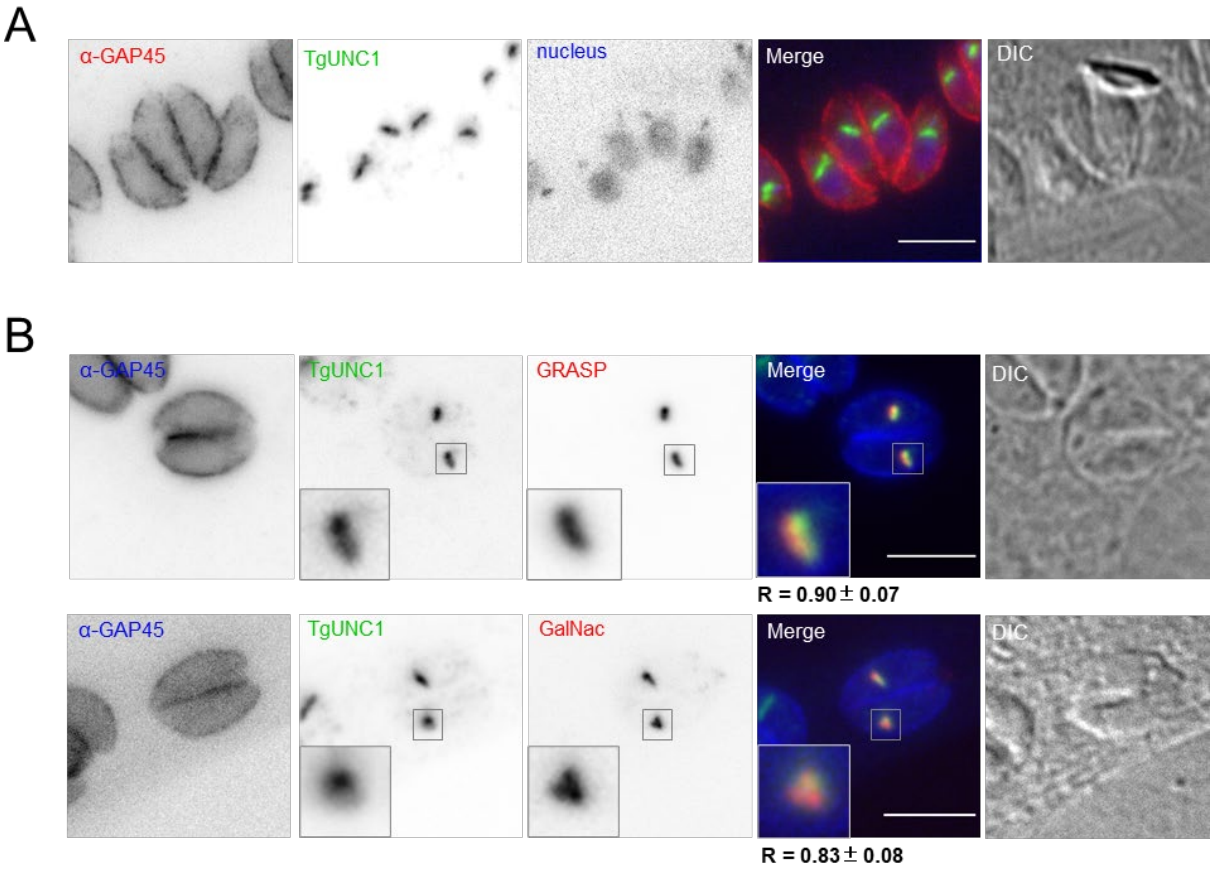

Fig. 5.3 Analysis of the localisation of TgUNC1
(A) Immunofluorescence assay reveals TgUNC1 to localise as a defined structure close to the nucleus. (B) Simultaneous staining of TgUNC1-3xHA with α-HA and transiently expressed, fluorescent tagged markers of the cis- and trans- Golgi network (cis-Golgi: GRASP; trans-Golgi: GalNac) demonstrates a colocalisation between TgUNC1 and the Golgi apparatus. Colocalisation was quantified by calculating the Pearson correlation coefficient (R) of 20-25 parasites using the ImageJ plugin JACoP (Bolte &

Cordelières, 2006). Mean values and standard deviation are shown under the respective images. Parasite shape is visualised with a α-GAP45 antibody, the nuclei are stained with Hoechst in (A). DIC: differential interference contrast, scale bar: 5 µm.

The localisation of TgUNC1 in extracellular parasites seems to be identical to intracellular parasites (Fig. 5.4).

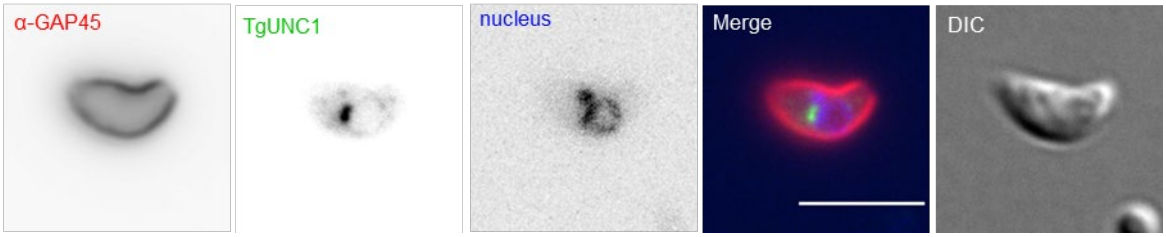

Fig. 5.4 Analysis of the localisation of TgUNC1 in extracellular parasites
Localisation of TgUNC1 in extracellular parasites is comparable to similar like in intracellular parasites. Parasite shape is visualised with a α-GAP45 antibody, the nucleus is stained with Hoechst. DIC: differential interference contrast, scale bar: 5 µm.

5.2.3 TgUNC1 is not essential for parasite growth and organelle morphology

To get a better insight into the function of TgUNC1, the behaviour of the parasite after TgUNC1 loss was observed. With regard to the phenotypic screening by Sidik et al. from 2016, the protein might be important for the fitness of the parasite. Despite the negative score of -2.26, the conditional knockout of *unc1* showed no obvious growth defect, as seen by plaque assay (Fig. 5.5A). Consequently, it was possible to isolate a null mutant of *unc1* after induction of the conditional knockout mutant with rapamycin, that showed neither an obvious growth defect nor any morphological change of the cis- or trans-Golgi in IFA (Fig. 5.5B). Next, organellar markers were used to analyse the morphology of different organelles, such as dense granules, rhoptries, micronemes, apicoplast, the inner membrane complex or the nucleus. Same as with the Golgi apparatus, no abnormalities could be observed (Fig. 5.5C). Consistent with the observation in the western blot, no protein was detectable in the knockout mutant of *unc1* in

the IFAs (Fig. 5.5B). The null mutant of *unc1* was easily kept in cell culture for extended time without the occurrence of any obvious defects.

.

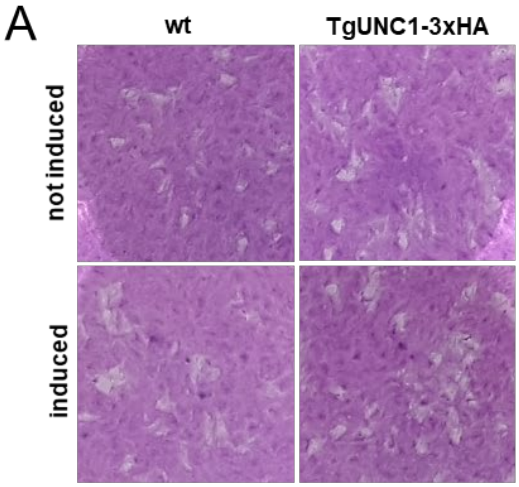

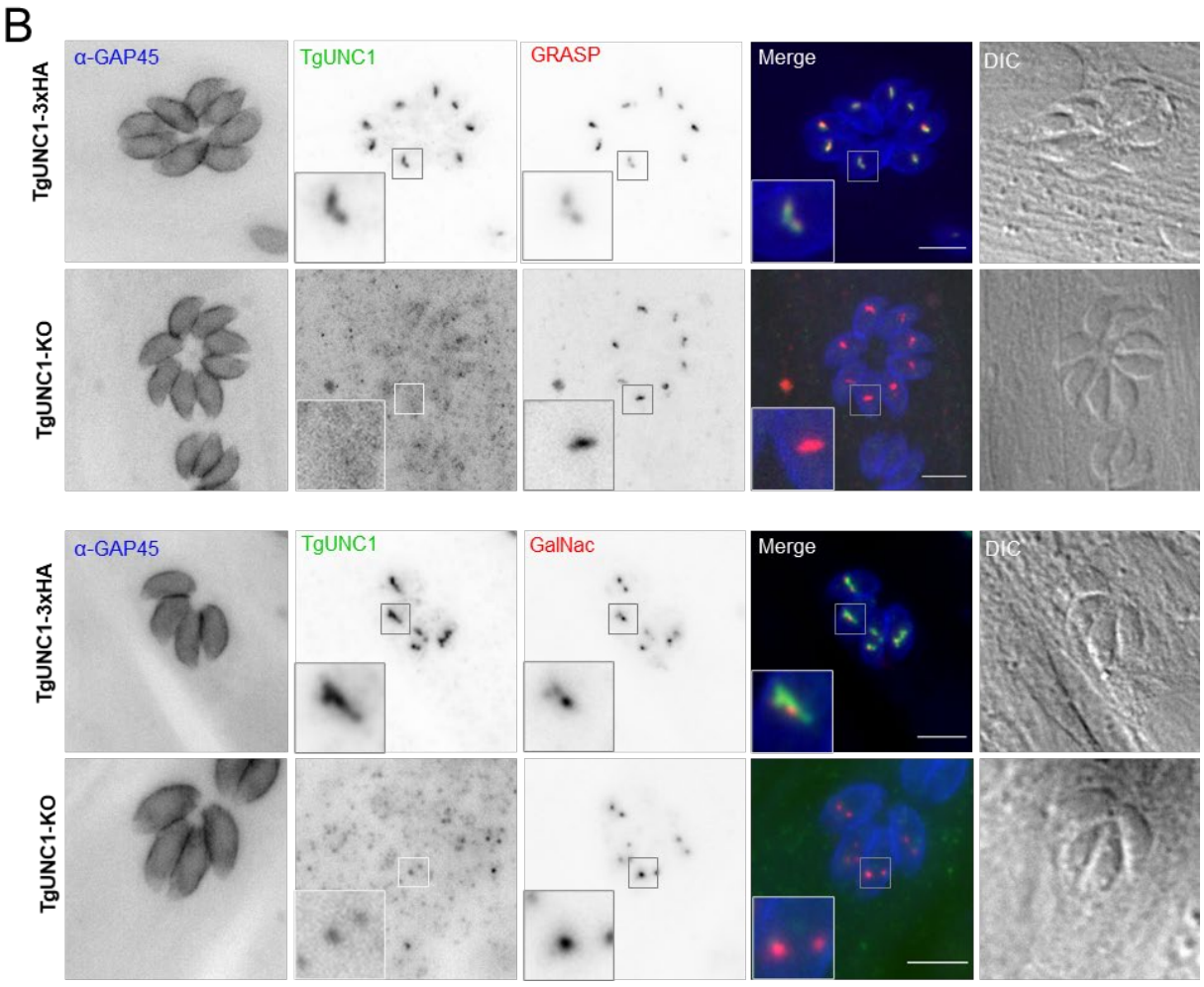

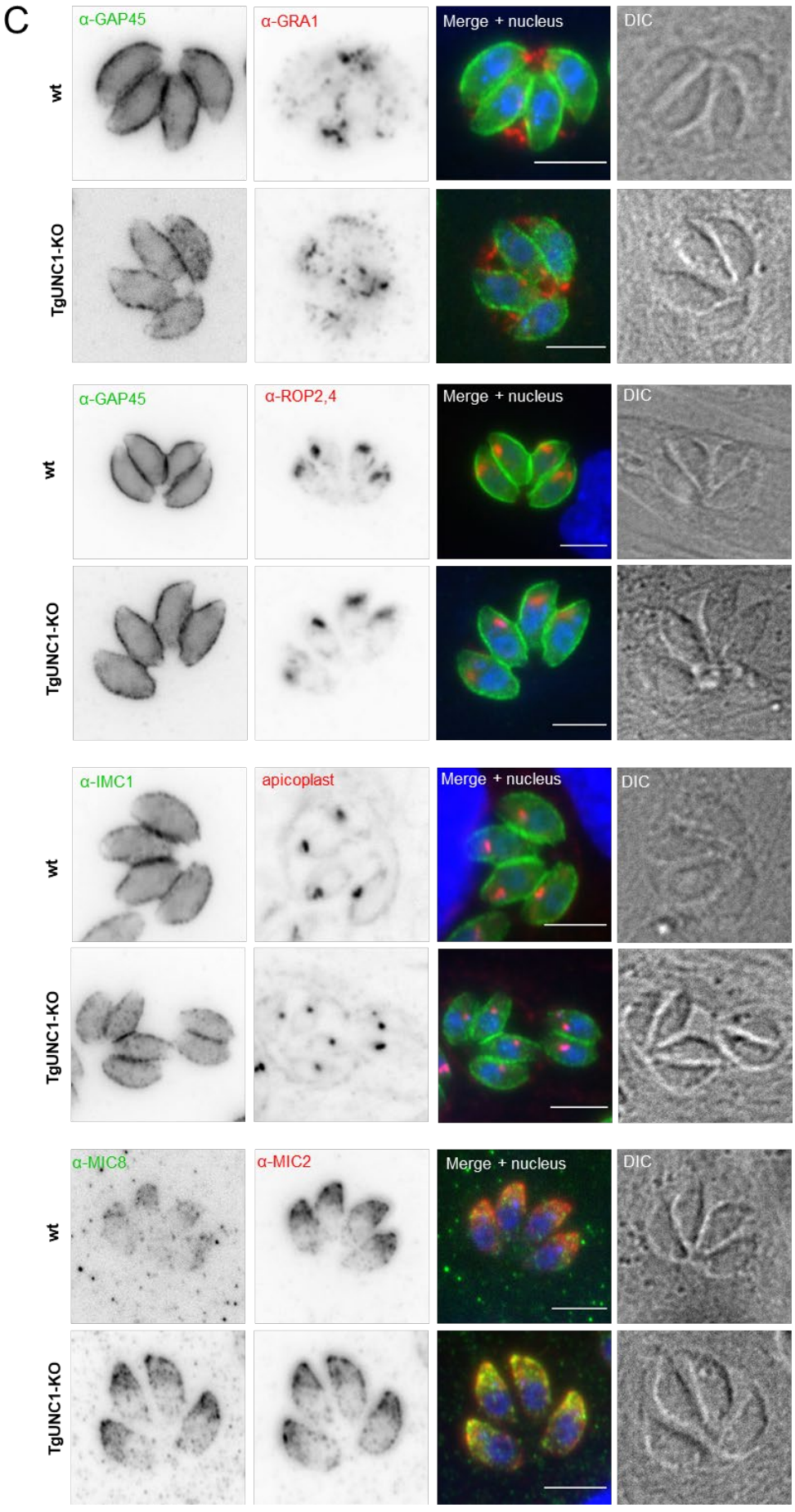
C
α-GAP45
α-GRA1
Merge + nucleus
DIC
wt
TgUNC1-KO
α-GAP45
α-ROP2,4
Merge + nucleus
DIC
wt
TgUNC1-KO
α-IMC1
apicoplast
Merge + nucleus
DIC
wt
TgUNC1-KO
α-MIC8
α-MIC2
Merge + nucleus
DIC
wt
TgUNC1-KO

Fig. 5.5 Analysis of the conditional knockout mutant of TgUNC1
(A) Plaque assay shows that loss of TgUNC1 is not affecting the parasite's growth. (B) Immunofluorescence analysis of the TgUNC1-3xHA line or an isolated knockout mutant of TgUNC1 (TgUNC1-KO) showed normal shape of the parasites and their Golgi apparatus which was visualised by a transiently expressed, fluorescent tagged marker protein of the cis-Golgi (GRASP) or the trans-Golgi (GalNac). (C) IFA of different marker proteins on the wildtype (wt) and an isolated *unc1* null mutant (TgUNC1-KO) showed normal shape of all organelles analysed in this experiment. The shape of the parasites is visualised with an α-GAP45 antibody or α-IMC1, dense granules with α-GRA1, rhoptries with α-ROP2,4, micronemes with α-MIC2 or α-MIC8 and the naturally biotinylated apicoplast with a streptavidin conjugate. The nuclei are stained with Hoechst. DIC: differential interference contrast, scale bar: 5 µm.

5.3 Characterisation of TgSLP2

5.3.1 Generation and analysis of transgenic parasites for TgSLP2

An endogenous tag was integrated at the C-terminus of TgSLP2 using CRISPR/ Cas9 (Stortz et al., 2019). To visualise the protein in live parasites, attempts were made to label the protein with a fluorescent tag, but it was only possible to insert a small epitope tag (3xHA). The correct genomic integration of the tag was confirmed by PCR and sequencing (Fig. 5.6). Probably due to the big protein size and low expression levels, it was not possible to verify the correct protein size by western blotting.

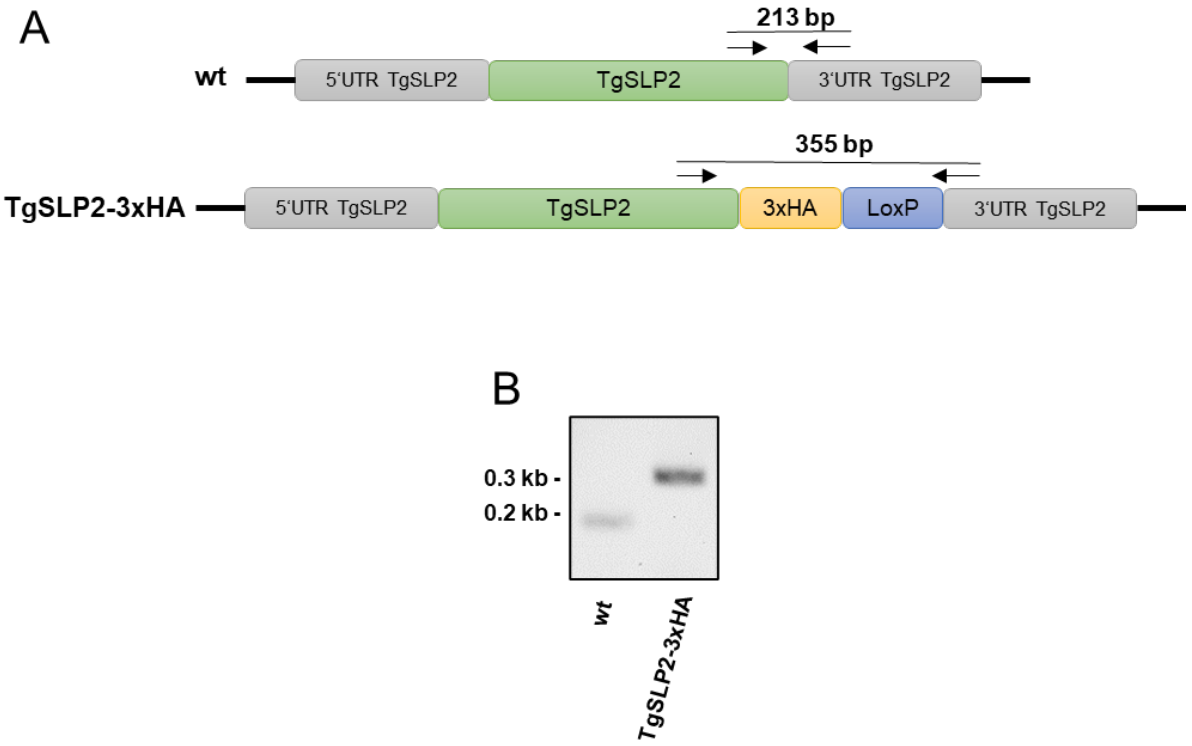

Fig. 5.6 Generation and confirmation of the endogenous tagged line of TgSLP2
(A) Schematic overview of the TgSLP2 locus before genetic manipulation (endogenous) and after C-terminal tagging (TgSLP2-3xHA). (B) PCR analysis confirms the correct integration of the tag. Primer positions and length of PCR products are indicated in (A).

5.3.2 TgSLP2 localises as a diffused punctuated pattern throughout the parasite

The subcellular localisation of TgSLP2 was unclear. It was localised as a diffused stippled pattern within the parasite and at the intravacuolar network (Fig. 5.7A). Simultaneous staining of TgSLP2 and the nucleus visualised with a transiently expressed fluorescently labelled histone 2B (H2B-RFP; Gubbels et al., 2006) was performed and it appeared that TgSLP2 does not accumulate in the nucleus (Fig. 5.7B). In extracellular parasites, the localisation of TgSLP2 seems to be similar to that in intracellular parasites (Fig. 5.7C).

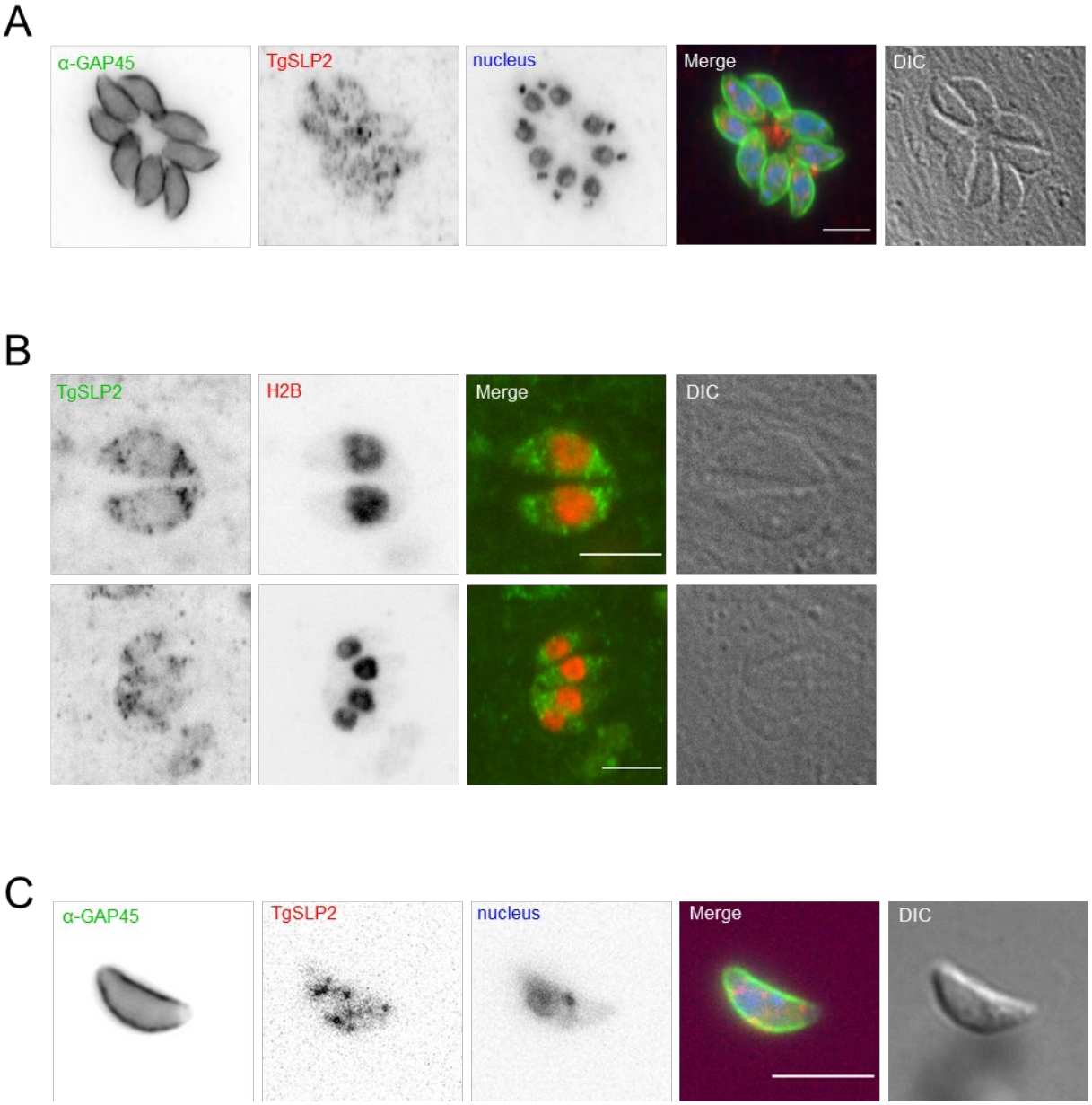

Fig. 5.7 Analysis of the localisation of TgSLP2
(A) Immunofluorescence assay of transgenic TgSLP2-3xHA parasites shows a diffuse punctuated pattern through the whole parasite and the intravacuolar network. (B) Simultaneous staining of TgSLP2 and a transiently expressed histone 2B (H2B) reveals that TgSLP2 is not accumulating in the nucleus. (C) The localisation of TgSLP2 in extracellular parasites seems to be similar to intracellular parasites. TgSLP2 is visualised with α-HA antibody staining, the parasite shape is visualised with an α-GAP45 antibody in (A) and (C). The nuclei are stained with Hoechst in (A) and (C). DIC: differential interference contrast, scale bar: 5 µm.

Since the SUN-binding counterparts (KASH domain proteins) bind to cytoskeletal proteins in opisthokonts (Padmakumar et al., 2005; Starr & Han, 2002; Zhen et al., 2002; Patterson et al., 2004; Fridolfsson & Starr, 2010), it would be interesting to investigate whether TgSLP2 might colocalise with the F-actin network. Therefore, an F-actin-binding chromobody tagged with emerald (CbEmerald; Periz et al., 2017) was transiently expressed in TgSLP2-3xHA tagged parasites. Surprisingly, the localisation and expression of TgSLP2 appeared to change, which can only be explained by a cross-reaction of the α-HA antibody with the F-actin-binding CbEmerald, especially in case of a strong signal for actin filaments (Fig. 5.8A). In parasites that did not receive the plasmid upon transfection, the TgSLP2 signal is weaker, shows the stippled pattern previously described, and is only visible in an overexposed image (Fig. 5.8A, arrow). As control, parasites expressing CbEmerald and wildtype parasites were stained with the α-HA antibody. While wildtype parasites did not show any signal for α-HA, in the CbEmerald line, there is colocalisation between CbEmerald and α-HA detectable (Fig. 5.8B, images taken by Janessa Grech).

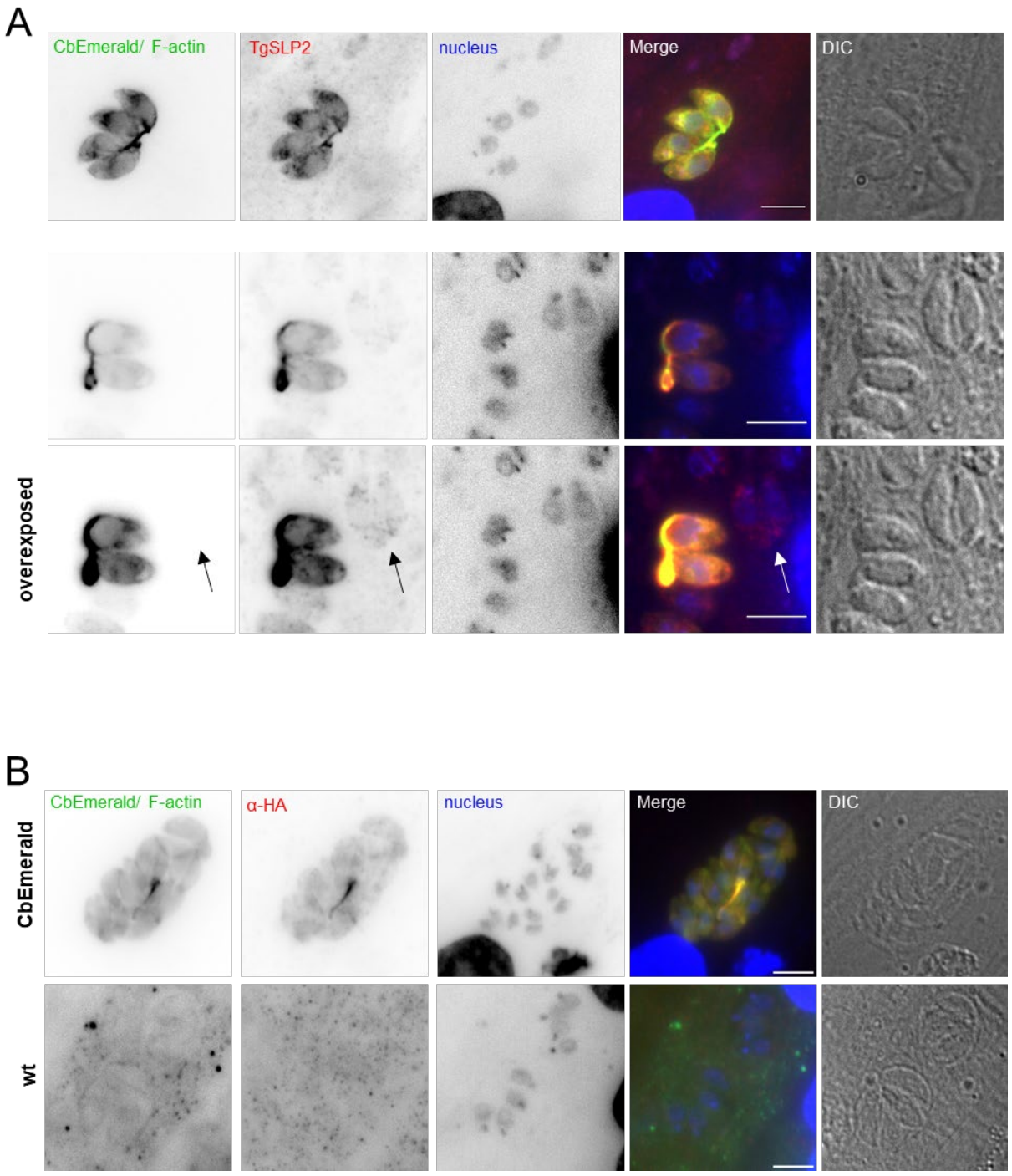

Fig. 5.8 The F-actin-binding Chromobody Emerald cross-reacts with the α-HA antibody
Immunofluorescence assay of TgSLP2-3xHA parasites and transiently expressing F-actin-binding CbEmerald shows a change of the localisation of TgSLP2 to the strong actin filaments, which can be explained by a cross-reaction of the chromobody and the α-HA antibody. The arrow in the overexposed images points to a vacuole that did not receive the transient expressed CbEmerald showing the previously observed pattern of TgSLP2. (B) As control, wildtype parasites and parasites expressing only CbEmerald were stained with α-HA. Only in parasites expressing CbEmerald, colocalisation between CbEmerald and the α-HA antibody was detectable. The nuclei are stained with Hoechst. DIC: differential interference contrast, scale bar: 5 µm. Images in (B) were taken by Janessa Grech.

As previously described, it was not possible to generate a parasite line in which TgSLP2 is fluorescently labelled. For this reason, it was not possible to co-stain F-actin and TgSLP2 in the same parasite line. Instead, the effect of actin-remodelling drugs on TgSLP2 was observed by using the actin-stabilising drug jasplakinolide (Jas; Bubb et al., 1994; Poupel & Tardieux, 1999; Periz et al., 2017) or cytochalasin D (cytD) to depolymerise actin filaments (Goddette & Frieden, 1986; Periz et al., 2017). As a control, parasites were incubated with DMSO. Neither treatment with Jas nor with cytD had an effect on the localisation of TgSLP2 (Fig. 5.9).

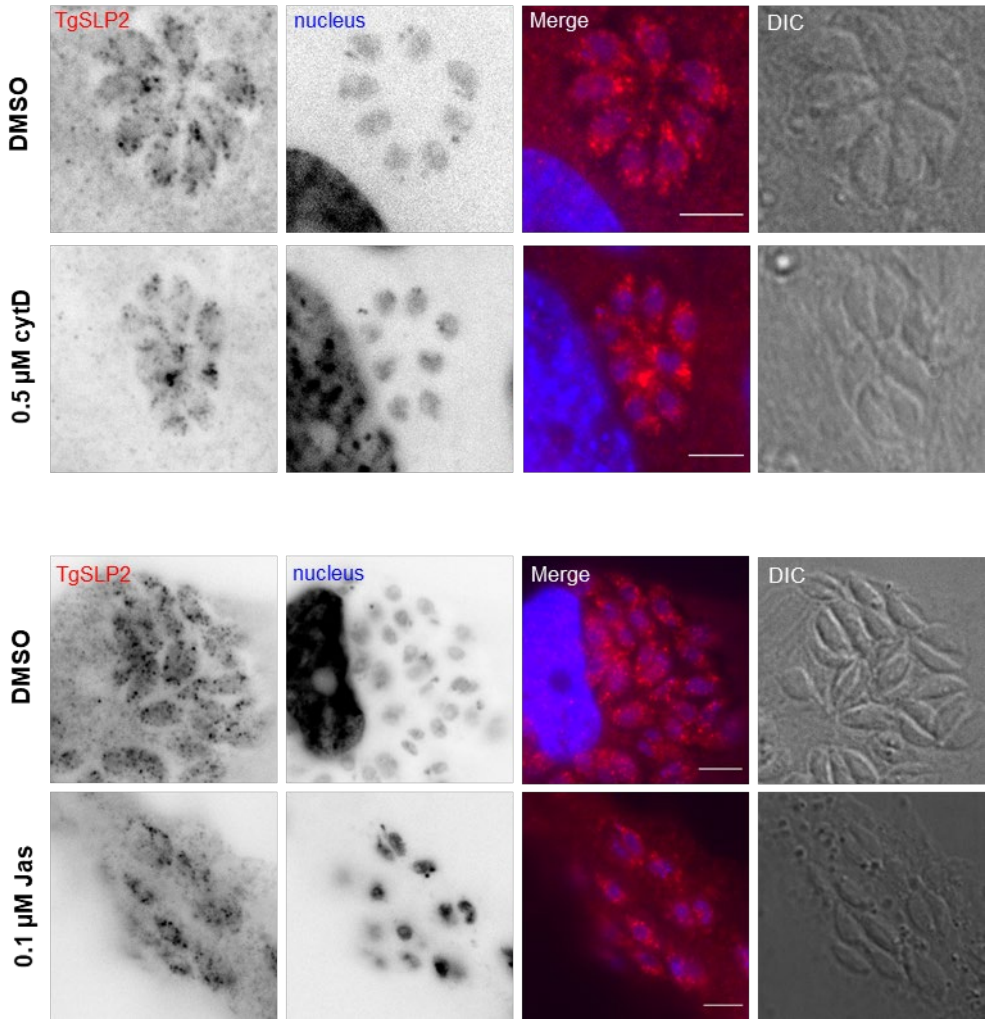

Fig. 5.9 Actin remodelling drugs do not have an effect on TgSLP2 localisation
TgSLP2-3xHA tagged parasites were treated for 1 hour with either 0.5 µM cytochalasin D (cytD) to destabilise the F-actin network or with 0.1 µM jasplakinolide (Jas) which has a stabilising effect on F-actin. As control, parasites were incubated in DMSO. TgSLP2 was visualised with α-HA, the nuclei are stained with Hoechst. DIC: differential interference contrast; scale bar: 5 µM.

To verify that the drugs have an effect on F-actin, the experiment was performed in another parasite line stably expressing CbEmerald and the other SUN-like protein in *T. gondii* (TgSLP1), which will be discussed later in point 5.4.3.

5.3.3 Attempts to conditionally knockout TgSLP2

To get better insight in the function of TgSLP2, it would be interesting to see how the parasite behaves after loss of TgSLP2. Similar to the conditional knockout strategy used for TgUNC1 and TgSLP1 (see 5.4.1), it was attempted to integrate a second LoxP site at the 5'end of *slp2*. Four sgRNAs at different positions to integrate the LoxP site were designed (Fig. 5.10A). The first attempt was an sgRNA that binds only a few base pairs upstream of the start codon. Despite several transfection attempts, it was not possible to isolate clones that integrated the LoxP site. To exclude a destruction of the 5'UTR, another sgRNA binding upstream of the 5'UTR was designed, but again, no clones with integrated LoxP could be isolated. The genomic locus of TgSLP2 is densely packed and a second gene (TGGT1_207110) with a negative phenotypic score of -3.68 (Sidik et al., 2016) is just upstream of TgSLP2 (Fig. 5.10A). Therefore, an sgRNA binding upstream of TGGT1_207110 was designed, but again, no clones with integrated LoxP sites could be isolated. As a last try, an sgRNA cutting within the first base pairs of *slp2* in combination with a template repairing the locus in frame was designed. Since this approach also failed, as an alternative to the DiCre system, it was attempted to use a strategy based on conditional U1 small nuclear ribonucleic particles (snRNP)-mediated gene silencing (Pieperhoff et al., 2015) and another based on the auxin-inducible degron (AID) system (Brown et al., 2017; Brown et al., 2018) to create a conditional knockout of TgSLP2 (Fig. 5.10B-C). However, both methods failed and no integrands could be isolated. Together this suggests that the genomic locus of TgSLP2 is refractory to genetic modifications.

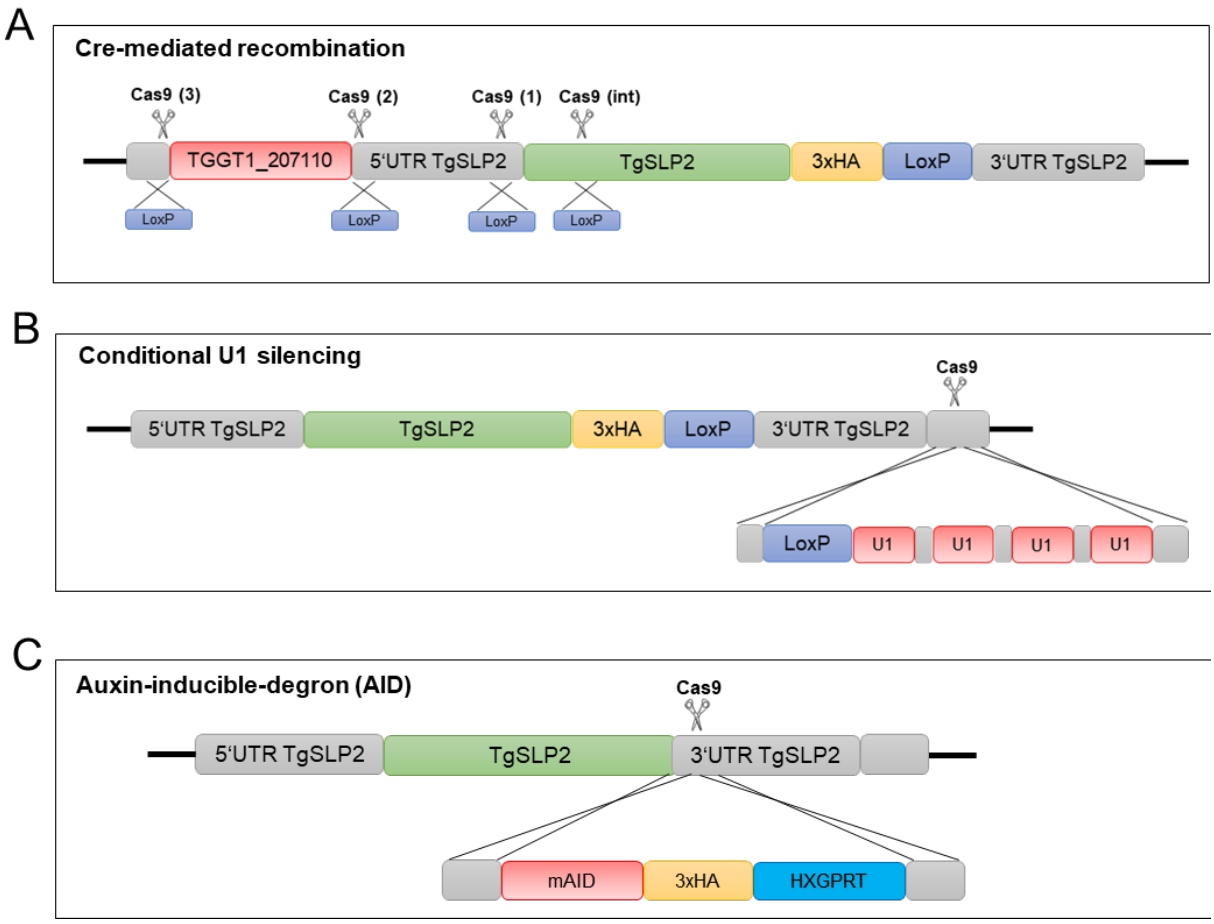

Fig. 5.10 Schematic overviews of various attempts to conditionally knockout TgSLP2
(A) Overview of the different positions of four sgRNAs designed to integrate a second LoxP site in TgSLP2-3xHA parasites to create a conditional knockout based on the DiCre-mediated recombination system. (B) Overview of the genomic integration of U1 sites to use a strategy based on conditional U1 silencing to create a conditional knockout of TgSLP2. (C) Overview of the genomic integration of mAID-3xHA-HXGPRT to create a conditional knockout of TgSLP2 based on the auxin-inducible-degron system. All integrations are based on CRISPR/ Cas9 (Stortz et al., 2019).

5.4 Characterisation of TgSLP1

5.4.1 Generation and analysis of transgenic parasites for TgSLP1

To determine the localisation of TgSLP1, the C-terminus of *slp1* was endogenously tagged with a yellow fluorescent protein (sYFP2) in RH-Δ*ku80*-DiCre parasites using CRISPR/ Cas9 (Stortz et al, 2019). The resulting coding sequence of *slp1-syfp2* was flanked by LoxP sites, allowing the excision of this locus after induction with rapamycin (Fig. 5.11A). Genomic integration of the tag and Cre-mediated excision was verified by PCR and sequencing and by western blot analysis (Fig. 5.11B-C).

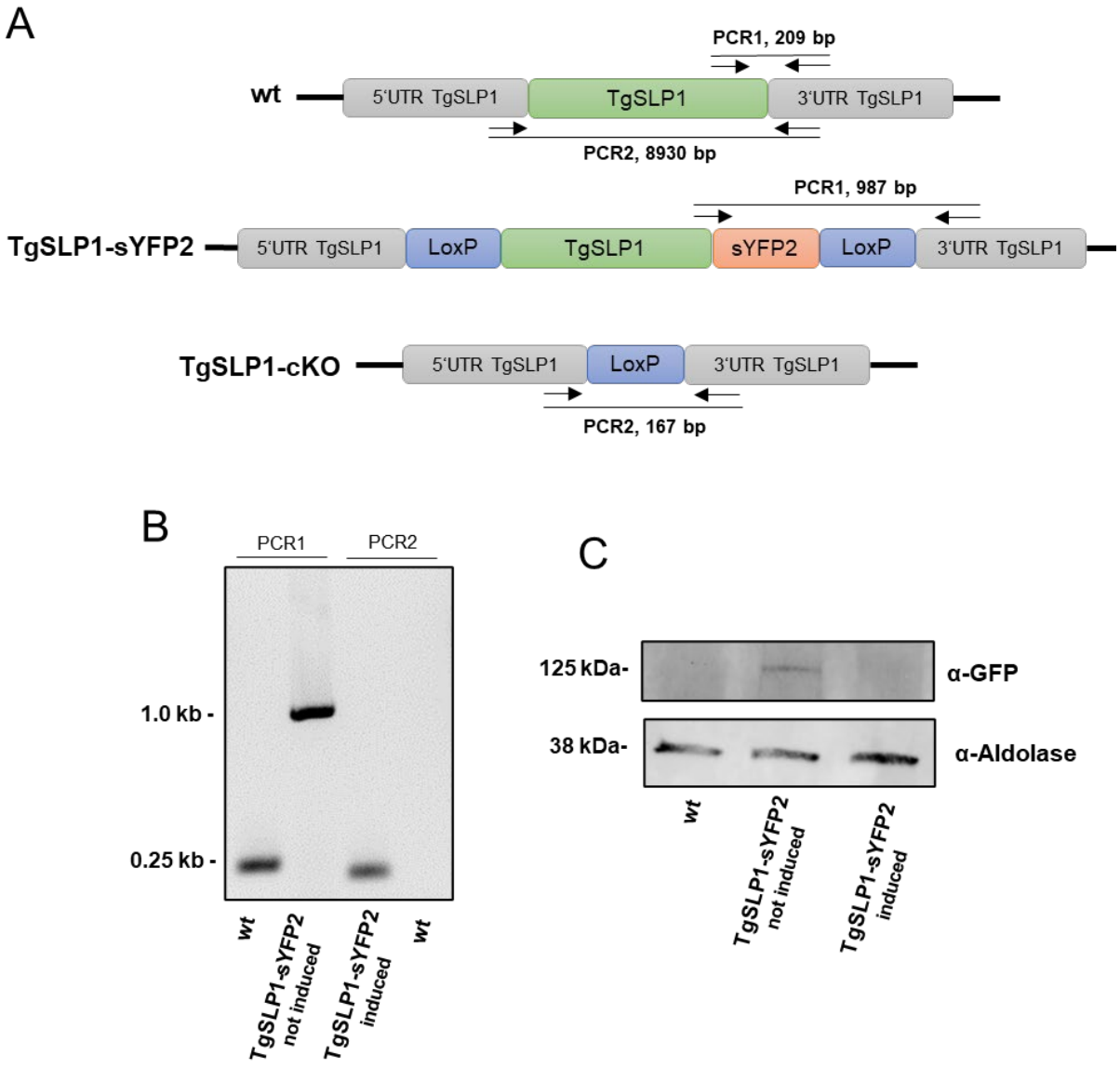

Fig. 5.11 Generation and confirmation of the conditional knockout of TgSLP1
(A) Schematic overview of the TgSLP1 locus before genetic manipulation (endogenous), after C-terminal tagging and integration of LoxP-sites (TgSLP1-sYFP2) and upon excision of the gene using DiCre induction (TgSLP1-cKO). (B) PCR analysis confirms the correct integration of the tag and excision of *slp1* after 48 hours of rapamycin treatment. Primer positions and length of PCR products are indicated in (A). Note that there is no PCR product for the wildtype PCR2 due to the length of almost 9000 bp. (C) Western blot analysis using α-GFP antibody on the wildtype (wt) and not induced or induced TgSLP1-sYFP2 lines verifies the expected protein size of around 88 kDa and protein depletion under induced conditions. α-Aldolase is used as loading control.

5.4.2 Analysis of the localisation of TgSLP1

5.4.2.1 TgSLP1 is involved in nuclear division and colocalises with the mitotic spindle

To assess the localisation of TgSLP1, IFA analysis was carried out. Interestingly, though a clonal line was obtained, not all parasites expressed TgSLP1-sYFP2, leading to the hypothesis that this protein is expressed cell cycle dependent. In an asynchronous culture, some vacuoles had no visible signal, while in others TgSLP1 appeared as a single dot or two dots near the nucleus, visualised by a transiently expressed histone 2B (H2B) tagged with mRFP (Fig. 5.12; Gubbels et al., 2006).

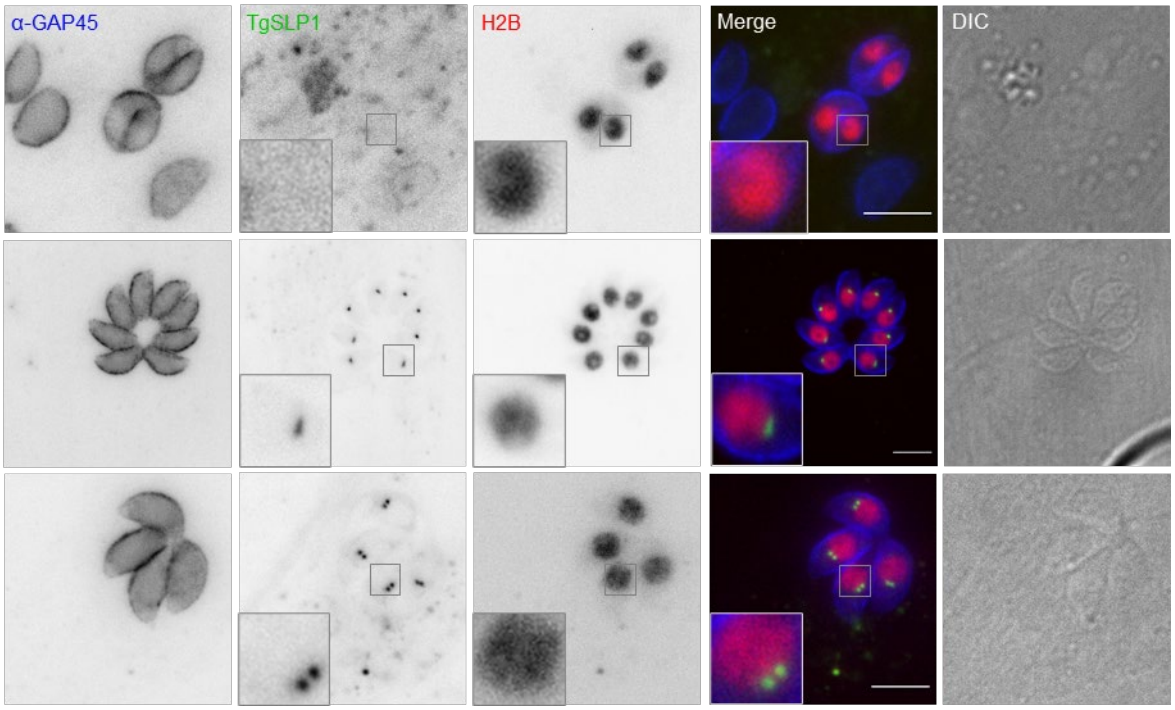

Fig. 5.12 TgSLP1 localisation in an asynchronous culture
Immunofluorescence analysis of transgenic TgSLP1-sYFP2 parasites and transiently expressed, fluorescent tagged histone 2B (H2B) reveals a close localisation of TgSLP1 to the nucleus. Parasite shape is visualised with α-GAP45. DIC: differential interference contrast, scale bar: 5 µm.

This observation suggests that TgSLP1 might be involved in nuclear division. To label microtubular structures during cell division, TLAP4 (TGGT1_201760), a protein previously described to localise to the cortical microtubules and the centrioles (Liu et al., 2016) was endogenously tagged with mCherry at its N-terminus in TgSLP1-sYFP2 expressing parasites using CRISPR/ Cas9 (Stortz et al., 2019). The correct genomic integration of the tag was confirmed by PCR and sequencing (Fig. 5.13).

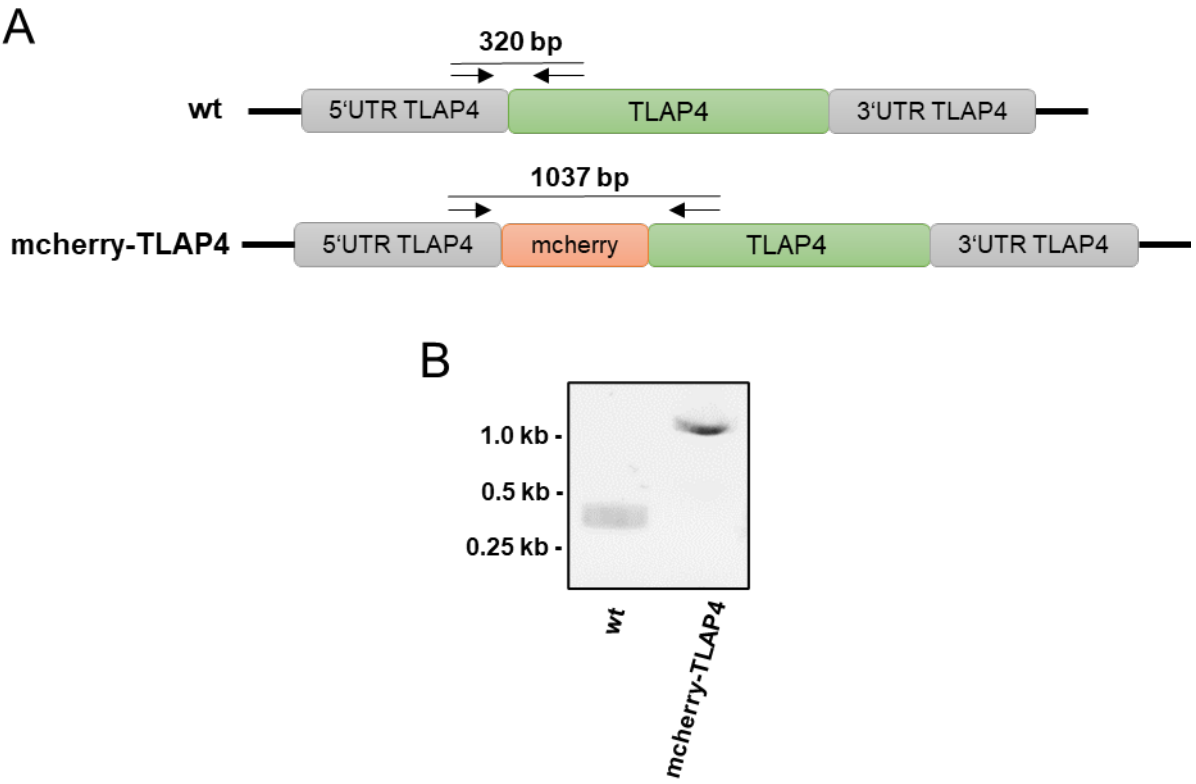

Fig. 5.13 Generation and confirmation of endogenously tagged TLAP4
(A) Schematic overview of wildtype (wt) and the N-terminally, mCherry tagged parasite line of TLAP4. (B) PCR analysis confirms the correct integration of the tag. Primer positions and length of PCR products are indicated in (A).

Although an overexpressed version of TLAP4 seems to be a good marker for microtubular structures including the mitotic spindle, as previously demonstrated (Liu et al., 2016; Fig. 5.14A), the endogenous tagged protein appears to be concentrated at the apical tip of cortical microtubules (Fig. 5.14B).

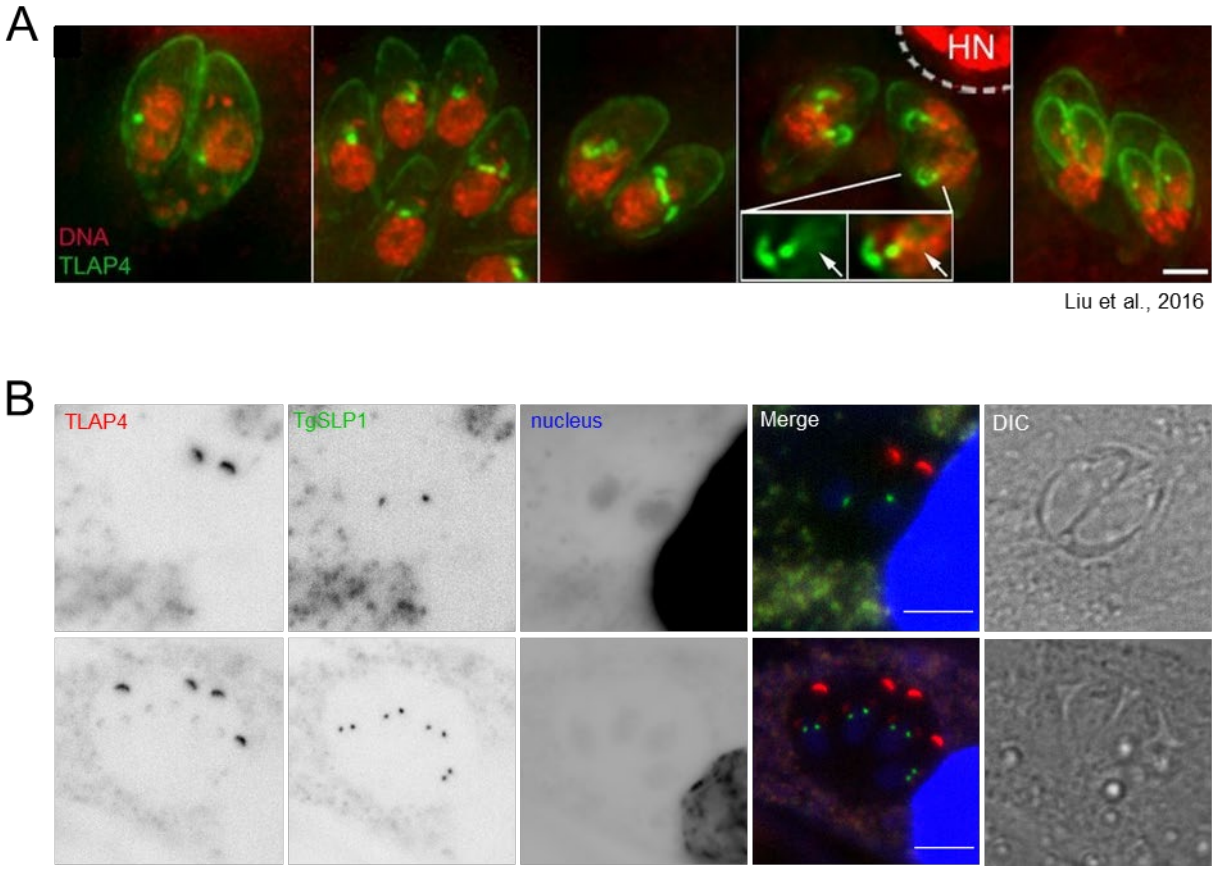

Fig. 5.14 Localisation of overexpressed and endogenously tagged TLAP4
(A) Immunofluorescence analysis of transgenic parasites expressing *ptub-mEmeraldFP-TLAP4*. The extra copy of TLAP4 marks microtubular structures including the mitotic spindle. The nucleus is stained with Hoechst. HN: host cell nucleus. Scale bar: 2 µm. Figure is adapted from Liu et al., 2016. © 2016 Liu, He, et al. CC BY 3.0 license (B) IFA of endogenously tagged TLAP4 with mCherry at the N-terminus shows that the endogenously labelled protein is localised at the apical tip of maternal cortical microtubules and at a lower level also at the apical tip of emerging daughter parasite microtubules. The nuclei are stained with Hoechst. DIC: differential interference contrast, scale bar: 5 µm.

To label microtubular structures, an extra copy of α-tubulin labelled with mCherry (Hu et al., 2002b) was transiently expressed in the transgenic TgSLP1-sYFP2 parasite line. Analysis of these parasites revealed that TgSLP1 colocalises with the mitotic spindle, which is formed during cell division and separates the duplicated chromosomes. The IFA shows the localisation of TgSLP1 and α-tubulin in not dividing and in dividing parasites. The Pearson correlation coefficient was calculated to quantify the degree of colocalisation (Fig. 5.15).

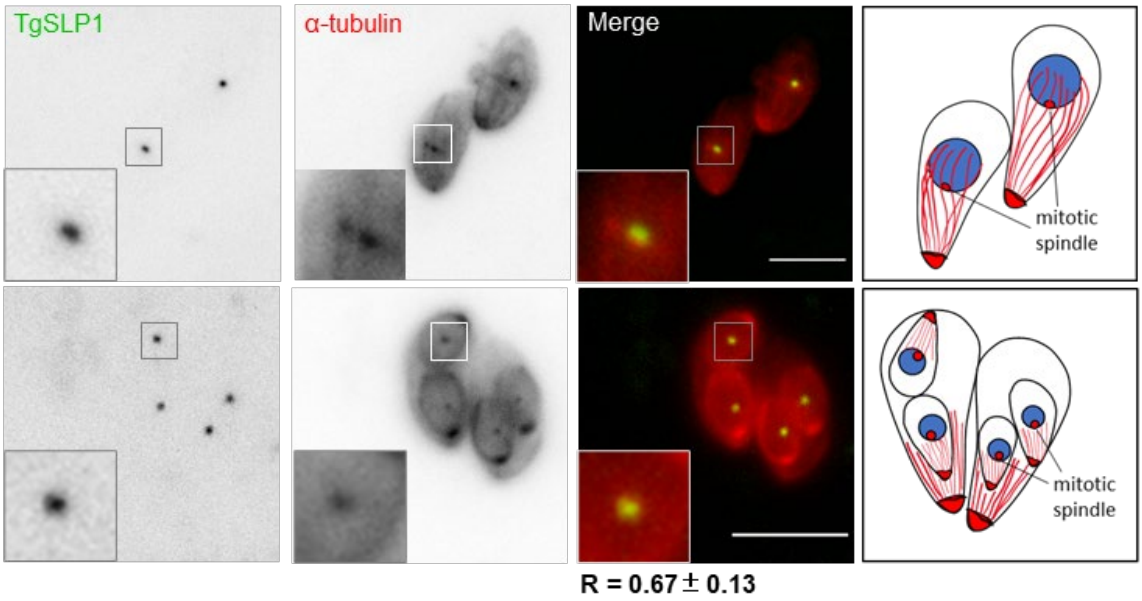

Fig. 5.15 TgSLP1 colocalises with the mitotic spindle in *T. gondii* tachyzoites
Immunofluorescence analysis of TgSLP1-sYFP2 parasites transiently expressing fluorescent tagged α-tubulin. The upper channels show not dividing parasites, lower channels show parasites that are in division. The colocalisation was quantified by calculating the Pearson correlation coefficient (R) of 20-25 parasites using the ImageJ plugin JACoP (Bolte & Cordelières, 2006). Mean value and standard deviation are shown under the respective image. Scale bar: 5 µm.

5.4.2.2 TgSLP1 colocalises with MORN1 and VPS31

To provide further subcellular colocalisation, an additional copy of YFP tagged MORN1 (Gubbels et al., 2006) was transiently transfected into endogenously TgSLP1-mCherry expressing parasites. The correct integration of the mCherry tag was verified via PCR and sequencing (data not shown).

MORN1 localises specifically to the apical and posterior end of the IMC, but also to the centrocone, a specialised nuclear structure that is thought to organise the mitotic spindle and plays a central role in apicoplast segregation and daughter cell formation (Gubbels et al., 2006; Lorestani et al., 2010). As expected, fluorescence microscopy demonstrated a colocalisation between the two proteins at the centrocone in dividing and not dividing parasites. For quantification of the colocalisation, the Pearson correlation coefficient was calculated (Fig. 5.16).

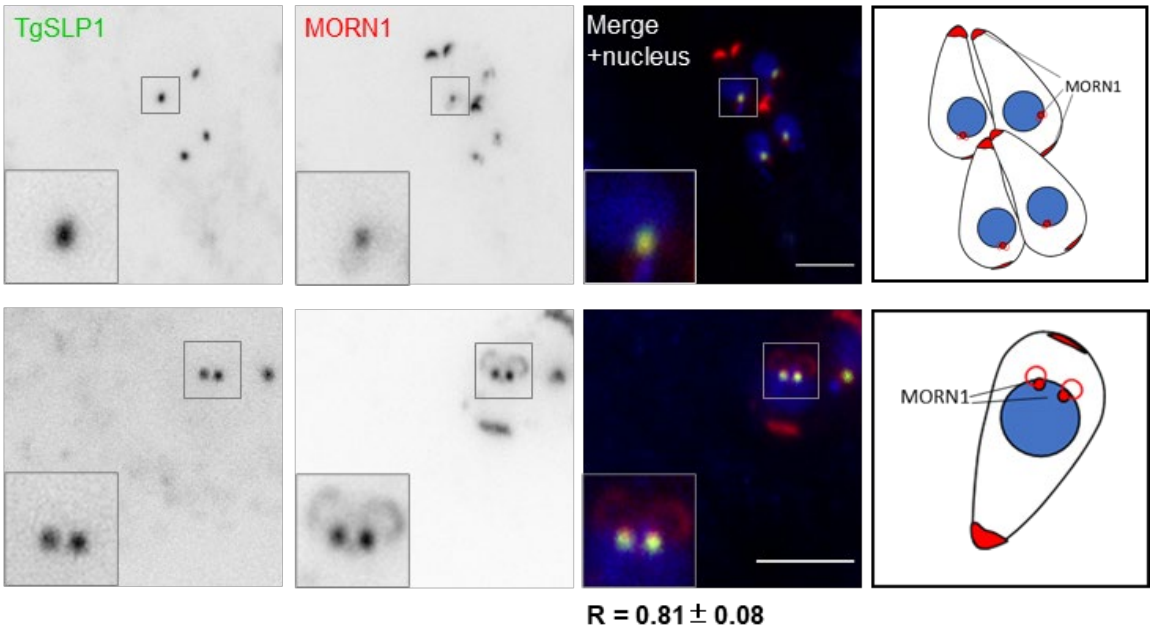

Fig. 5.16 TgSLP1 colocalises with MORN1 at the centrocone
Immunofluorescence analysis of TgSLP1-mcherry parasites transiently expressing fluorescent tagged MORN1. The upper channels show not dividing parasites, lower channels show parasites that are in division. The colocalisation was quantified by calculating the Pearson correlation coefficient (R) of 20-25 parasites using the ImageJ plugin JACoP (Bolte & Cordelières, 2006). Mean value and standard deviation are shown under the respective image. The nuclei are stained with Hoechst. Scale bar: 5 µm.

Furthermore, colocalisation was observed between TgSLP1 and VPS31 (vacuolar protein sorting-associated protein 31; TGGT1_256910), a component of the endosomal sorting complex required for transport (ESCRT) III, which is thought to be important for the cleavage of various membranes. VPS31 was endogenously tagged with 3xHA in TgSLP1-sYFP2 parasites and validated via PCR and sequencing (data not shown).

A conditional knockout mutant of VPS31 shows, that it is not essential for growth and parasites lacking this protein show normal morphology of the nucleus and the IMC (Dr. Elena Jiménez-Ruiz, unpublished data).

As shown in Figure 5.17, TgSLP1 colocalises with VPS31 in non-dividing and dividing parasites (Fig. 5.17A). However, it appears that TgSLP1 divides slightly earlier than VPS31 (Fig. 5.17B).

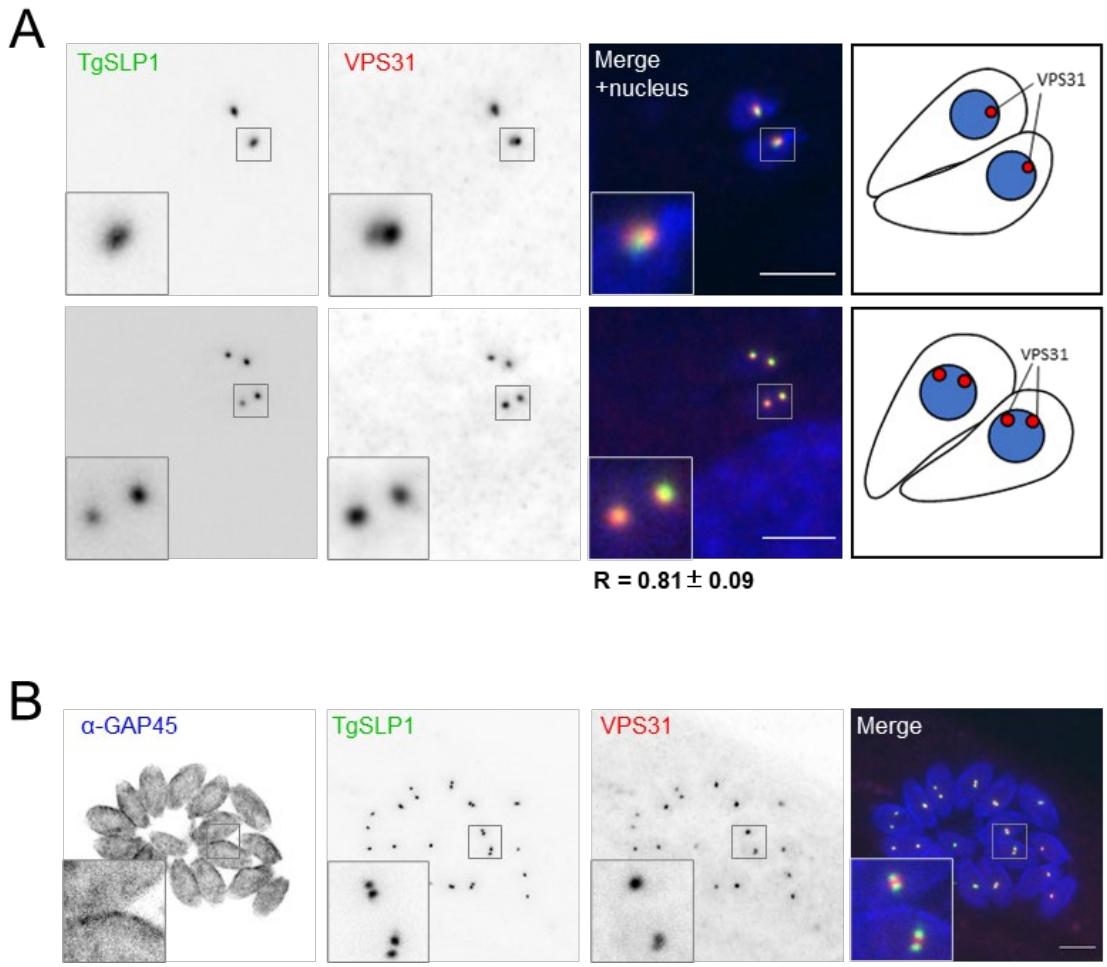

Fig. 5.17 TgSLP1 colocalises with the ESCRT-III component VPS31
(A) Immunofluorescence analysis of endogenously tagged TgSLP1-sYFP2 and VPS31-3xHA reveals a colocalisation between the two proteins. The upper channels show not dividing parasites, lower channels show parasites that are in division. The colocalisation was quantified by calculating the Pearson's correlation coefficient (R) of 20-25 parasites using the ImageJ plugin JACoP (Bolte & Cordelières, 2006). Mean value and standard deviation are shown under the respective image. Nuclei are stained with Hoechst. (B) In some vacuoles it appears that TgSLP1 divides a little earlier than VPS31. Parasite shape is visualised with an α-GAP45 antibody. Scale bar: 5 µm.

The localisation of TgSLP1 seems to be cell cycle dependent, as further analysed in the following chapter. Interestingly, extracellular parasites with and without TgSLP1 expression were observed (Fig. 5.18). This might be due to the experimental setting, where intracellular parasites are mechanically released from the host cells, fixed and prepared for microscopy. Parasites that have just started the division process may still express TgSLP1, although it is not needed when parasites are extracellular. As will be discussed later, TgSLP1 appears to be important for cell division, therefore the analysis in this study was limited to intracellular

parasites. However, it cannot be excluded, that TgSLP1 plays a separate role in host cell invasion.

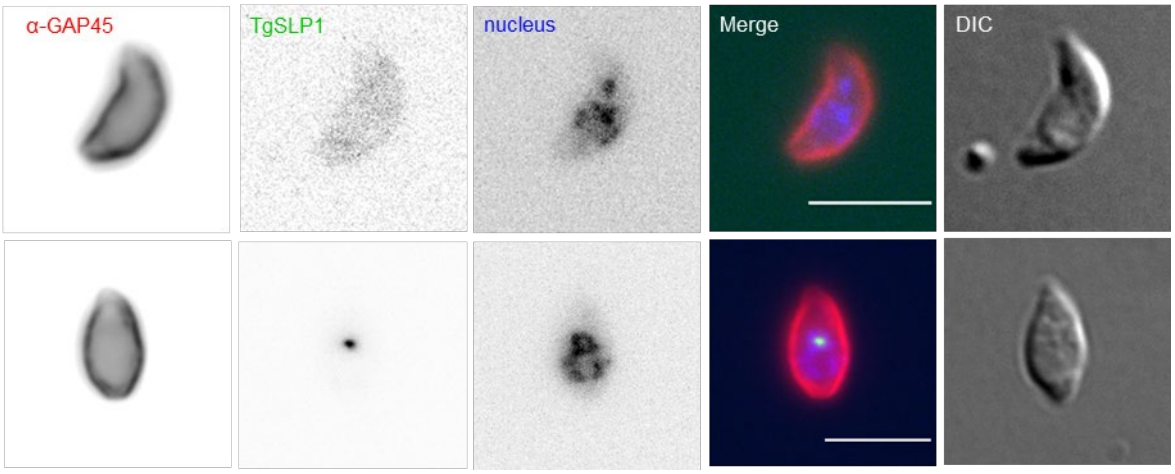

Fig. 5.18 TgSLP1 expression in extracellular parasites
(A) Immunofluorescence assay of TgSLP1-sYFP2 in extracellular parasites, mechanically released from host cells. While TgSLP1-sYFP2 is detectable in some parasites, it is not in others. The parasite shape is visualised with an α-GAP45 antibody, the nucleus is stained with Hoechst. DIC: differential interference contrast, scale bar: 5 µm.

5.4.2.3 Dynamic localisation of TgSLP1 throughout the tachyzoite division cycle

To obtain a better insight into the timing of expression, an antibody raised against centrin1 to visualise the centrosome and thus the cell cycle stage of *T. gondii* parasites was used (Fig. 5.19). Tachyzoite endodyogeny is characterised by three phases consisting of the main phases G1 and S, with mitosis (M-phase) immediately following the completion of DNA replication. With the formation of apical daughter complexes, cytokinesis begins in late S-phase and overlaps with mitosis (Radke et al., 2001). While parasites enter G1-phase with a single centrosome, no TgSLP1 was visible at this stage. When cells enter S-phase, the centrosome divides and a single TgSLP1 spot between the divided centrosomes was detectable. This indicates that while TgSLP1 appeared to remain associated with the centrosome, it divides slightly later. Finally, in late S-phase overlapping with beginning M-phase, TgSLP1 divides and shows a close association with the centrosome of the parasite (Fig. 5.19).

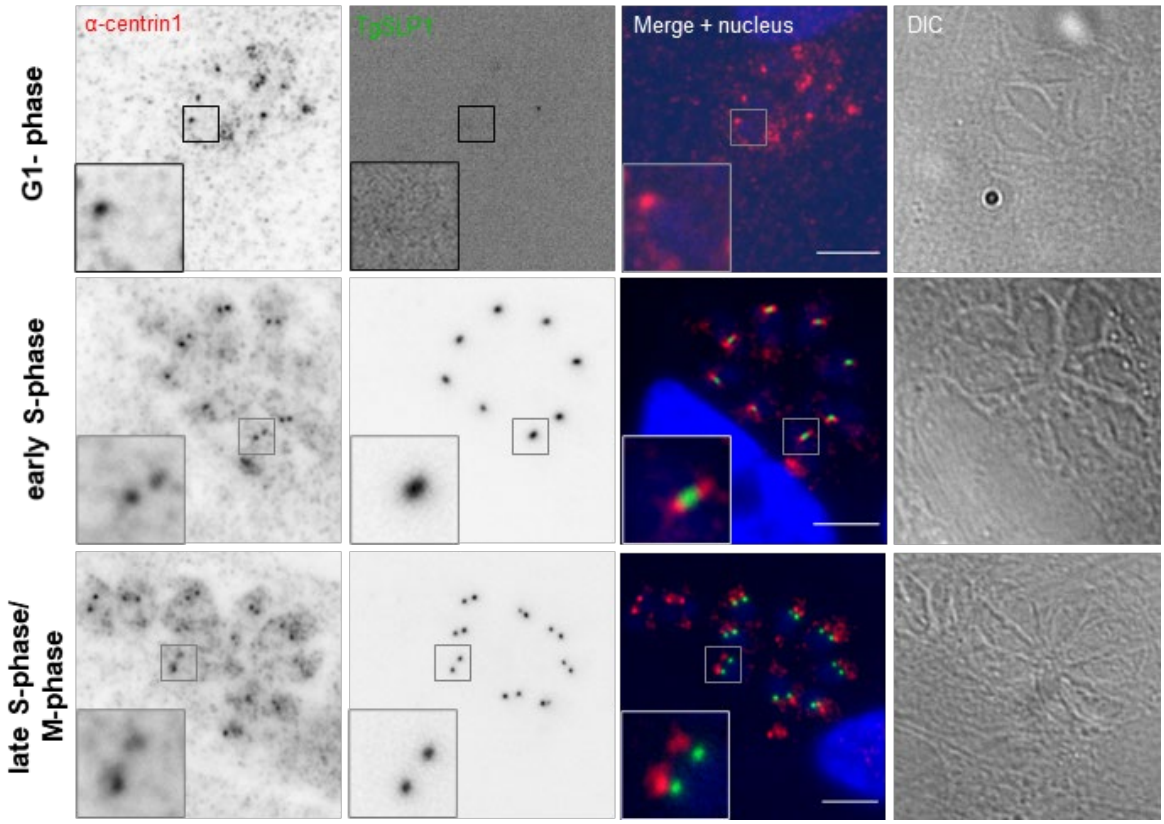

Fig. 5.19 Dynamic localisation of TgSLP1 throughout the tachyzoite division cycle
Immunofluorescence analysis through the tachyzoite division cycle shows that the expression and localisation of TgSLP1 is cell cycle dependent. The nuclei are stained with Hoechst, the cell cycle stages are defined by α-centrin1 antibody labelling the parasite's centrosome. DIC: differential interference contrast, scale bar: 5 µm.

To quantify the expression of TgSLP1 in the different phases of cell division, parasites were arrested in G1-phase using pyrrolidine dithiocarbamate (PDTC; Conde de Felipe et al., 2008) or in S-phase using hydroxyurea (HU; Melo et al., 2000). In a mixed parasite population, TgSLP1 was detectable in more than 70% of the vacuoles. In contrast, the majority of vacuoles arrested with PDTC in G1-phase showed little or no TgSLP1 expression (about 25%). As expected, most parasites (more than 98%) arrested with HU in S-phase showed TgSLP1 expression (Fig. 5.20A). The successful arrest was controlled by staining the centrosome with α-centrin1 antibody and subsequent quantification (Fig. 5.20B).

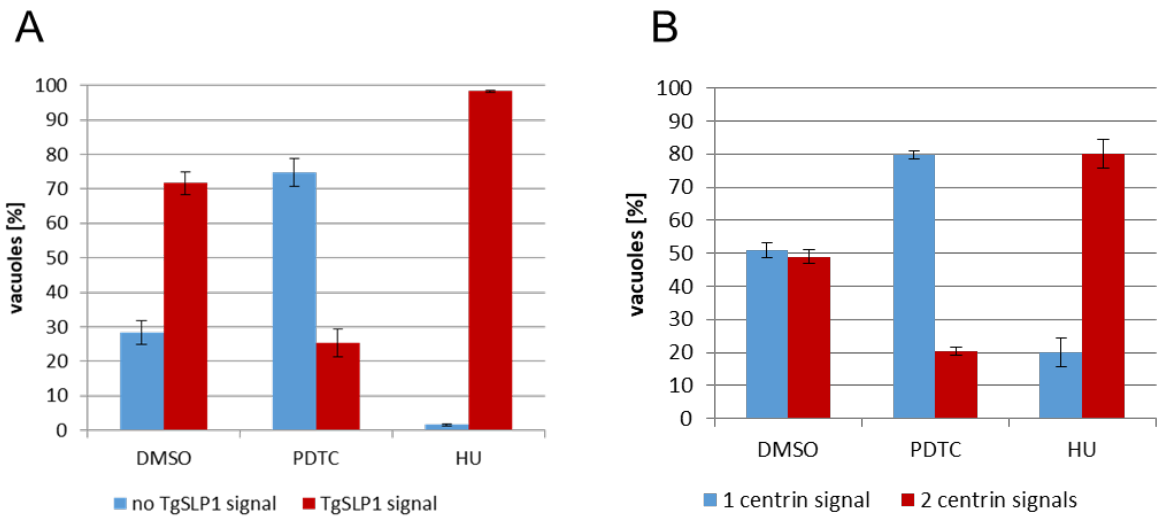

Fig. 5.20 Quantification of TgSLP1 expression in parasites arrested at different stages of the cell cycle
(A) TgSLP1-sYFP2 expression in parasites from a mixed population (DMSO), parasites arrested in G1-phase using pyrrolidine dithiocarbamate (PDTC) or in S-phase using hydroxyurea (HU) were analysed depending on their TgSLP1-sYFP2 expression. (B) Successful cell cycle arrest was monitored by α-centrin1 staining. In (A) and (B), 100 vacuoles were counted per condition, the experiments were done in biological and technical triplicates. Mean values of three independent assays are shown, error bars indicate the standard deviation.

The dynamic localisation of TgSLP1 was also observed using live cell imaging. Therefore, TgSLP1 was C-terminally tagged with mCherry in parasites expressing CbEmerald to visualise the F-actin network (Periz et al., 2017).

Stills from movies depicting different stages of the parasite's division cycle are shown in Figure 5.21. The formation of daughter parasites within the mother demonstrates the onset of cytokinesis, concomitant with TgSLP1 division. It seems that TgSLP1 localises close to the actin polymerisation centre during parasite division. (Fig. 5.21, 30-60 min). When daughter cells emerge from the mother cell, TgSLP1 disappeared (Fig. 5.21, 90-150 min).

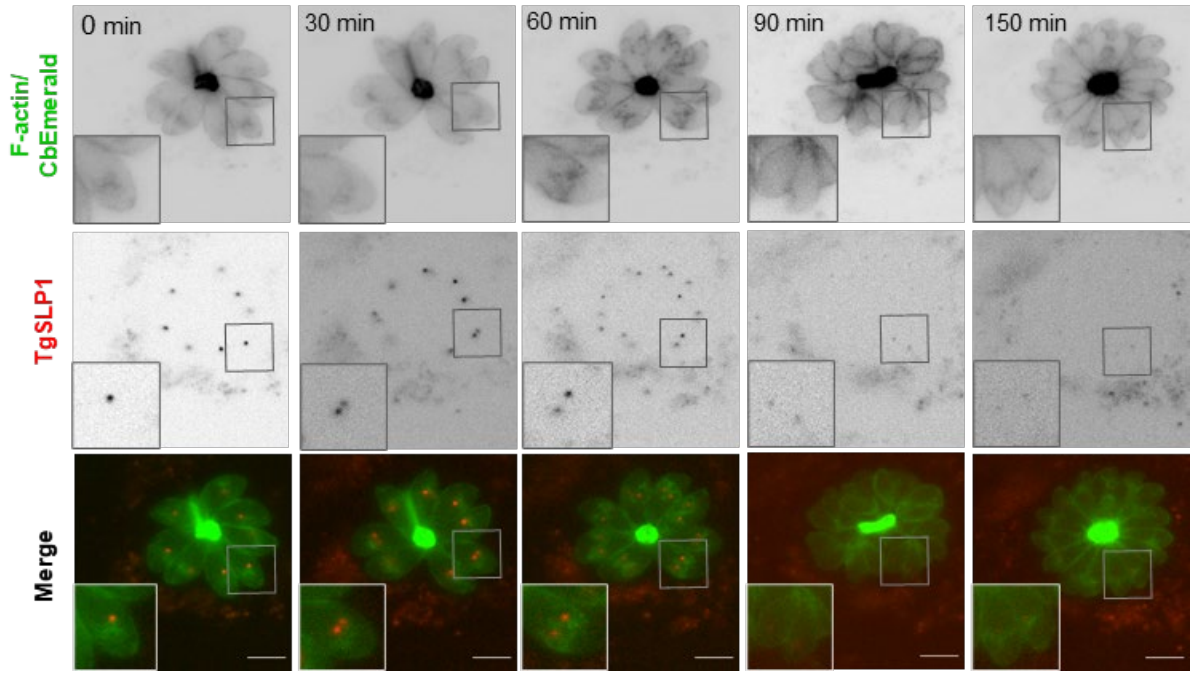

Fig. 5.21 Time-laps analysis of TgSLP1 and F-actin localisation during parasite division
TgSLP1 was tagged with mCherry in a parasite line expressing CbEmerald to visualise F-actin. At the beginning, the parasites are already in S-phase, recognisable by TgSLP1 expression. After 30-60 minutes, TgSLP1 divides and daughter parasites emerge within the mother parasite. Finally, when division is completed, TgSLP1 disappears. Scale bar: 5 µm.

Figure 5.22 shows stills from a movie of dividing TgSLP1-sYFP2 tagged parasites transiently expressing mCherry tagged α-tubulin (Hu et al., 2002b). Similar as observed in the CbEmerald expressing parasites, TgSLP1 starts to divide when daughter cells are formed within the mother parasite (Fig. 5.22, 30-60 min). The final separation representing the end of endodyogeny when the mother is consumed by the daughter parasites, TgSLP1 disappears (Fig. 5.22, 90-150 min).

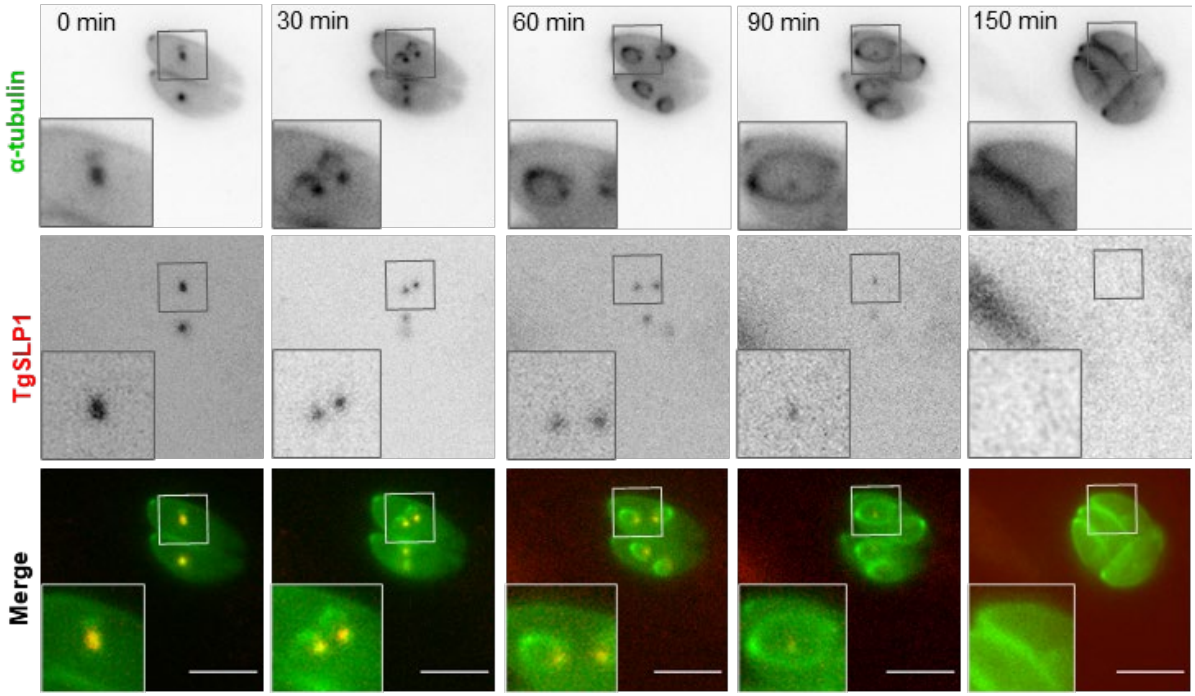

Fig. 5.22 Time-laps analysis of TgSLP1 and α-tubulin localisation during parasite division
Fluorescently labelled α-tubulin was transiently expressed in a TgSLP1-sYFP2 parasite line. The time-laps begins at S-phase with parasites expressing TgSLP1 which is colocalising with the mitotic spindle. After 30-60 minutes, the spindle and TgSLP1 are dividing and daughter parasites arise within the mother parasite. After 90 minutes, TgSLP1 starts to disappear and after 150 minutes, the mother is consumed by the daughter parasites and division is completed. Scale bar: 5 µm.

5.4.3 Effect of actin modulating drugs on TgSLP1

As described in several organisms, SUN domain proteins are anchored in the inner nuclear membrane through the interaction of nucleoskeletal proteins and interact with KASH domain proteins, which in turn interact with cytoskeletal proteins such as actin or tubulin-interacting proteins (Padmakumar et al., 2005; Starr & Han, 2002; Zhen et al., 2002; Patterson et al., 2004; Fridolfsson & Starr, 2010). In parasites expressing the F-actin binding CbEmerald, it seems that the actin polymerisation center is close to TgSLP1 (Fig. 5.21). For this reason, it was tested whether actin remodelling drugs have an impact on the localisation of TgSLP1. Jasplakinolide (Jas) treatment was performed to stabilise the actin cytoskeleton (Bubb et al., 1994; Poupel & Tardieux, 1999; Periz et al., 2017) whereas cytochalasin D (cytD) was used to depolymerise actin filaments (Goddette & Frieden, 1986; Periz et al., 2017). As control, parasites were incubated with DMSO. The experiment was performed using a TgSLP1-mCherry tagged

parasite line expressing CbEmerald to visualise the F-actin network. While the actin filaments became longer and thicker in the presence of Jas, cytD leads to a destabilisation and depolymerisation of the actin filaments. Neither Jas nor cytD had any observable effect on TgSLP1 localisation in dividing and not dividing intracellular tachyzoites (Fig. 5.23).

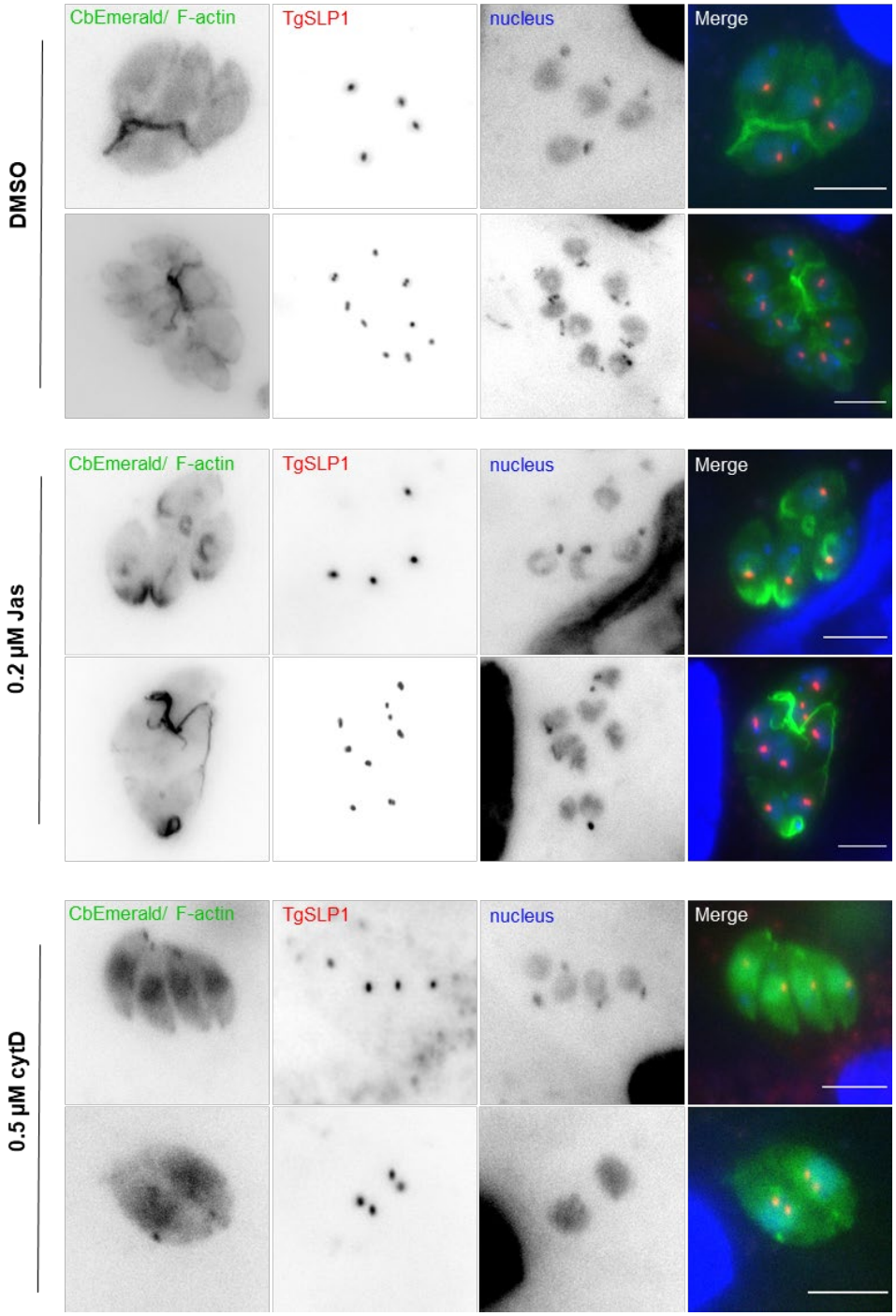

Fig. 5.23 The localisation of TgSLP1 is not influenced by actin remodelling drugs
TgSLP1 was fluorescently tagged in parasites expressing CbEmerald to visualise the F-actin network and were treated for 1 hour with either 0.5 µM cytochalasin D (cytD) to destabilise the F-actin network

or with 0.2 µM jasplakinolide (Jas) which has a stabilising effect on F-actin. As control, parasites were incubated in DMSO. Nuclei are stained with Hoechst. Scale bar: 5 µM.

5.4.4 Analysis of the conditional knockout of TgSLP1

5.4.4.1 TgSLP1 is essential for the survival of *T. gondii* tachyzoites

To investigate the role of TgSLP1 in *T. gondii*, the conditional knockout line was induced with 50 nM rapamycin. The viability of the conditional TgSLP1-KO parasites was tested by a plaque assay and no growth was detectable under induced conditions after seven days in culture (Fig. 5.24A), in good agreement with the low fitness score of -4.52 (Sidik et al., 2016). The plaque assay was additionally left in culture for 16 days. While wildtype and non-induced parasites completely lysed all cells, the induced TgSLP1-cKO parasites failed to form plaques (Fig. 5.24B).

Phenotypic analysis of individual *T. gondii* vacuoles was performed using an immunofluorescence assay to determine why parasites lacking TgSLP1 failed to grow. Immunoblot analysis demonstrates that the TgSLP1 signal was undetectable 48 hours post induction (Fig. 5.24C). Without TgSLP1, the parasites were deformed and it appeared that the nucleus failed to divide (Fig. 5.24C).

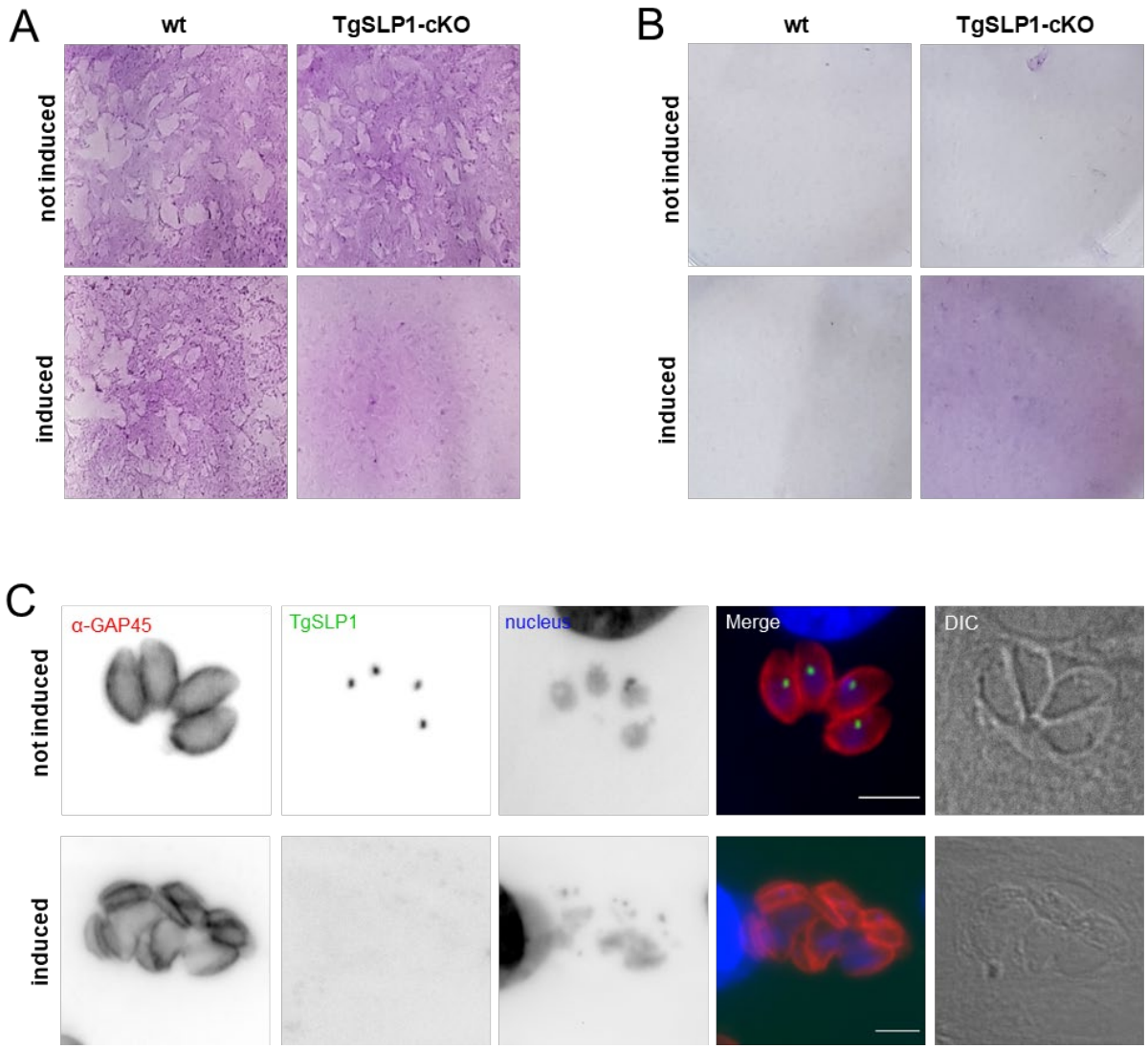

Fig. 5.24 Analysis of the conditional knockout mutant of TgSLP1
(A-B) Plaque assay shows that loss of TgSLP1 is strongly affecting parasite growth. 1000 parasites of the indicated strains were incubated on HFF cells for 7 days (A) or 16 days (B) either with 50 nM rapamycin (induced) or DMSO (not induced) and stained with Giemsa to visualise plaques. (C) Immunofluorescence analysis of the TgSLP1 conditional knockout line not induced or induced with 50 nM rapamycin for 48 hours. TgSLP1 cannot be detected under induced conditions. The shape of the parasites is visualised with α-GAP45 antibody, the nuclei are stained with Hoechst, DIC: differential interference contrast, scale bar: 5 µm.

5.4.4.2 TgSLP1 is essential for nuclear division in *T. gondii* tachyzoites

Nearly all vacuoles showed a strong defect in karyokinesis. While some parasites from one vacuole harbour an extremely enlarged nucleus, others lack nuclear DNA and only possess DNA from the apicoplast, which was also detected with Hoechst (Fig. 5.25, arrows). Some

vacuoles showed additional, severe nuclear missegregation with nuclear DNA outside the IMC (Fig. 5.25, arrowheads).

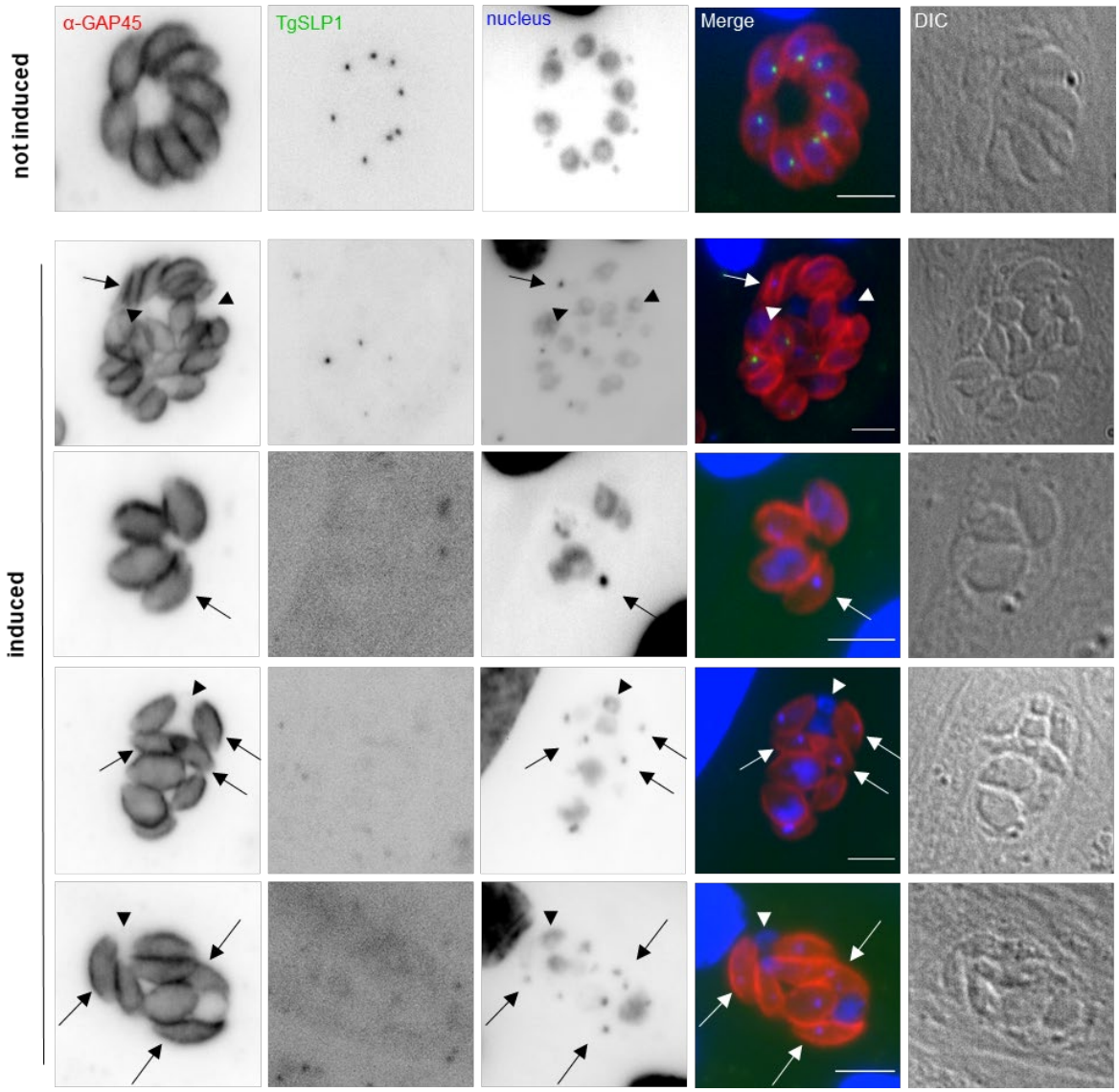

Fig. 5.25 Parasites lacking TgSLP1 have severe nuclear defects
Immunofluorescence analysis of the TgSLP1 conditional knockout line not induced or induced with rapamycin for 48 hours. Arrows mark parasites without nucleus; arrowheads mark a nucleus outside of the IMC. Parasite shape is visualised with α-GAP45 and the nuclei are stained with Hoechst. DIC: differential interference contrast, scale bar: 5 µm.

A quantification of the observations is shown in Figure 5.26. More than 90% of all vacuoles showed the strong defect in nuclear division after 48 hours of induction and almost 50% had extra nuclear DNA outside the IMC. The few remaining normal-shaped vacuoles still showed signal for TgSLP1, indicating that induction in these vacuoles failed or the time of induction was not sufficient. The fact that parasites could not form plaques under induced conditions even after 16 days indicates a delayed induction (Fig. 5.24B).

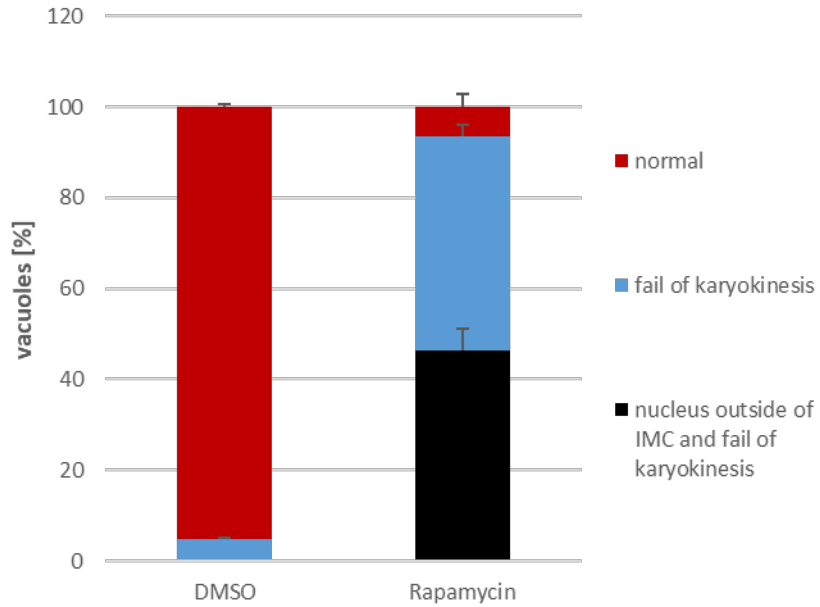

Fig. 5.26 Quantification of nuclear defects in parasites lacking TgSLP1
The diagrams show the quantification of vacuoles with nuclear loss and thus failed karyokinesis and vacuoles with additional nuclear DNA outside the IMC. 100 vacuoles were counted each under induced (50 nM rapamycin for 48 hours) and not induced (DMSO) conditions. The experiment was done in biological triplicates. Error bars indicate the standard deviation.

Interestingly, the deletion of TgSLP1 resulted in diffuse and disorganised localisation of the centrosome marker centrin1, indicating that TgSLP1 is a crucial part of the centrosome required for its integrity (Fig. 5.27).

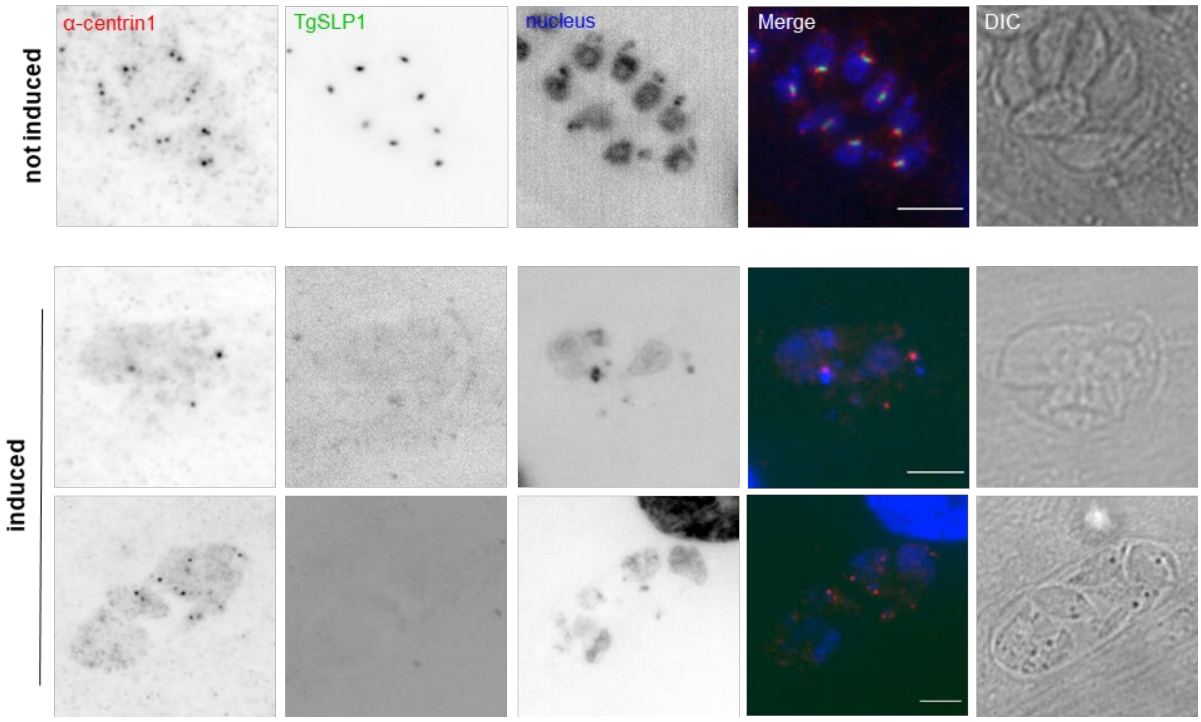

Fig. 5.27 The integrity of the centrosome is lost in parasites lacking TgSLP1
Immunofluorescence analysis of the TgSLP1 conditional knockout line not induced or induced with rapamycin for 48 hours. The centrosome of the parasites is visualised with α-centrin1 and the nuclei are stained with Hoechst. DIC: differential interference contrast, scale bar: 5 µm.

5.4.4.3 TgSLP1 is important for the localisation and the expression of the ESCRT III component VPS31

As shown in section 5.4.2.2, VPS31, a component of the ESCRT III complex colocalises with TgSLP1. The aim was to analyse the expression and localisation of VPS31 in *slp1*-depleted parasites. Parasites endogenously tagged with TgSLP1-sYFP2 and VPS31-3xHA were treated with rapamycin for 48 hours to excise *slp1* and immunofluorescence assay followed by microscopy was performed. Interestingly, the distribution of VPS31 between parasites of a vacuole was unequal in parasites lacking TgSLP1. In some individual parasites it was undetectable (Fig. 5.28, arrows) while in others it was still present as one dot, as in TgSLP1 expressing parasites (Fig. 5.28, induced, upper channel, arrowheads). In other vacuoles, the signal of VPS31 was either very diffuse (Fig. 5.28, induced, lower channel, arrowheads) or absent (Fig. 5.28, arrows).

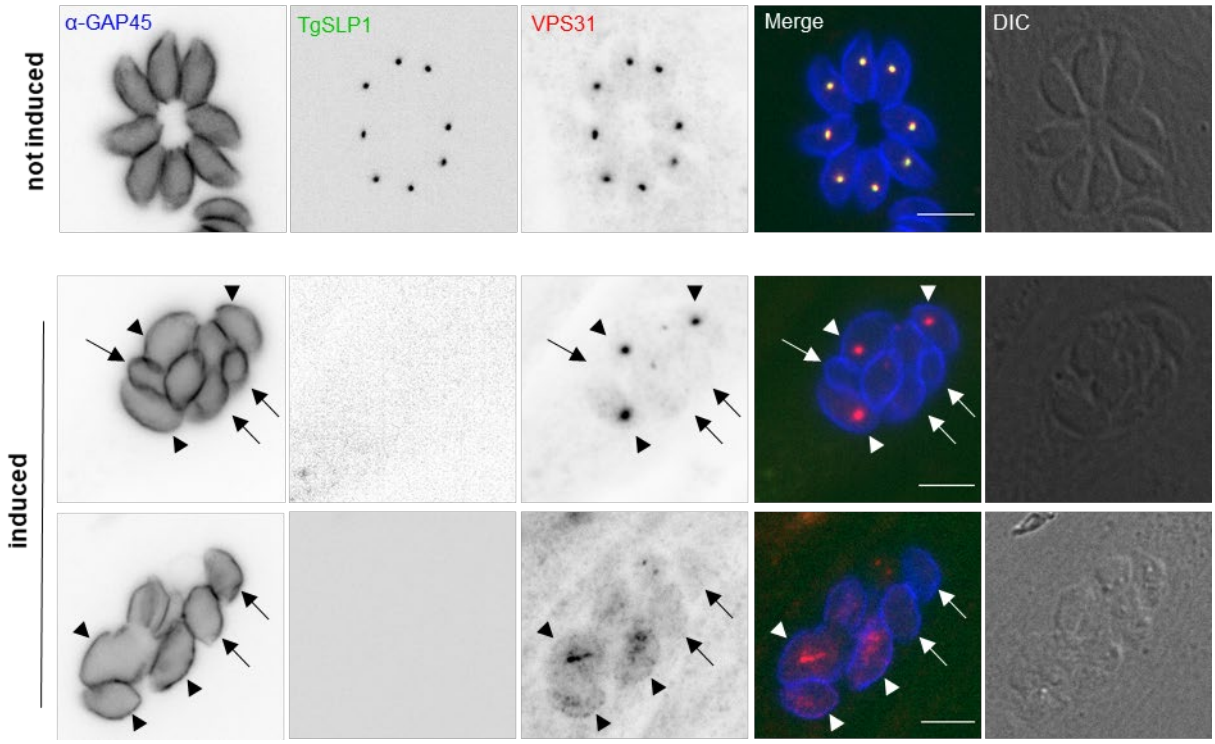

Fig. 5.28 TgSLP1 is important for the expression and localisation of VPS31
Immunofluorescence analysis of parasites endogenously tagged with VPS31-3xHA in the conditional knockout line TgSLP1-sYFP2. Arrows indicate individual parasites with no VPS31 expression, arrowheads show individual parasites either with normal VPS31 expression (induced, upper channel) or diffused VPS31 expression (induced, lower channel). Shape of the parasites is visualised with α-GAP45, VPS31 is visualised with α-HA. DIC: differential interference contrast, scale bar: 5 µm.

These observations and the colocalisation between the two proteins leads to the conclusion that TgSLP1 may be closely associated with VPS31. Nevertheless, further analysis such as pulldown experiments need to be performed to demonstrate a possible association between the ESCRT III complex and TgSLP1. Since this was not the aim here, it was not pursued further in this study.

5.4.4.4 Microtubular structure in *slp1*-depleted parasites

To analyse the effect of the *slp1* deletion on the microtubules, microscopy of parasites transiently expressing α-tubulin tagged with mCherry (Hu et al., 2002b) and TgSLP1-sYFP2 or of parasites endogenously tagged with TLAP4-mCherry and TgSLP1-sYFP2 was performed under induced and not induced conditions. As observed in the IFAs previously, the parasites exhibit a greatly altered shape after 48 hours of treatment with 50 nM rapamycin. Without

TgSLP1, some parasites from one vacuole are extremely swollen and possess a huge nucleus, whereas others from the same vacuole are small and do not have any nuclear DNA. In addition, the organisation and orientation of the parasites within the vacuole is disorganised (Fig. 5.29).

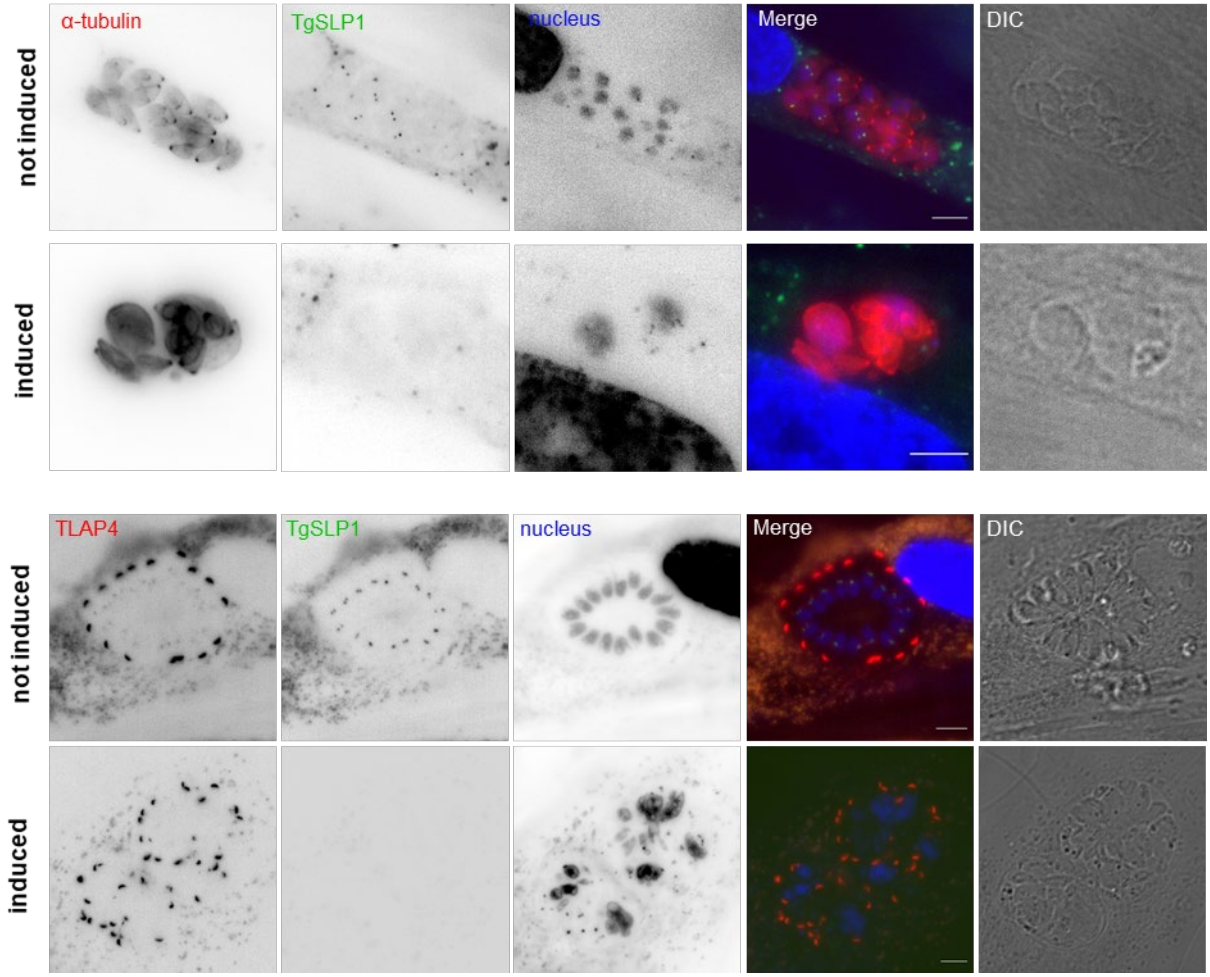

Fig. 5.29 Microtubular structures in parasites lacking TgSLP1
Immunofluorescence analysis of the microtubules in *slp1*-depleted parasites. Microtubules are labelled with either a transient expressed, fluorescently labelled α-tubulin or TLAP4, endogenously tagged with mCherry. Parasites were incubated either in DMSO (not induced) or with 50 nM rapamycin (induced) for 48 hours. Transiently expressed α-tubulin labels microtubular structures including the mitotic spindle, while endogenously tagged TLAP4 only marks the apical part of the cortical microtubules of mother and daughter cells. The nuclei are stained with Hoechst. DIC: differential interference contrast, scale bar: 5 µm.

5.4.4.5 Secretory organelles in *slp1*-depleted parasites

To observe the effect of *slp1* depletion on the secretory organelles of *T. gondii,* an immunofluorescence assay of GRA1, a dense granule protein, the rhoptry proteins ROP2,4 and the micronemal protein MIC2 was performed. Although the vacuoles are disorganised and parasites lacking TgSLP1 are extremely deformed, the secretory organelles and the secretory pathway appear to be unaffected and, as expected, do not appear to be the cause for parasite death in *slp1*-depleted parasites (Fig. 5.30).

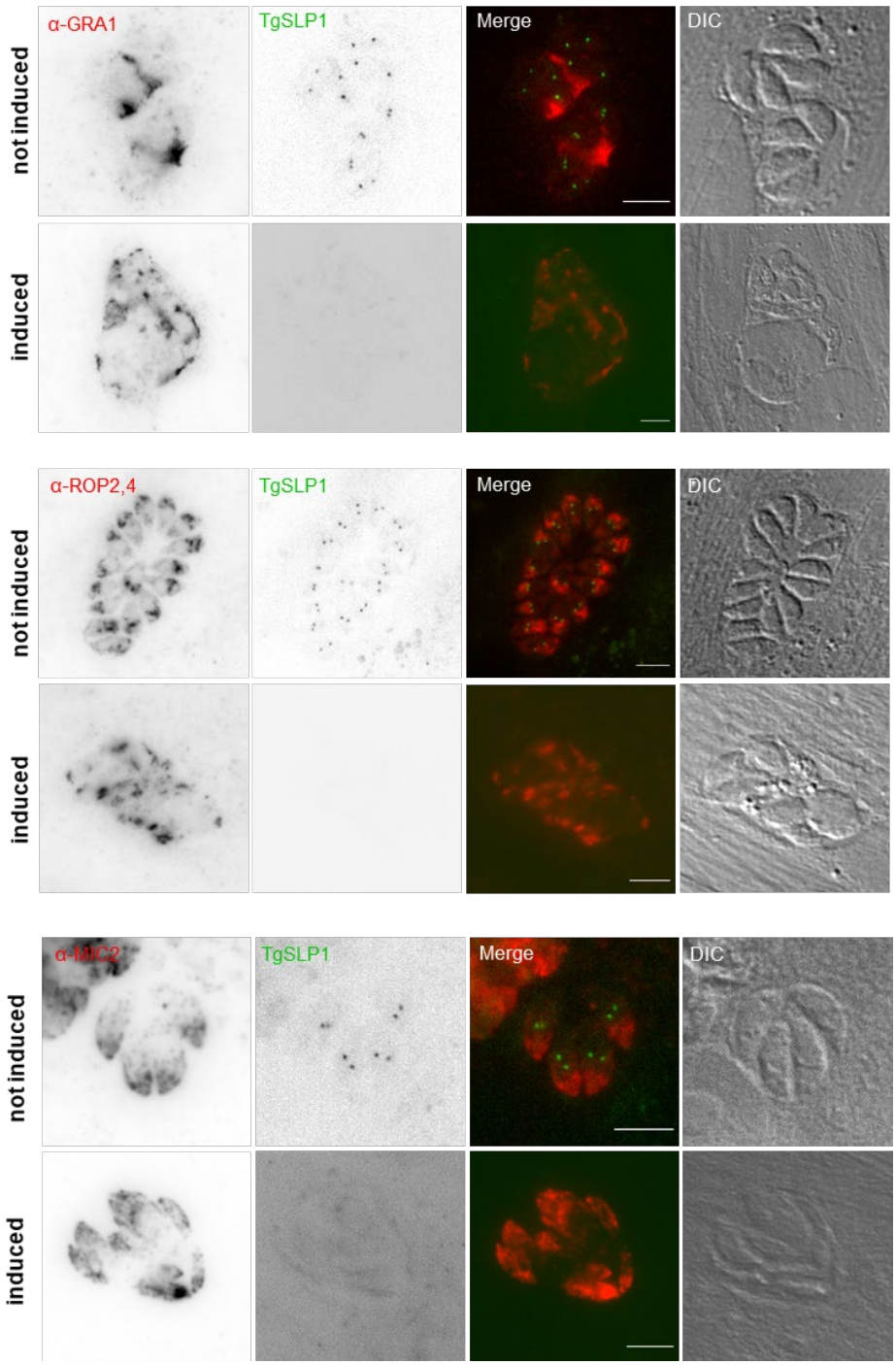

Fig. 5.30 Secretory organelles in *slp1*-depleted parasites
The IFA analysis shows that TgSLP1 downregulation does not affect the secretory organelles such as dense granules (α-GRA1), rhoptries (α-ROP2,4) and micronemes (α-MIC2), although the shape of the parasites is heavily altered under induced conditions as previously described. DIC: differential interference contrast, scale bar: 5 µm.

5.4.4.6 Mitochondria and apicoplast in *slp1*-depleted parasites

Similar to the secretory organelles, the mitochondria and the apicoplast were observed with antibodies in parasites lacking TgSLP1. The shape of both mitochondria and apicoplast does not appear to be greatly affected, and the distribution of these organelles is equal among parasites within a vacuole (Fig. 5.31).

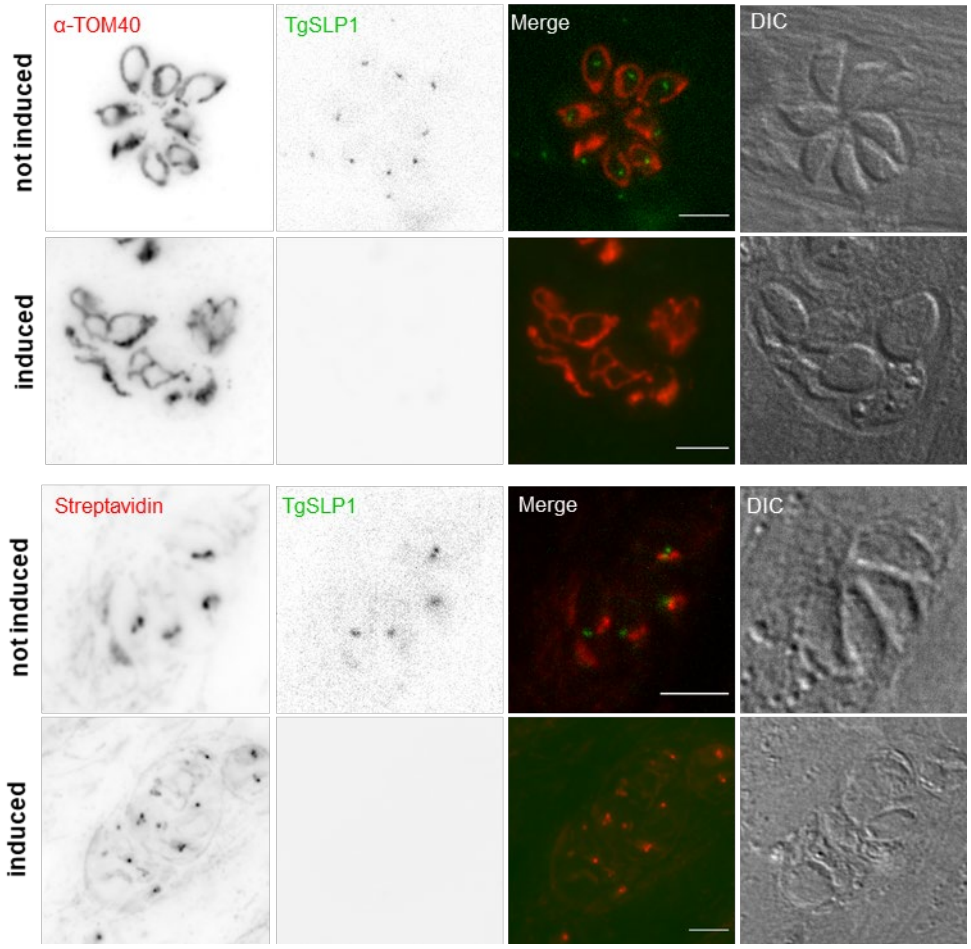

Fig. 5.31 Mitochondria and apicoplast in *slp1*-depleted parasites
IFA analysis shows that down regulation of TgSLP1 does not affect the mitochondria or the apicoplast, although the parasites are strongly deformed under induced conditions as previously described. The mitochondria are visualised with α-TOM40 antibody and the naturally biotinylated apicoplast is stained with a streptavidin conjugate. DIC: differential interference contrast, scale bar: 5 µm.

5.4.5 Proximity-dependent labelling of proteins (TurboID)

To identify interaction partners of TgSLP1, proximity labelling was used. To do this, a method called TurboID, an adapted version of the BioID system that is based on proximity-dependent labelling of proteins was used (Branon et al., 2018; Zhou et al., 2021). Similar to the fluorescent labelling, TgSLP1 was C-terminally tagged with TurboID using CRISPR/ Cas9 (Stortz et al., 2019). The correct integration of the tag was confirmed by PCR and sequencing.

Biotinylation of proteins was tested by immunofluorescence assay using a streptavidin conjugate. To this end, parasites were incubated with 150 µM biotin for 10 or 30 minutes or 4 hours or as a control, without biotin. After the time points, the samples were fixed with 4% PFA and stained with the streptavidin conjugate. Samples were stained with Hoechst to visualise nuclear and apicoplast DNA. The apicoplast is visible in the Hoechst stains as a small dot next to the nucleus (Fig. 5.32, arrowheads). While the naturally biotinylated apicoplast is visible in all samples (Fig. 5.32, arrowheads), TgSLP1 is only visible in the samples incubated with biotin (Fig. 5.32, arrows).

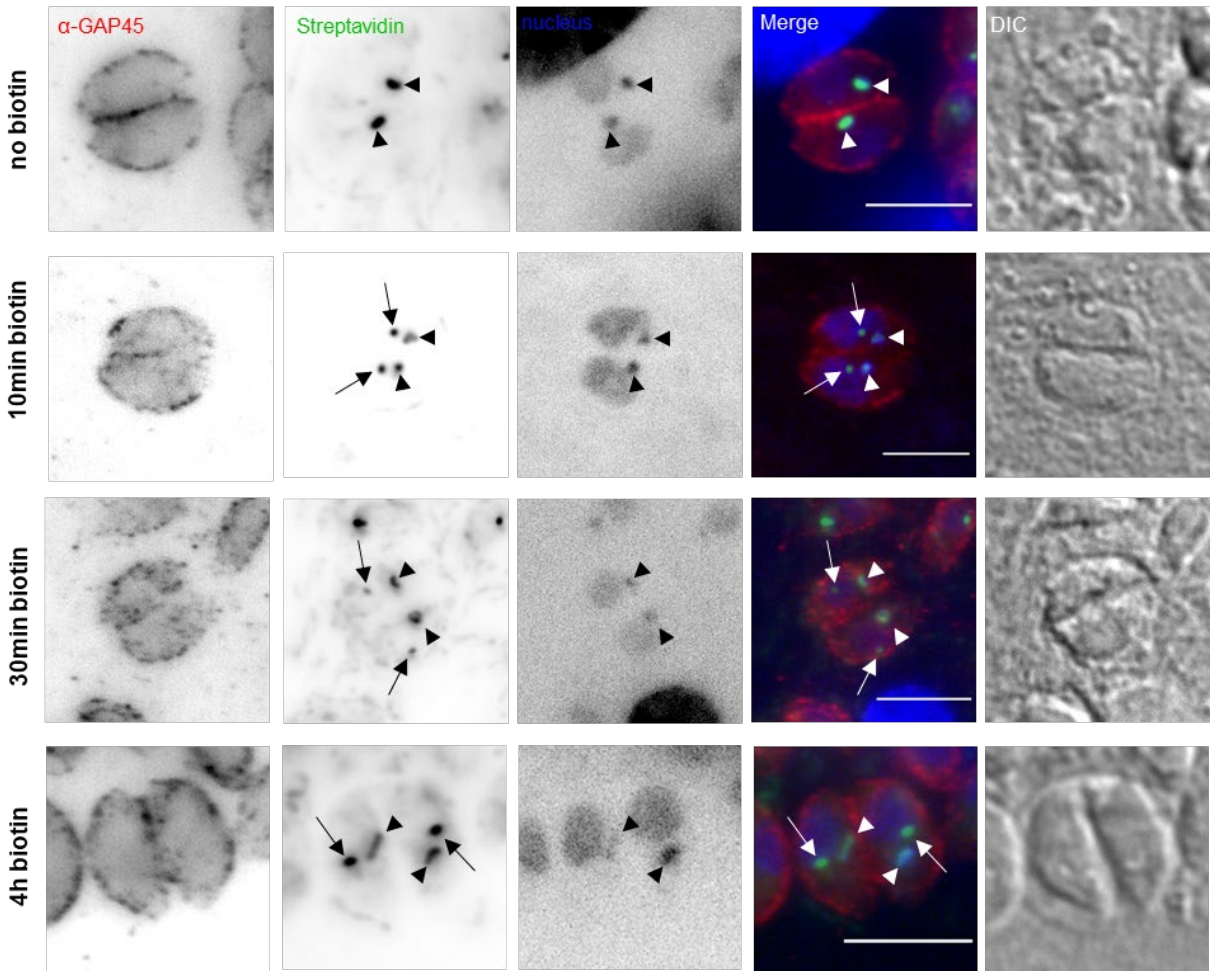

Fig. 5.32 Biotinylation of proteins was tested using a fluorescent streptavidin conjugate
The IFA shows endogenous tagged TgSLP1-TurboID parasites incubated without biotin or incubated with 150 µM biotin for 10 minutes, 30 minutes or 4 hours. After fixation, the parasites were treated with a streptavidin conjugate to visualise biotinylated proteins. Arrowheads point to the naturally biotinylated apicoplast which is visible in all samples, whereas TgSLP1 is only detectable in the samples incubated with biotin (arrows). The shape of the parasites is visualised with α-GAP45 antibody and the nuclei including the apicoplast are stained with Hoechst. DIC: differential interference contrast. Scale bar: 5 µm.

Although biotinylated proteins could be detected after 10 minutes of incubation, the experiment was performed using 4 hours of incubation, in order to identify more proteins during the limited expression time of TgSLP1. Whole cell lysates from purified parasites were loaded onto an SDS-gel and western blot analysis was performed to detect differences in the degree of biotinylation. While biotinylated proteins were detectable in all cell lysates, the TgSLP1-TurboID sample incubated with biotin showed an increased level of biotinylated proteins compared to the other samples (Fig. 5.33).

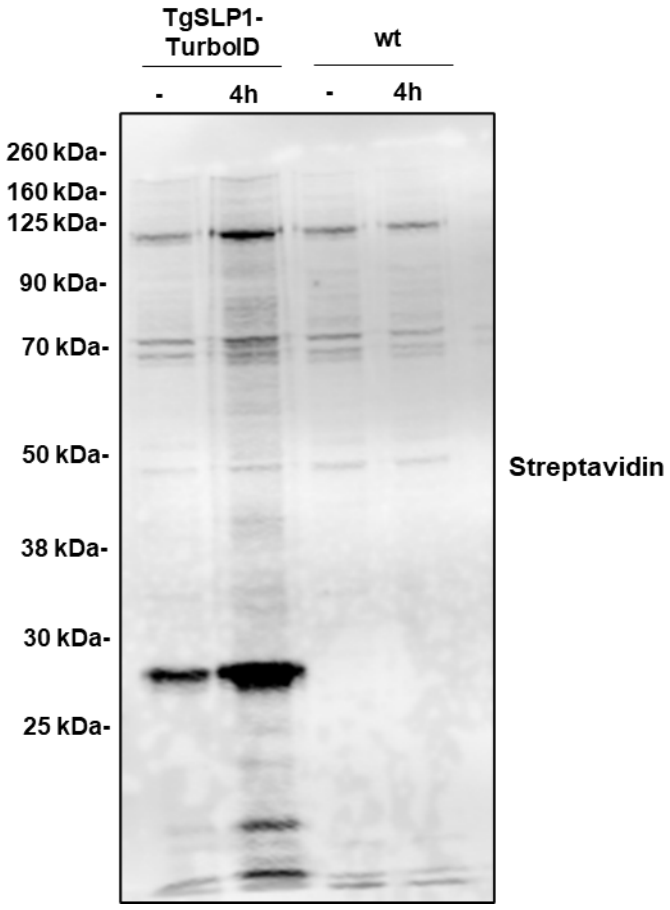

Fig. 5.33 Detection of biotinylated proteins from whole parasite lysates
Western blot analysis of biotinylated proteins in the wildtype and the TgSLP1-TurboID parasite line with and without addition of 150 µM biotin for 4 hours. To detect biotinylated proteins, Streptavidin IRDye 800CW was used.

To purify biotinylated proteins, immunoprecipitation experiments were performed using magnetic streptavidin beads and the eluate was sent for mass spectrometry. For this purpose, intracellular wildtype and TgSLP1-TurboID parasites were incubated with 150 µM biotin for 4 hours, harvested and purified from the host cells. 5% each of the input, flow-through, first wash and eluate of the pull-down experiment were loaded on an SDS-gel and western blot analysis was performed using a streptavidin conjugate to visualise biotinylated proteins. While the wildtype sample did not contain many biotinylated proteins, the eluate from TgSLP1-TurboID parasites showed protein bands of different sizes (Fig. 5.34).

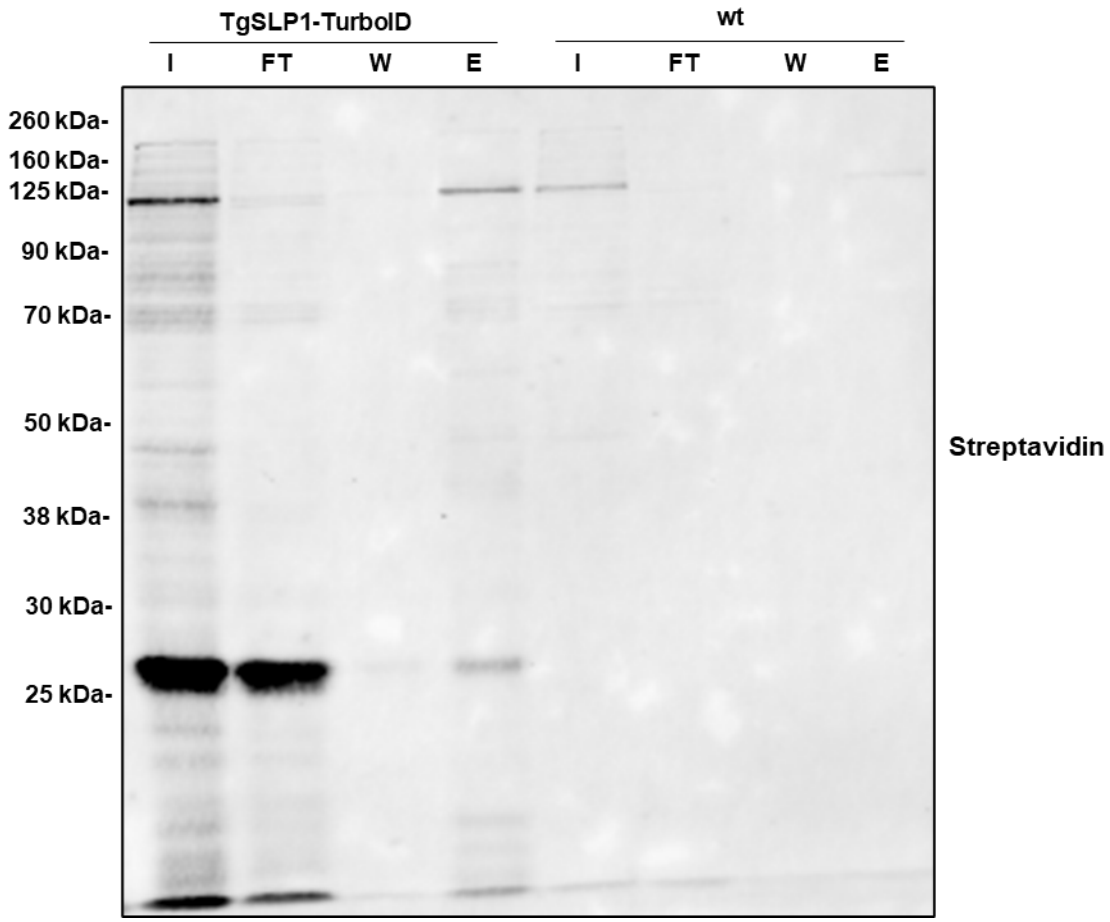

Fig. 5.34 Immunoprecipitation of biotinylated proteins in wildtype and TgSLP1-TurboID parasites
Western blot analysis on the different fractions of immunoprecipitation performed on the wildtype (wt) and TgSLP1-TurboID parasites after incubation with 150 µM biotin for 4 hours. I: Input, FT: Flow-through, W: 1st Wash, E: Eluate. Biotinylated proteins were detected using Streptavidin IRDye 800CW.

The eluates were analysed by mass spectrometry from the Glasgow Polyomics facility. Two major biotinylated proteins were detected in both samples (wildtype and TgSLP1-TurboID), the acetyl-CoA carboxylase ACC1, an apicoplast protein and the mitochondrial pyruvate carboxylase. These two proteins were described to contain biotin (Zuther et al., 1999; Jelenska et al., 2001), indicating that the experiment basically worked. Unexpectedly, TgSLP1 was not pulled out. Some proteins were only detected in the TgSLP1-TurboID sample, those with a mascot probability score (Score MS) of more than 20 and which were identified by more than two peptides are listed in Table 5.1 including the phenotypic scores based on the genome-wide screen by Sidik and colleagues and the LOPIT localisation predictions from the study by Barylyuk and colleagues (Sidik et al., 2016; Barylyuk et al., 2020).

Table 5.1 List of mass spectrometry results from the TgSLP1-TurboID pull-down
Gene IDs, descriptions of the respective genes from ToxoDB, mascot probability score (Score MS), phenotypic score based on the genome-wide CRISPR/ Cas9 screen (Sidik et al., 2016) and the LOPIT localisation prediction (Barylyuk et al., 2020) are shown.

Gene ID		Score MS	Phenotypic score	LOPIT
TGGT1_231640	alveolin domain containing intermediate filament IMC1	195	-4	IMC
TGGT1_271050	SAG-related sequence SRS34A	168	1.72	Plasmamembrane, peripheral 1
TGGT1_309590	rhoptry protein ROP1	122	1.59	Rhoptries
TGGT1_240590	DNA-directed RNA polymerase II RPB5	108	-5.78	40S ribosome/ Nucleus- non-chromatin
TGGT1_261250	histone H2A1	98	-3.39	Nucleolus
TGGT1_284180	hypothetical protein	45	-2.68	no data
TGGT1_251870	histone H2Bb	44	1.72	Nuclear, chromatin
TGGT1_239260	histone H4	39	-4.81	Nuclear, chromatin
TGGT1_245720	SWI2/SNF2-containing protein	39	-0.25	Endomembrane vesicles
TGGT1_305620	hypothetical protein	35	-3.78	no data
TGGT1_210690	ribosomal protein RPS6	34	-4.58	40S ribosome
TGGT1_291830	putative DNA double-strand break repair rad50 ATPase	26	1.33	no data
TGGT1_210815	hypothetical protein	23	1.55	no data
TGGT1_309300	SAG-related sequence SRS55A	23	-0.35	no data

Some of the proteins detected by mass spectrometry are not expected to be in close association with TgSLP1 (IMC1; SAG-related sequence SRS34A; ROP1; DNA-directed RNA polymerase II RPB5; ribosomal protein RPS6; SAG-related sequence SRS55A) and were therefore excluded. Also the histones, the SWI2/SNF2-containing protein and the putative DNA double-strand break repair rad50 ATPase were excluded. The hypothetical proteins could be interesting candidates as SUN-binding partners. A potential KASH-like protein is expected to be important for parasite fitness, hence the protein with the positive phenotypic score of 1.55 (TGGT1_210815) can also be excluded. Only the two hypothetical proteins with negative phenotypic scores (TGGT1_284180, -2.68 and TGGT1_305620, -3.78) could be interesting candidates as they have not been previously described. Unfortunately, no LOPIT localisation data are available for these proteins. Since TgSLP1 was not detected in the pull-down and the

experiment was only performed once, there is no guarantee that the experiment worked properly. In order to reproduce the results, it is necessary to perform the experiment in at least triplicates.

5.5 Identification of potential KASH domain proteins

By performing standard homology searches, it was not possible to identify any KASH domain protein in *T. gondii* or other apicomplexan parasites. The reason for this could be either the complete absence or a very low sequence similarity with opisthokont KASH domain proteins as it is the case in plants (Zhou et al., 2012; Meier et al., 2016). A study from 2014 developed a computational method to identify plant KASH proteins based on the similarities between opisthokont KASH proteins and WPP domain-interacting proteins, which until then were the only known KASH proteins in plants (Zhou et al., 2014). The algorithm, called DORY, searches for protein sequences that fulfil certain properties of known KASH domains. These are: immediately at the C-terminus of a transmembrane domain, between 9 and 40 amino acids in length, being the C-terminus of a protein and terminating in four amino acids with the specific pattern PPPX (Zhou et al., 2014). This specific pattern has been shown to be crucial for interacting with the SUN domain in opisthokonts (Padmakumar et al., 2005). Using this algorithm on the genome of *Toxoplasma gondii* strain GT1 (ToxoDB-50_TgondiiGT1_annotatedproteins.fasta; Gajria et al., 2008), two potential KASH-like proteins could be identified. Both are annotated as hypothetical proteins (TGGT1_279360 and TGGT1_321410) and have been further characterised as described in this chapter.

5.5.1 The potential KASH domain protein TGGT1_279360

The hypothetical protein TGGT1_279360 was identified as a potential KASH domain protein by the DORY program (Zhou et al., 2014). The phenotypic score from the CRISPR/ Cas9 screen (Sidik et al., 2016) is -5.12, hence the protein is predicted to have negative effects on the parasite fitness. Although the protein appears to be expressed in tachyzoites (Hassan et al., 2017), the protein is not listed in the subcellular localisation prediction from Barylyuk et al. from 2020. It has one transmembrane domain and the putative KASH tail sequence contains

the specific amino acid pattern PPPX, which has been shown to be essential for binding the SUN domain in mammalian cells (Padmakumar et al., 2005).

The protein was C-terminally tagged with mCherry and 3xHA using CRISPR/ Cas9 (Stortz et al., 2019) and the correct integration of the tag was verified by PCR and sequencing (Fig. 5.35).

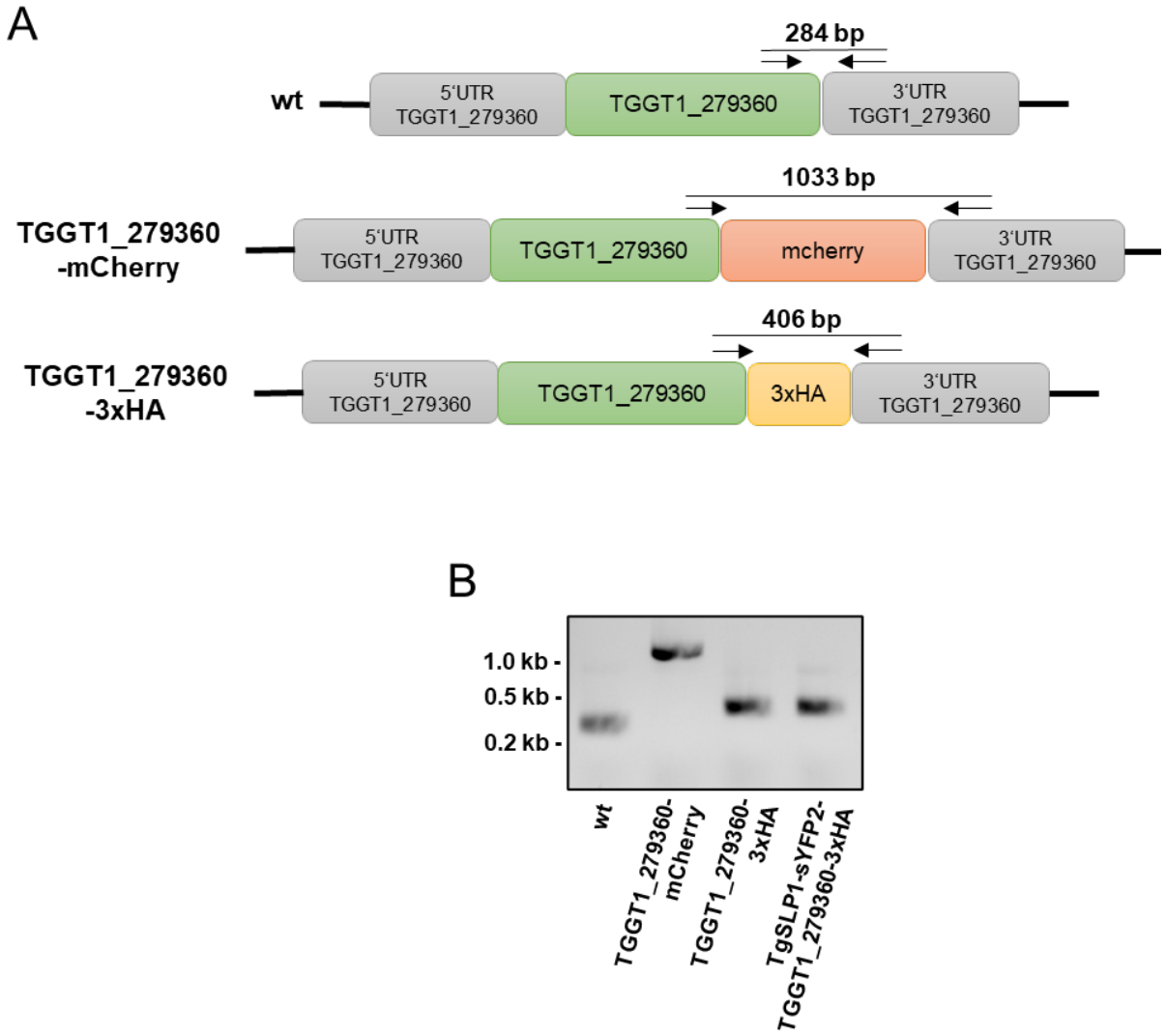

Fig. 5.35 Generation and confirmation endogenously tagged parasite lines of TGGT1_279360
(A) Schematic overview of wildtype (wt) and C-terminal mCherry or 3xHA tagged parasite lines of TGGT1_279360. (B) PCR analysis confirms the correct integration of the tags. Primer positions and length of PCR products are indicated in (A).

The localisation of TGGT1_279360 within the parasite was analysed using an immunofluorescence assay, showing that the protein is localised close to the nucleus (Fig. 5.36).

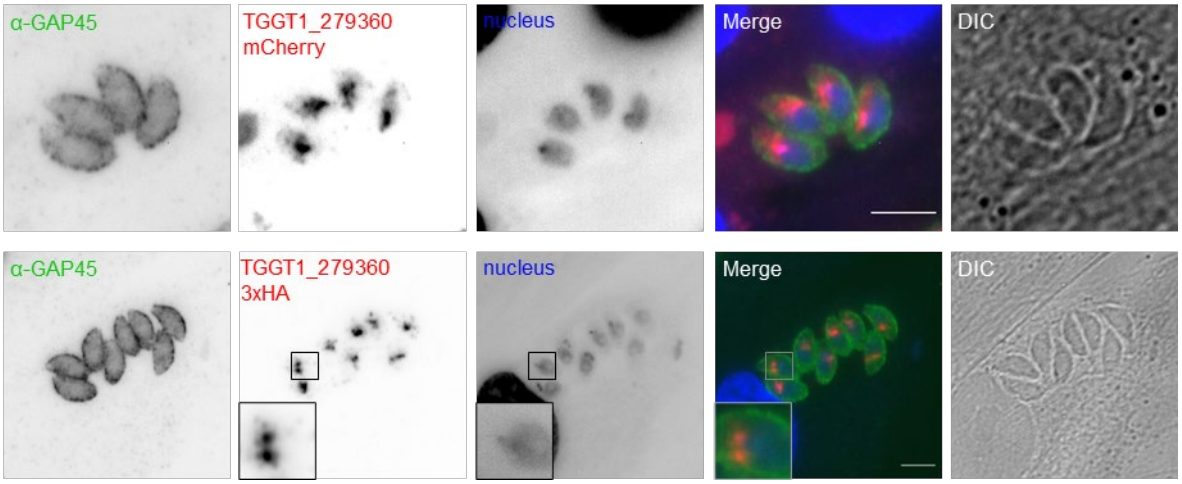

Fig. 5.36 Analysis of the localisation of TGGT1_279360
Immunofluorescence assay of transgenic TGGT1_279360-mCherry or TGGT1_279360-3xHA parasites shows a distinct localisation close to the nucleus. The shape of the parasites is visualised with an α-GAP45 antibody, the nuclei are stained with Hoechst and the 3xHA tag is visualised with an α-HA antibody. DIC: differential interference contrast, scale bar: 5 µm.

Additionally, live cell imaging was performed with the fluorescent tagged parasite line and, interestingly, the localisation of TGGT1_279360 between the vacuoles was not consistent. In some parasites, it appeared as a clear, distinct structure near the nucleus as in fixed parasites (Fig. 5.37, upper channel) while in others, TGGT1_279360 is localised as a diffuse, stippled pattern and appears to migrate in vesicles through the parasite (Fig. 5.37, lower channel).

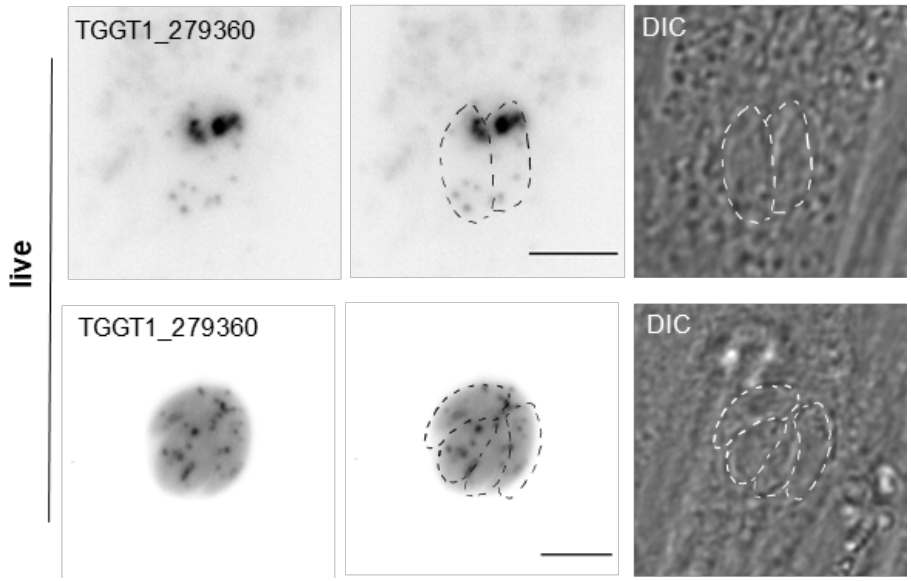

Fig. 5.37 Analysis of the localisation of TGGT1_279360 in live parasites

TGGT1_279360-mCherry parasites were imaged using live cell microscopy. Two different patterns of the proteins in different vacuoles could be observed. The outlines of the parasites are indicated with dashed lines. DIC: differential interference contrast, scale bar: 5 µm.

To compare the localisation of TGGT1_279360 with the SUN domain protein TgSLP1, TGGT1_279360 was endogenously tagged with a 3xHA tag in the TgSLP1-sYFP2 parasite line. Similar to the other parasite lines, the correct integration of the tag was verified by PCR and sequencing (Fig. 5.35). Although TGGT1_279360 seems to localise close to TgSLP1 in most of the vacuoles, there is no colocalisation observable between the two proteins (Fig. 5.38).

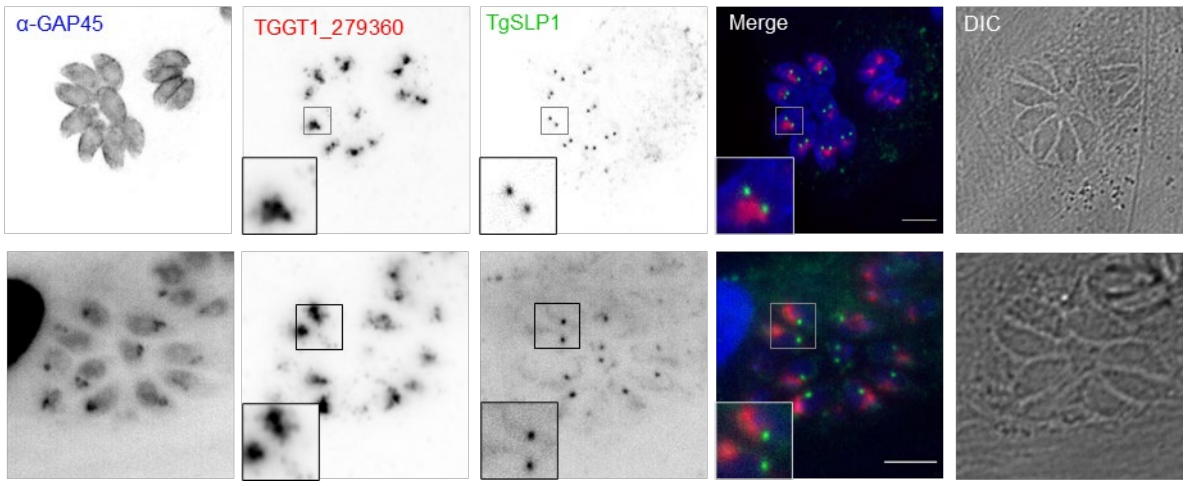

Fig. 5.38 There is no colocalisation between TGGT1_279360 and TgSLP1
TGGT1_279360 was endogenously tagged with 3xHA in the TgSLP1-sYFP2 parasite line and an immunofluorescence assay was performed. The shape of the parasites is visualised with an α-GAP45 antibody and the 3xHA tag is visualised with an α-HA antibody. DIC: differential interference contrast, scale bar: 5 µm.

Our observations suggest that the protein is localised to the Golgi or ER rather than the nucleus. However, to confirm this hypothesis, further colocalisation analyses with marker proteins would have to be performed. To be a suitable KASH domain protein candidate, TGGT1_279360 would have to interact with TgSLP1 and thus localise at the same position in the parasite. For this reason, this protein was not analysed further in this study.

5.5.2 The potential KASH domain protein TGGT1_321410

The second protein that was identified by the DORY algorithm is a hypothetical protein and was referred to as TGGT1_321410. With a phenotypic score of -2.2, the genome-wide screening suggests that the protein is important for the parasite fitness (Sidik et al., 2016). The subcellular localisation prediction from the LOPIT study by Barylyuk et al. in 2020, suggests the protein to localise at the nucleus (chromatin) or on the internal/ cytosolic leaflet of the plasma membrane, depending on the prediction algorithm used. Similar to TGGT1_279360, it has a transmembrane domain.

To find out the subcellular localisation of TGGT1_321410, it was C-terminally tagged with mCherry using CRISPR/ Cas9 (Stortz et al., 2019) and the integration of the tag was confirmed by PCR and sequencing. To analyse the localisation with regard to TgSLP1, TGGT1_321410 was also tagged in the TgSLP1-sYFP2 parasite line (Fig. 5.39).

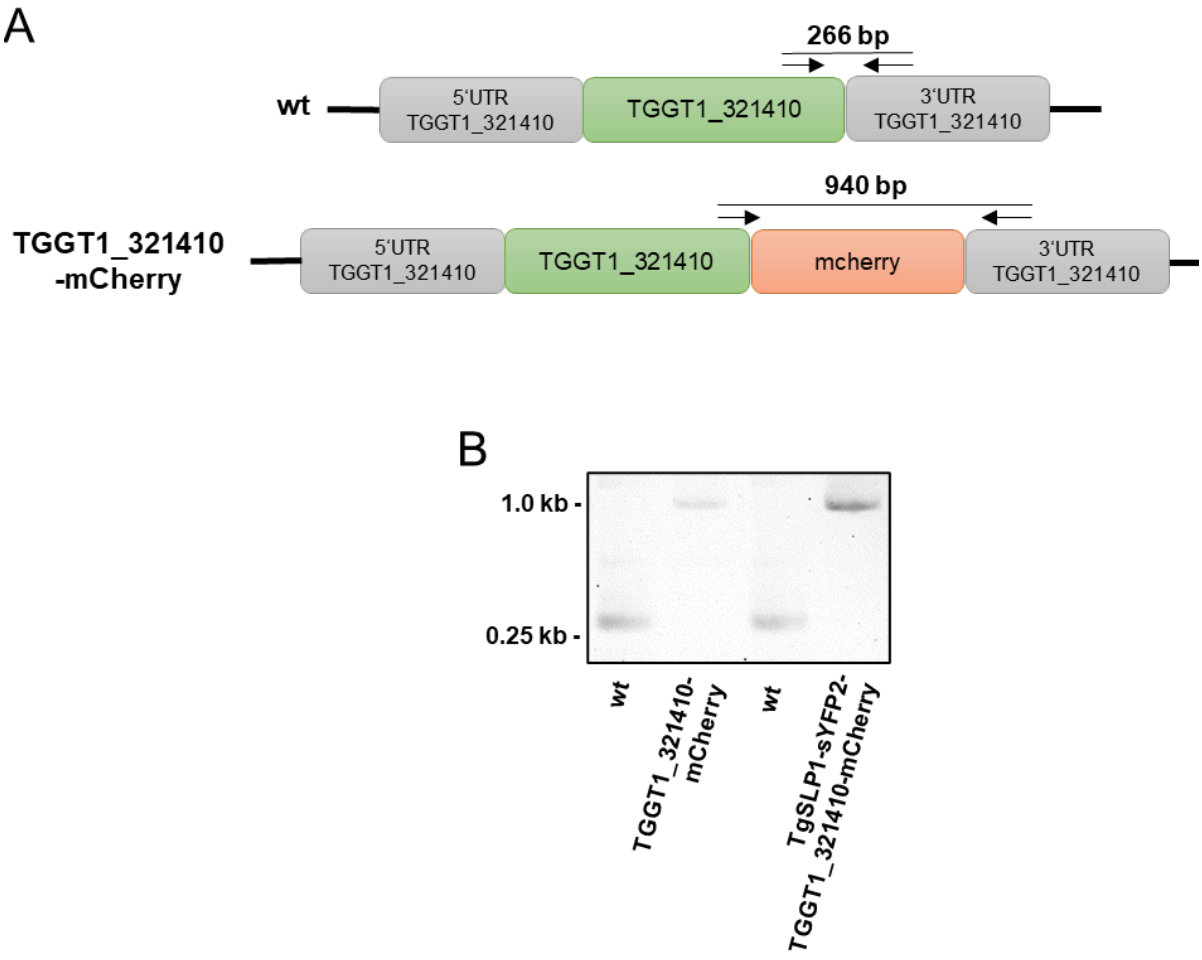

Fig. 5.39 Generation and confirmation endogenously tagged parasite lines of TGGT1_321410
(A) Schematic overview of wildtype (wt) and C-terminal mCherry tagged parasite lines of TGGT1_321410. (B) PCR analysis confirms the correct integration of the tags. Primer positions and length of PCR products are shown in (A).

To determine the localisation of TGGT1_321410 in *T. gondii* tachyzoites, an immunofluorescence assay was performed. Similar to the other potential KASH domain protein, TGGT1_279360, TGGT1_321410 localises as a clear structure close to the nucleus.

Although TgSLP1 seems to localise close to TGGT1_321410 in some vacuoles, there is no colocalisation between the two proteins visible (Fig. 5.40).

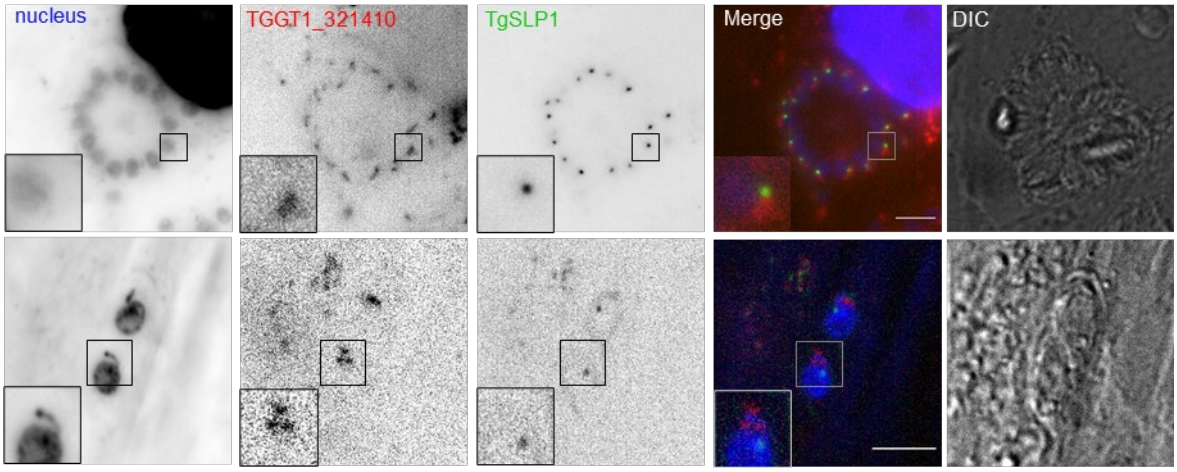

Fig. 5.40 IFA shows no colocalisation between TGGT1_321410 and TgSLP1
TGGT1_321410 was endogenously tagged with mCherry in the TgSLP1-sYFP2 parasite line and an immunofluorescence assay was performed. The 3xHA tag is visualised with an α-HA antibody, the nuclei are stained with Hoechst. DIC: differential interference contrast, scale bar: 5 µm.

The protein seems to localise at the Golgi which was confirmed with a transiently expressed marker for the trans-Golgi network (GalNac; Nishi M., 2008, unpublished; Fig. 5.41).

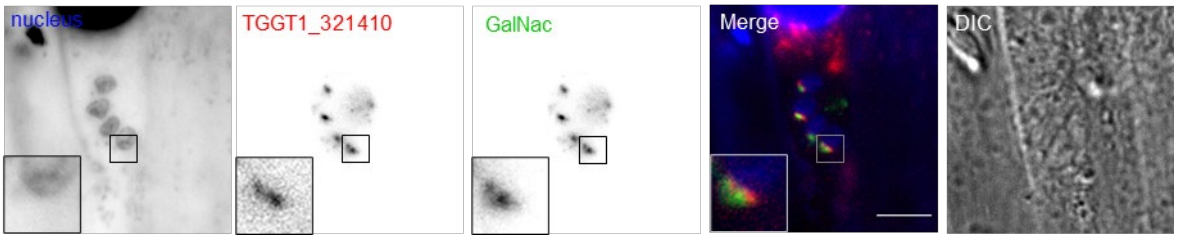

Fig. 5.41 TGGT1_321410 colocalises with the Golgi apparatus
A fluorescent tagged marker of the trans-Golgi network (GalNac) was transiently expressed in parasites that were endogenously tagged with mCherry at the C-terminus of TGGT1_321410. The 3xHA tag is visualised with an α-HA antibody, the nuclei are stained with Hoechst. DIC: differential interference contrast, scale bar: 5 µm.

TGGT1_321410 seems to localise to the parasite's Golgi apparatus. However, the aim was to find a potential KASH-like binding partner for the SUN-like protein TgSLP1. Since TGGT1_321410 does not colocalise with TgSLP1, it was not pursued further in this study.

6 Discussion

6.1 Nuclear-cytoskeletal connections in apicomplexan parasites

The connection between the nucleus and the cytoskeleton is central to maintain a variety of cellular processes, including transmission of mechanical forces across the nuclear envelope during cell migration and the attachment of the centrosome to the nucleus during cell division. In metazoans, plants and single cell organisms like yeast, the cytoskeletal-nuclear bridge involves the LINC complex that is comprised of SUN domain proteins at the inner nuclear membrane, interacting with nuclear lamins and KASH domain proteins at the outer nuclear membrane, interacting with cytoskeletal elements such as actin (Padmakumar et al., 2005; Crisp et al., 2006).

LINC complexes and its components have been found and characterised in most eukaryotes. To date, there is no LINC complex described in apicomplexan parasites, however, comparable processes have been observed. In migrating cells, the LINC complex appears to play a role in moving the nucleus through confined spaces (McGregor et al., 2016). A recent study on the apicomplexan parasite *T. gondii* described F-actin dynamics during invasion of host cells and demonstrated a meshwork of F-actin surrounding the nucleus, facilitating nuclear deformation and protection during the invasion process (Del Rosario et al., 2019). This observation has disproved the assumption that F-actin exclusively acts in the space between the IMC and the PM (Del Rosario et al., 2019; Frénal et al., 2017) and suggests that F-actin plays an important role during invasion, similar to the squish and squeeze model that has been proposed in other migrating eukaryotes (McGregor et al., 2016; Del Rosario et al., 2019).

In this study, the two SUN domain proteins TgSLP1 and TgSLP2 and the UNC-50 domain protein TgUNC1 were identified in the genome of the apicomplexan parasite *T. gondii.* Moreover, two proteins being potential KASH-like candidates (TGGT1_279360; TGGT1_321410) were identified using an algorithm called DORY, which was originally programmed to identify non-canonical KASH-like proteins in plants (Zhou et al., 2012).

6.2 TgUNC1 localises at the Golgi apparatus and is not essential for *T. gondii* survival

TgUNC1 differs from the other two Sad1/ UNC family proteins existing in *T. gondii*. It has an UNC-50 domain and multiple annotated transmembrane domains.

Homologues were identified and characterised earlier in the nematode *C. elegans,* yeast and mammals (Lewis et al., 1987; Chantalat et al., 2003; Fitzgerald et al., 2000). Worms lacking *unc-50* have defects in movement and it appears that UNC-50 promotes transport of assembled acetylcholine receptors to the cell surface (Lewis et al., 1987). The yeast homologue *GMH1* is dispensable for vegetative growth. It is an integral membrane protein localised in the Golgi that plays a role in ARF GTPase dependent transport vesicle budding and sorting (Chantalat et al., 2003). In mammals, UNCL is an inner nuclear membrane RNA-binding protein that localises to the ER and the inner nuclear membrane where it is involved in cell surface expression of neuronal nicotinic receptors (Fitzgerald et al., 2000).

The results show that TgUNC1 is localised to the Golgi network of the parasite, where it appears to play no critical role for asexual parasite growth and Golgi architecture. The localisation agrees with the prediction from the hyperLOPIT study (Barylyuk et al., 2020). Despite the negative phenotypic score of -2.26 (Sidik et al., 2016), parasites lacking TgUNC1, seem not to have an impairment in fitness, when grown *in vitro.* A possible explanation could be the different setting of the experiments. While TgUNC1-KO parasites were not in competition with other parasite lines in the present study, parasites in the CRISPR/ Cas9 screening were grown in parasite pools consisting of different mutants. After different time points, genomic DNA was isolated and sequenced to determine which mutants survived (Sidik et al., 2018). Mutants with a slight growth defect are displaced by other, normally growing parasites. These slight growth defects may not be noticed in a pure clonal culture. This hypothesis could be tested with in a competition assay with wildtype parasites.

The subcellular localisation and the observation that TgUNC1 is dispensable for normal parasite morphology and growth led us to conclude that this protein is not a good candidate for being a member of an apicomplexan LINC complex and therefore it was not pursued further in this study.

6.3 The SUN-like protein TgSLP2

One of the SUN-like proteins identified in the genome of *T. gondii* was referred to as TgSLP2. Because of the unspecific, punctuated localisation through the whole parasite, the question arose whether TgSLP2 might localise to the F-actin network. It was not possible to test this with the available tools due to a cross-reaction between the α-HA antibody and the F-actin-binding chromobody. Instead, the effect of actin stabilising and destabilising drugs on TgSLP2 was tested and no impact on the expression or localisation of TgSLP2 could be observed.

The SUN domain of TgSLP2 is located in the middle of the protein. “Mid-SUN” proteins have been characterised in *A. thaliana* (AtSUN3 and AtSUN4; Graumann et al., 2014) and in mice (Opt; Sohaskey et al., 2010). AtSUN3 and AtSUN4 localise to the nuclear envelope and the ER. In *A. thaliana,* both C-term SUN and mid-SUN domain proteins have been shown to interact with each other, as well as with the KASH domain protein AtWIP1, and are involved in a protein complex network at the nuclear envelope that is reminiscent of the LINC complex found in other species (Graumann et al., 2014). In mice, the mid-SUN protein Opt is localised to the ER and may act as an adaptor protein connecting the rough ER to the cytoskeleton (Sohaskey et al., 2010). The subcellular localisation prediction from the LOPIT study suggests that TgSLP2 localises to the ER (Barylyuk et al., 2020). Based on the observations in the immunofluorescence assays, the *T. gondii* mid-SUN protein TgSLP2 might indeed partially colocalise with the ER. This would have to be verified by colocalisation analysis with ER marker proteins.

So fat it has not been possible to generate a conditional knockout mutant of TgSLP2. Based on the negative phenotypic score of -3.86 suggested from the CRISPR/ Cas9 genome-wide screen (Sidik et al., 2016), it was hypothesised that the protein might be essential and therefore the genomic locus is susceptible for genomic modifications.

In a recent study, a method called splitCas9 was adapted to *T. gondii* by creating parasites that express two separate subunits of the Cas9 enzyme fused to either an FKBP or a FRB domain. The two domains interact upon addition of rapamycin and Cas9 activity is restored. Using this parasite line, specific genes can be knocked down by induction with rapamycin in parasites expressing an sgRNA binding within the particular gene (Li et al., 2022). This method could be used to generate a knockdown mutant of TgSLP2.

Due to problems in generating a conditional knockout mutant and based of the observations made in this study, it was determined that TgSLP2 is not a good candidate to be a member of an apicomplexan LINC complex. Therefore, the characterisation of this protein was not pursued further. However, there is insufficient information to definitively rule out TgSLP2 as part of a nuclear-cytoskeletal bridge complex.

6.4 TgSLP1 localises to the mitotic spindle and is essential for nuclear division and parasite survival

This study shows that TgSLP1 is a member of the SUN domain family in the apicomplexan parasite *T. gondii* and provides evidence that it is essential for cell division in the tachyzoite stage. TgSLP1 localises to the mitotic spindle and seems to be closely associated to the centrosome during the asexual division cycle of *T. gondii.* Parasites lacking TgSLP1 show a severe defect in centrosome integrity and nuclear segregation. A schematic representation of how TgSLP1 might be involved in endodyogeny and what consequences a lack of this protein has for the parasites is shown in Figure 6.1. The centrosome (Fig. 6.1, yellow) localises at the outer nuclear membrane outside of the nucleus. The mitotic spindle (Fig. 6.1, red) localises in the perinuclear space between the outer and inner nuclear membrane. In G1-phase, there is no TgSLP1 detectable in immunofluorescence assay. When division starts, in early S-phase, the centrosome divides and TgSLP1 (Fig. 6.1, green) appears. The mitotic spindle divides and so does TgSLP1 in the following late S-phase and mitosis. Later in cell division, when daughter cells emerge within the mother parasite, TgSLP1 starts to disappear.

In parasites lacking TgSLP1, the centrosome and the mitotic spindle appear to mislocalise and nuclear division is completely disorganised (Fig. 6.1, right).

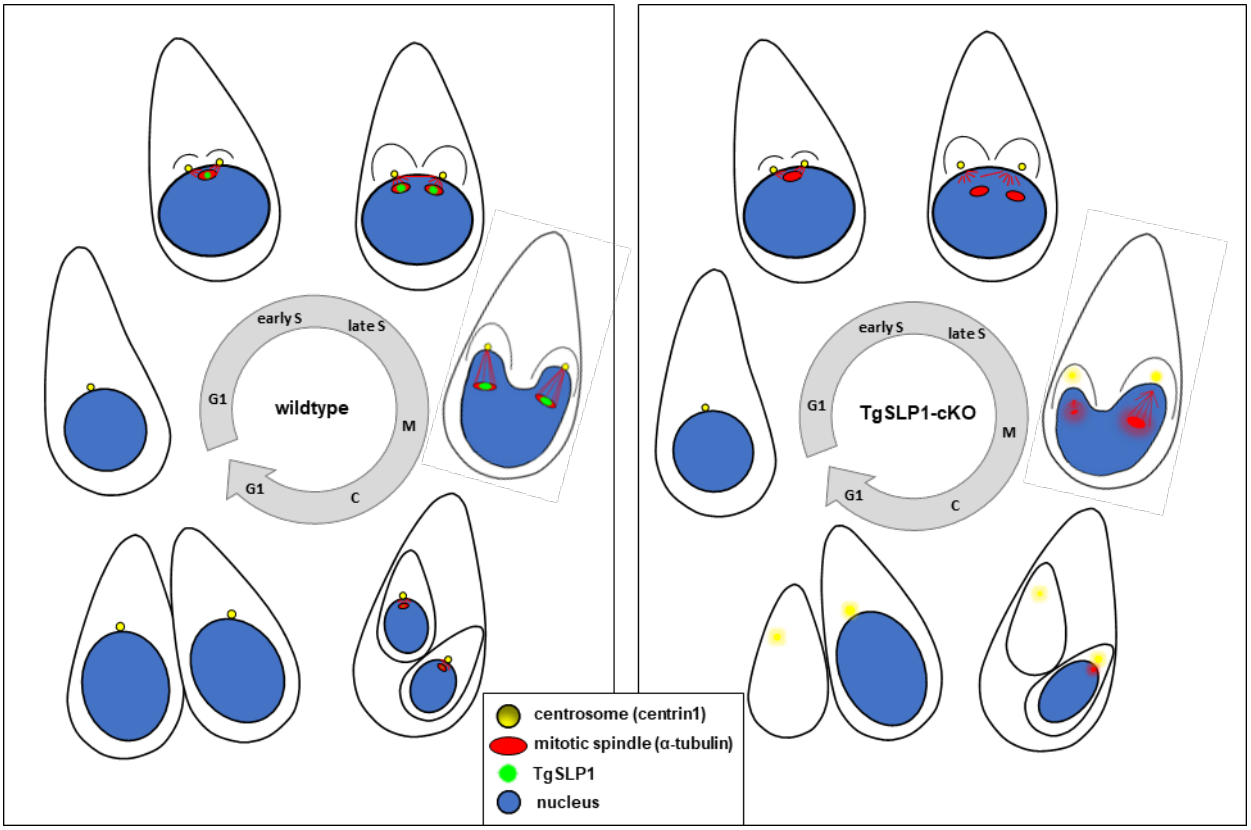

Fig. 6.1 Model of TgSLP1 localisation and function in *T. gondii*
Schematic summary of *T. gondii* centrosome (yellow), mitotic spindle (red), nucleus (blue) and TgSLP1 (green) organisation during endodyogeny in wildtype and TgSLP1-cKO parasites.

The observations on TgSLP1 are in good agreement with the function of SUN domain proteins in other species. Studies in mammals (Zhang et al., 2009), *C. elegans* (Malone et al., 2003; Zhou et al., 2009) and yeast (Chen et al., 2019) show non-canonical LINC complexes connecting the centrosome to the nucleus. For example, the SUN domain proteins SUN1 and SUN2 form complexes with the KASH domain protein Syne-2/ Nesprin-2 to couple the nucleus to the centrosome during neurogenesis and neuronal migration in mice (Zhang et al., 2009). In the nematode *C. elegans*, depletion of *sun-1* causes centrosomes to become detached from the nucleus, demonstrating that the linkage of the SUN-KASH pair SUN-1 and ZYG-12 connects the centrosome to the nucleus (Malone et al., 2003; Zhou et al., 2009). A recent study in budding yeast reveals an atypical, centrosome-associated LINC complex formed by the SUN protein Mps3 and the KASH-like protein Mps2 during mitosis (Chen et al., 2019).

The DiCre system was used to conditionally knockout TgSLP1 (Andenmatten et al., 2013). A disadvantage of this method is its relatively slow kinetics, making it difficult to distinguish between primary and secondary effects (Jiménez-Ruiz et al., 2014). In parasites lacking TgSLP1, the centrosome appears to fall apart and lose its integrity (Fig. 5.27). Despite this, the apicoplast seems to divide normally (Fig. 5.25, Fig. 5.31), although it is believed to separate in association with the centrosome (Striepen et al., 2000). Daughter budding seems not to be affected in TgSLP1-KO parasites, as well as the segregation of other organelles like mitochondria and secretory organelles. Here, centrin1 was used as a marker for the centrosome, but in more detail it labels the centrioles located at the outer core of the centrosome (Striepen et al., 2000; Suvorova et al., 2015). While nuclear segregation is regulated by the inner core of the centrosome, daughter budding is coordinated by the outer core of the centrosome (Suvorova et al., 2015). Since daughter budding and apicoplast division appear to be normal in TgSLP1-KO parasites, disintegration of the centrosome (or at least centrin1) seems likely be a secondary effect.

The phenotypes observed in TgSLP1 are similar to the recently demonstrated knockout of the inner core protein TgCep250L1 (Tomasina et al., 2022). Parasites lacking TgCep250L1 are unable to survive, show severe nuclear segregation defects and the outer core of the centrosome detaches from the nucleus. Interestingly, either segregation or duplication of the outer core is affected, since most parasites possess the expected distribution of either one or two centrin1 dots (Tomasina et al., 2022). Whether the outer core of the centrosome in TgSLP1-depleted parasites disintegrates instead of just detaching from the nucleus cannot be assessed with the data generated here. In Fig. 5.27, it seems that not all parasites have equal distributed centrin1 dots like it was observed in TgCep250L1 knockout parasites (Tomasina et al., 2022) but this observation might be due to the slow kinetics of the DiCre system. Faster knockout systems such as auxin-inducible-degron (AID) or the ddFKBP system would be helpful to elucidate how TgSLP1 affects centrosome integrity and to distinguish between primary and secondary effects (Brown et al., 2018; Herm-Götz et al., 2007; Jiménez-Ruiz et al., 2014). The study by Tomasina et al. also shows that TgCep250L1 depletion does not affect the segregation of daughter cells and of other organelles such as the apicoplast or the mitochondria, which was also not observed in TgSLP1-depleted parasites.

Since the phenotype of TgSLP1 knockout parasites is reminiscent of those lacking TgCep250L1 and likely acts in the nuclear cycle (which is coordinated by the inner core of the centrosome), it would be interesting to monitor the fate of the inner core upon TgSLP1 depletion using TgCep250L1 as marker.

Additionally, the exact localisation of TgSLP1 has to be determined. A suitable method besides electron microscopy is ultrastructure expansion microscopy (U-ExM), a method based on the physical, three-dimensional expansion of immunolabeled biological samples without altering internal features, using standard fluorescence microscopy (Gambarotto et al., 2019). Recently, this method was successfully adapted for *T. gondii* (Tosetti et al., 2020) and could reveal the precise localisation of TgSLP1 in the centrocone, thus providing clues to its ultimate function.

Tubulin recruitment to the centrocone has been shown to occur just before centrosome duplication in late G1-phase (Chen et al., 2015). TgSLP1 is cell cycle dependent and not detectable in G1-phase. This observation is consistent with spindle microtubule formation monitored using TgEB1-YFP as a marker protein for the spindle pole and spindle microtubules (Chen et al., 2015). It would be interesting to determine whether spindle microtubule formation occurs simultaneously with the appearance of TgSLP1, using TgEB1 as a marker protein.

Overall, the precise localisation of TgSLP1 could be determined (for instance with expansion microscopy) using appropriate marker proteins of the nuclear division machinery such as TgEB1 for spindle microtubules and the spindle pole and TgCep250L1 for the inner core centrosome in addition to the outer core marker centrin1 (Chen et al., 2015; Tomasina et al., 2022; Suvorova et al., 2015). Furthermore, the kinetochore and the centromeres can be monitored using marker proteins such as Ndc80 or Nuf2 (kinetochore; Farrell & Gubbels, 2014) and CenH3 or Chromo1 (centromeres; Brooks et al., 2011; Gissot et al., 2012). Moreover, the fate of the centrosome, the kinetochore, the spindle microtubules and the centromeres in absence of TgSLP1 will shed light on the function of TgSLP1 during nuclear division.

The results of this study, consistent with observations in other organisms, allow us to conclude that TgSLP1 may be part of an apicomplexan, centrosome-associated LINC complex.

Nevertheless, we still lack a KASH-like protein as a binding partner of TgSLP1. Interestingly, other centrosome-associated LINC complexes possess SUN-binding partners that differ from the typical KASH domain proteins. For instance, *C. elegans* ZYG-12 has three isoforms, two on the nuclear envelope, harbouring a transmembrane-containing KASH domain and one, localised to the centrosome lacking the KASH domain (Zhou et al., 2009). Furthermore, the yeast KASH-like protein Mps2 lacks the typical C-terminal KASH motif, but it interacts with the SUN protein Mps3 similar to conserved SUN-KASH binding. In an attempt to identify potential interaction partners of TgSLP1, proximity labelling and a pulldown experiment were performed using TurboID, an improved method of BioID (Branon et al., 2018; Zhou et al., 2021), but due to inconsistent results, no KASH-like protein could be identified with this method. Immunoprecipitation experiments with the TgSLP1-sYFP2 or an epitope tagged TgSLP1 (for example 3xHA) followed by mass spectrometry analysis would be a good alternative and helpful to discover binding partners of TgSLP1 as potential KASH domain proteins.

6.5 Potential KASH proteins

Since it was not possible to identify KASH domain proteins using standard homology searches, an algorithm called DORY, originally programmed to identify non-canonical KASH-like proteins in plants (Zhou et al., 2012) was applied and two potential candidates were identified.

The hypothetical protein TGGT1_279360 has one transmembrane domain and a potential C-terminal KASH tail with a characteristic PPPX motif, which has been described as essential for SUN domain binding (Padmakumar et al., 2005; Sosa et al., 2012). The phenotypic score proposed by the genome-wide CRISPR/ Cas9 screen (Sidik et al., 2016) is -5.12, hence the protein is believed to be essential for *T. gondii* survival. Since KASH domain proteins have been described as essential in other organisms (Kim et al., 2015), one would expect that a KASH-like protein would also be essential in *T. gondii.*

Another candidate has been identified as a potential KASH-like protein, namely the hypothetical protein TGGT1_321410. It also possesses a transmembrane domain and seems to be important for parasite fitness according to the genome-wide screen by Sidik et al. in 2016 (phenotypic score: -2.2). The LOPIT localisation study predicts that the protein localises

to the nucleus and the plasma membrane depending on the prediction algorithm (Barylyuk et al., 2020), making the protein a good candidate for a KASH-like protein in *T. gondii.*

To examine the localisation of the two proteins with respect to TgSLP1, both were endogenously tagged in parasites expressing endogenously labelled TgSLP1-sYFP2. While both TGGT1_279360 and TGGT1_321410 were tightly localised to the nucleus, they do not colocalise with TgSLP1. Based on the localisation pattern, it was hypothesised that both proteins are localised in the parasite's Golgi apparatus, which was confirmed by a transiently expressed marker of the trans-Golgi network (GalNac) in TGGT1_321410. Colocalisation confirmation with a marker protein was not performed for TGGT1_279360. Since the aim was to identify KASH-like proteins that bind to the SUN domain protein TgSLP1, these proteins are expected to colocalise with TgSLP1, which was not the case for any of the hypothetical proteins. Therefore, both were not analysed further in this study.

6.6 Conclusion

SUN domain and KASH domain proteins are the typical components of LINC complexes. Although LINC complexes are well characterised in most eukaryotic cells, no data are available in apicomplexan parasites, but observations suggest that similar mechanisms exist. This study identifies a SUN-like protein in the apicomplexan parasite *T. gondii* and demonstrates its importance during nuclear division, suggesting that TgSLP1 is part of an apicomplexan-specific, centrosome-associated LINC complex, although a KASH-like binding partner remains to be discovered.

7 Summary

Apicomplexan parasites include some of the most important pathogens, such as *Plasmodium* spp., the causative agent of malaria, or *Toxoplasma gondii,* the causative agent of toxoplasmosis. As obligate intracellular parasites, Apicomplexa invade host cells in an active process, where they replicate within a parasitophorous vacuole, followed by egress and lysis of the host cell. *T. gondii* parasites use a unique mode of cell division called endodyogeny, in which two daughter cells form within the mother parasite.

The linker of nucleoskeleton and cytoskeleton (LINC) complex connects the nucleus to the cytoskeleton and allows transmission of mechanical forces across the nuclear envelope. In opisthokonts, its core components are KASH (Klarsicht, ANC-1 and Syne Homology) domain proteins, localised to the outer nuclear membrane and SUN (Sad1 and UNC-84) domain proteins, located to the inner nuclear membrane.

Although no LINC complex is described in apicomplexan parasites, it can be speculated that they might have similar mechanisms integrating the nucleus and cytoskeleton. In this study, a UNC-50 domain and two SUN domain proteins in the *T. gondii* genome were identified as potential candidates for core components of the LINC complex. In addition to characterising the three SUN-like candidates, attempts were made to identify KASH domain proteins in *T. gondii* using TurboID and bioinformatic research. Two proteins were identified and their subcellular localisation determined, but no further characterisation was performed.

The UNC-50 protein (TgUNC1) was localised to the Golgi apparatus and did not appear to be essential for the parasite. Visualisation of a SUN domain protein, TgSLP2 (SUN-like protein 2), revealed a diffuse, punctuated pattern throughout the parasite. In contrast, the SUN domain protein TgSLP1 (SUN-like protein 1) showed stage-specific expression, localised to the mitotic spindle and the centrocone, a nuclear structure that plays a central role in daughter cell formation. Conditional knockout of TgSLP1 leads to failure of nuclear division and loss of centrosome integrity. This study shows that TgSLP1 is highly essential for nuclear division and thus for the survival of the parasite.

8 Zusammenfassung

Einige der bedeutendsten Krankheitserreger wie *Plasmodium* spp., der Erreger der Malaria und *Toxoplasma,* der Verursacher von Toxoplasmose, gehören zum Stamm der Apicomplexa. Als strikt intrazelluläre Parasiten dringen Apicomplexa aktiv in Wirtszellen ein und vermehren sich innerhalb einer parasitophoren Vakuole, gefolgt von der Zerstörung der Wirtszelle. *T. gondii* vermehrt sich durch Endodyogeny, ein besonderer Prozess, in dem zwei Tochterzellen in einem Mutterparasiten entstehen.

Der LINC (linker of nucleoskeleton and cytoskeleton)-Komplex verbindet den Zellkern mit dem Zytoskelett und ermöglicht die Übertragung mechanischer Kräfte über die Kernhülle. Die Hauptkomponenten in Opisthokonten sind Proteine mit einer KASH (Klarsicht, ANC-1 und Syne Homologie) Domäne, die sich an der äußeren Kernmembran befinden und Proteine mit einer SUN (Sad1 und UNC-84) Domäne, die sich an der inneren Kernmembran befinden. Es wird vermutet, dass Apicomplexa über ähnliche Mechanismen verfügen um das Zytoskelett mit dem Zellkern zu verbinden. In dieser Studie wurde ein Protein mit einer UNC-50 Domäne und zwei Proteine mit einer SUN Domäne im Genom von *T. gondii* als potentielle Kandidaten für Kernkomponenten des LINC-Komplexes identifiziert. Zusätzlich zur Charakterisierung der drei SUN-ähnlichen Kandidaten wurden Versuche unternommen, mithilfe von TurboID und bioinformatischer Recherche Proteine mit einer KASH Domäne zu identifizieren. Es wurden zwei Proteine gefunden und deren Lokalisation in der Zelle bestimmt, allerdings wurde keine weitere Charakterisierung durchgeführt.

Das UNC-50 Protein (TgUNC1) konnte im Golgi Apparat lokalisiert werden und scheint nicht essentiell für den Parasiten zu sein. Eines der SUN Domänen Proteine (TgSLP2 für SUN-like Protein 2) weist ein diffuses, unterbrochenes Muster im gesamten Parasiten auf. Im Gegensatz dazu wurde eine zellzyklus-spezifische Expression des anderen SUN Domänen Proteins (TgSLP1 für SUN-like Protein 1) beobachtet, welches an der mitotischen Spindel und an dem Centrocone lokalisiert, einer speziellen Struktur am Zellkern, die eine zentrale Rolle bei der Bildung von Tochterzellen spielt. Ein Knockout von TgSLP1 führt zum Versagen der Kernteilung und zum Verlust der Integrität des Zentrosoms. Diese Studie zeigt, dass TgSLP1 für die Kernteilung und damit für das Überleben des Parasiten höchst essentiell ist

9 References

Alexander, D. L. et al., 2005. Identification of the moving junction complex of Toxoplasma gondii: a collaboration between distinct secretory organelles. *PLoS Pathog,* 1(2), p. e17.

Andenmatten, N. et al., 2013. Conditional genome engineering in Toxoplasma gondii uncovers alternative invasion mechanisms. *Nat Methods.,* 10(2), pp. 125-7.

Anderson-White, B. et al., 2012. Cytoskeleton assembly in Toxoplasma gondii cell division. *Int Rev Cell Mol Biol,* Volume 298, pp. 1-31.

Apel, E. D., Lewis, R. M., Grady, M. R. & Sanes, J. R., 2000. Syne-1, a Dystrophin- and Klarsicht-related protein associated with synaptic nuclei at the neuromuscular junction. *J Biol Chem,* 275(41), pp. 31986-95.

Arrizabalaga, G. & Boothroyd, J. C., 2004. Role of calcium during Toxoplasma gondii invasion and egress. *Int J Parasitol,* 34(3), pp. 361-8.

Barylyuk, K. et al., 2020. A comprehensive subcellular atlas of the Toxoplasma proteome via hyperLOPIT provides spatial context for protein functions. *Cell Host Microbe.,* 28(5), pp. 752-766.

Black, M. W. & Boothroyd, J. C., 2000. Lytic cycle of Toxoplasma gondii. *Microbiol Mol Biol Rev,* 64(3), pp. 607-23.

Blader , I., Coleman, B., Chen, C.-T. & Gubbels, M.-J., 2015. The lytic cycle of Toxoplasma gondii: 15 years later. *Annu Rev Microbiol.,* Volume 69, pp. 463-85.

Blum, M. et al., 2021. The InterPro protein families and domains database: 20 years on. *Nucleic Acids Res,* 49(D1), pp. D344-D354.

Bolte, S. & Cordelières, F. P., 2006. A guided tour into subcellular colocalization anaylsis in light microscopy. *J Microsc.,* 224(3), pp. 213-32.

Branon, T. C. et al., 2018. Efficient proximity labeling in living cells and organisms with TurboID. *Nat Biotechnology,* 36(9), pp. 880-7.

Brooks, C. F. et al., 2011. Toxoplasma gondii sequesters centromeres to a specific nuclear region throughout the cell cycle. *Proc Natl Acad Sci U S A,* 108(9), pp. 3767-72.

Brown, K. M., Long, S. & Sibley, D. L., 2017. Plasma membrane association by N-acylation governs PKG function in Toxoplasma gondii. *mBio.,* 8(3), pp. e00375-17.

Brown, K. M., Long, S. & Sibley, D. L., 2018. Conditional knockdown of proteins using auxin-inducible degron (AID) fusions in Toxoplasma gondii. *Bio Protoc.,* 8(4), p. e2728.

Bubb, M. R., Knutson, J. R., Porter, D. K. & Korn, E. D., 1994. Actobinding induces the accumulation of actin dimers that neither nucleate polymerization nor self-associate. *J Biol Chem,* 269(41), pp. 25592-7.

Bunnik, E. M. et al., 2019. Comparative 3D genome organization in apicomplexan parasites. *Proc Natl Acad Sci U S A,* 116(8), pp. 3183-92.

Burg, J. L. et al., 1988. Molecular analysis of the gene encoding the major surface antigen of Toxoplasma gondii. *J Immunol.,* 141(10), pp. 3584-91.

Burke, B., 2018. LINC complexes as regulators of meiosis. *Curr Opin Cell Biol,* Volume 52, pp. 22-29.

Burke, B. & Stewart, C. L., 2002. Life at the edge: the nuclear envelope and human disease. *Nat Rev Mol Cell Biol,* 3(8), pp. 575-85.

Caldas, L. A. & de Souza, W., 2018. A window to Toxoplasma gondii egress. *Pathogens,* 7(3), p. 69.

Carruthers, V. B., 2002. Host cell invasion by the opportunistic pathogen Toxoplasma gondii. *Acta Trop.,* 81(2), pp. 111-22.

Carruthers, V. & Boothroyd, J. C., 2007. Pulling together: an integrated model of Toxoplasma cell invasion. *Curr Opin Microbiol,* 10(1), pp. 83-9.

Carruthers, V. B. & Sibley, D. L., 1997. Sequential protein secretion from three distinct organelles of Toxoplasma gondii accompanies invasion of human fibroblasts. *Eur J Cell Biol,* 73(2), pp. 114-23.

Carruthers, V., Giddings , O. K. & Sibley, D. L., 1999. Secretion of micronemal proteins is associated with toxoplasma invasion of host cells. *Cell Microbiol,* 1(3), pp. 225-35.

Cerutti, A., Blanchard, N. & Besteiro, S., 2020. The Bradyzoite: A key developmental stage for the persistence and pathogenesis of toxoplasmosis. *Pathogens,* 9(3), p. 234.

Cesbron-Delauw, M. F. et al., 1989. Molecular characterization of a 23-kilodalton major antigen secreted by Toxoplasma gondii. *Proc Natl Acad Sci U S A.,* 86(19), pp. 7537-41.

Chakraborty, S. et al., 2017. Potential sabotage of host cell physiology by apicomplexan parasites for their survival benefits. *Front Immunol,* Volume 8, p. 1261.

Chantalat, S. et al., 2003. A novel Golgi membrane protein is a partner of the ARF exchange factors Gea1p and Gea2p. *Mol Biol Cell,* 14(6), pp. 2357-71.

Chen, C.-T. & Gubbels, M.-J., 2013. The Toxoplasma gondii centrosome is the platform for internal daughter budding as revealed by a NEK1 kinase mutant. *J Cell Sci,* 126(15), pp. 3344-55.

Chen, C.-T. & Gubbels, M.-J., 2019. TgCep250 is dynamically processed through the division cycle and is essential for structural integrity of the Toxoplasma centrosome. *Mol Biol Cell,* 30(10), pp. 1160-9.

Chen, J. et al., 2019. Yeast centrosome components form a noncanonical LINC complex at the nuclear envelope insertion site. *J Cell Biol,* 218(5), pp. 1478-90.

Chi, Y.-H., Haller, K., Peloponese Jr, J.-M. & Jeang, K.-T., 2007. Histone acetyltransferase hALP and nuclear membrane protein hsSUN1 function in decondensation of mitotic chromosomes. *J Biol Chem,* 282(37), pp. 27447-58.

Clough, B. & Frickel, E.-M., 2017. The toxoplasma parasitophorous vacuole: an evolving host-parasite frontier. *Trends Parasitol,* 33(6), pp. 473-88.

Cohen, A. M., Rumpel, K., Coombs, G. H. & Wastling, J. M., 2002. Characterisation of global protein expression by two-dimensional electrophoresis and mass spectrometry: proteomics of Toxoplasma gondii. *Int J Parasitol.,* 31(1), pp. 39-51.

Cong, L. et al., 2013. Multiplex genome engineering using CRISPR/Cas systems. *Science,* 339(6121), pp. 819-23.

Conrad, M. N. et al., 2008. Rapid telomere movement in meiotic prophase is promoted by NDJ1, MPS3, and CSM4 and is modulated by recombination. *Cell,* 133(7), pp. 1175-87.

Courjol, F. & Gissot, M., 2018. A coiled-coil protein is required for coordination of karyokinesis and cytokinesis in Toxoplasma gondii. *Cell Microbiol,* 20(6), p. e12832.

Crisp, M. et al., 2006. Coupling of the nucleus and cytoplasm: role of the LINC complex. *J Cell Biol.,* 172(1), pp. 41-53.

Cronshaw, J. M. et al., 2002. Proteomic analysis of the mammalian nuclear pore complex. *J Cell Biol,* 158(5), pp. 915-27.

Curt-Varesano, A. et al., 2016. The aspartyl protease TgASP5 mediates the export of the Toxoplasma GRA16 and GRA24 effectors into host cells. *Cell Microbiol.,* 18(2), pp. 151-67.

Davis, W. M. & Jorgensen, E. M., 2022. ApE, A Plasmid Editor: A freely available DNA manipulation and visualization program. *Front. Bioinform.,* p. DOI:10.3389/fbinf.2022.818619.

De Magistris, P. & Antonin, W., 2018. The dynamic nature of the nuclear envelope. *Curr Biol,* 28(8), pp. 487-97.

Del Rosario, M. et al., 2019. Apicomplexan F-actin is required for efficient nuclear entry during host cell invasion. *EMBO Rep.,* 20(12), p. e48896.

Desmonts, G. et al., 1965. Etude epidemiologique sur la toxoplasmose: de l'influence de la cuisson des vidandes de boucherie sur la frequence de l'infection humaine. *Rev Fr Etudes Clin Biol.,* Volume 10, pp. 952-8.

Di Cristina, M. & Carruthers, V. B., 2018. New and emerging uses of CRISPR/Cas9 to genetically manipulate apicomplexan parasites. *Parasitology,* 145(9), pp. 1119-26.

Ding, D. Q., Chikashige, Y., Haraguchi, T. & Hiraoka, Y., 1998. Oscillatory nuclear movement in fission yeast meiotic prophase is driven by astral microtubules, as revealed by continuous observation of chromosomes and microtubules in living cells. *J Cell Sci.,* 111(Pt 6), pp. 701-12.

Ding, X. et al., 2007. SUN1 is required for telomere attachement to nuclear envelope and gametogenesis in mice. *Dev Cell,* 12(6), pp. 863-72.

Donald, R. G. & Roos, D. S., 1994. Homologous recombination and gene replacement at the dihydrofolate reductase-thymidylate synthase locus in Toxoplasma gondii. *Mol Biochem Parasitol.,* 63(2), pp. 243-53.

Dubey, J. P., 1998. Toxoplasma gondii oocyst survival under defined temperatures. *J Parasitol.,* 84(4), pp. 862-5.

Dubey, J. P., 2007. The history and life cycle of Toxoplasma gondii. In: *Toxoplasma gondii: The model apicomplexan - perspectives and methods.* London: Academic Press, pp. 1-17.

Dubey, J. P. & Frenkel, J. K., 1972. Cyst-induced toxoplasmosis in cats. *J Protozool.,* 19(1), pp. 155-77.

Dubey, J. P., Lindsay, D. S. & Speer, C. A., 1998. Structures of Toxoplasma gondii Tachyzoites, Bradyzoites and Sporozoites and biology and development of tissue cysts. *Clin Microbiol Rev,* 11(2), pp. 267-99.

Dubey, J. P., Miller, N. L. & Frenkel, J. K., 1970a. Characterization of the new fecal form of Toxoplasma gondii. *J Parasitol,* 56(3), pp. 447-56.

Dubey, J. P., Miller, N. L. & Frenkel, J. K., 1970b. The Toxoplasma gondii oocyst from cat feces. *J Exp Med.,* 132(4), pp. 636-62.

Dubremetz, J. F., 1973. Ultrastructural study of schizogonic mitosis in the coccidian, Eimeria necatrix (Johnson 1930). *J Ultrastruct Res,* 42(3), pp. 354-76.

Dubremetz, J. F., 2007. Rhoptries are major players in Toxoplasma gondii invasion and host cell interaction. *Cell Microbiol,* 9(4), pp. 841-8.

Egarter, S. et al., 2014. The toxoplasma Acto-MyoA motor complex is important but not essential for gliding motility and host cell invasion. *PLoS One,* 9(3), p. e91819.

Endo, T., Sethi, K. K. & Piekarski, G., 1982. Toxoplasma gondii: calcium ionophore A23187 - mediated exit of trophozoites from infected murine macrophages. *Exp Parasitol,* 53(2), pp. 179-88.

European Centre for Disease Prevention and Control, 2021. *Cryptosporidiosis, Annual epidemiological report for 2018,* Stockholm: ECDC.

Fan, J., Jin, H., Koch, B. A. & Yu, H.-G., 2020. Mps2 links Csm4 and Mps3 to form a telomere-associated LINC complex in budding yeast. *Life Sci Alliance,* 3(12), p. e202000824.

Ferguson, D. J., 2009. Toxoplasma gondii: 1908-2008, homage to Nicolle, Manceaux and Splendore. *Mem Inst Oswaldo Cruz,* 104(2), pp. 133-48.

Ferguson, D. J., Hutchison, W. M., Dunachie, J. F. & Siim, J. C., 1974. Ultrastructural study of early stages of asexual multiplication and microgametogony of Toxoplasma gondii in the small intestine of the cat. *Acta Pathol Microbiol Scand B Microbiol Immunol.,* 82(2), pp. 167-81.

Ferguson, D. J., Hutchison, W. M. & Siim, J. C., 1975. The ultrastructural development of the macrogamete and formation of the oocyst wall of Toxoplasma gondii. *Acta Pathol Microbiol Scand B.,* 83(5), pp. 491-505.

Ferguson, D. J. et al., 2008. MORN1 has a conserved role in asexual and sexual development across the apicomplexa. *Eukaryot Cell,* 7(4), pp. 698-711.

Fitzgerald, J. et al., 2000. UNCL, the mammalian homologue of UNC-50, is an inner nuclear membrane RNA-binding protein. *Brain Res,* 877(1), pp. 110-23.

Fortes , P. et al., 2003. Inhibiting expression of specific genes in mammalian cells with 5' end-mutated U1 small nuclear RNAs targeted to terminal exons of pre-mRNA. *Proc. Natl. Acad. Sci. U.S.A.,* 100(14), pp. 8264-9.

Fox, B. A., Ristuccia, J. G., Gigley, J. P. & Bzik, D. J., 2009. Efficient gene replacements in Toxoplasma gondii strains deficient for nonhomologous end joining. *Eukaryot Cell,* 8(4), pp. 520-9.

Francia, M. E. et al., 2020. A homolog of structural maintenance of chromosome 1 is a persistent centromeric protein which associates with nuclear pore components in Toxoplasma gondii. *Front Cell Infect Microbiol,* 10:295(eCollection 2020).

Francia, M. E. & Striepen, B., 2014. Cell division in apicomplexan parasites. *Nat Rev Microbiol.,* 12(2), pp. 125-36.

Frénal , K., Dubremetz, J.-F., Lebrun, M. & Soldati-Favre, D., 2017. Gliding motility powers invasion and egress in Apicomplexa. *Nat Rev Microbiol,* 15(11), pp. 645-60.

Frénal, K. et al., 2010. Functional dissection of the apicomplexan glideosome molecular architecture. *Cell Host Microbe,* 8(4), pp. 343-57.

Frenkel, J. K., 1973. Toxoplasma in and around us. *BioScience,* Volume 23, pp. 343-52.

Frenkel, J. K., Dubey, J. P. & Miller, N. L., 1970. Toxoplasma gondii in cats: Fecal stages identified as coccidian oocysts. *Science,* 167(3919), pp. 893-896.

Fridkin, A. et al., 2004. Matefin, a Caenorhabditis elegans germ line-specific SUN-domain nuclear membrane protein, is essential for early embryonic and germ cell development. *Proc Natl Acad Sci U S A,* 101(18), pp. 6987-92.

Fridolfsson, H. N. & Starr, D. A., 2010. Kinesin-1 and dynein at the nuclear envelope mediate the bidirectional migrations of nuclei. *J Cell Biol.,* 191(1), pp. 115-128.

Gajria, B. et al., 2008. ToxoDB: an integrated Toxoplasma gondii database resource. *Nucleic Acids Res.,* 36(Database issue), pp. D553-6.

Gaskins, E. et al., 2004. Identification of the membrane receptor of a class XIV myosin in Toxoplasma gondii. *J Cell Biol,* 165(3), pp. 383-93.

Gerace, L., Blum, A. & Blobel, G., 1978. Immunocytochemical localization of the major polypeptides of the nuclear pore complex-lamina fraction. Interphase and mitotic distribution. *J Cell Biol,* 79(2 Pt 1), pp. 546-66.

Göb, E., Schmitt, J., Benavente, R. & Alsheimer, M., 2010. Mammalian sperm head formation involves different polarisation of two novel LINC complexes. *PLoS One,* 5(8), p. e12072.

Goddette, D. W. & Frieden, C., 1986. Actin polymerization. The mechanism of action of cytochalasin D. *J Biol Chem,* 261(34), pp. 15974-80.

Goldman, M., Carver, R. K. & Sulzer, A. J., 1958. Reproduction of Toxoplasma gondii by internal budding. *J Parasitol,* 44(2), pp. 161-71.

Goodswen, S. J., Kennedy, P. J. & Ellis, J. T., 2013. A review of the infection, genetics, and evolution of Neospora caninum: From the past to the present. *Infect Genet Evol.,* Volume 13, pp. 133-150.

Gras, S. et al., 2017. Parasites lacking the micronemal protein MIC2 are deificient in surface attachement and host cell egress, but remain virulent in vivo. *Wellcome Open Res.,* 2(32).

Gras, S. et al., 2019. An endocytic-secretory cycle participated in Toxoplasma gondii in motility. *PLoS Biol,* 17(6), p. e3000060.

Graumann, K., Runions, J. & Evans , D. E., 2010. Characterization of SUN-domain proteins at the higher plant nuclear envelope. *Plant J,* 61(1), pp. 134-44.

Graumann, K. et al., 2014. Characterization of two distinct subfamilies of SUN-domain proteins in Arabidopsis and their interactions with the novel KASH-domain protein AtTIK. *J Exp Bot,* 65(22), pp. 6499-512.

Green, R. & Rogers, E. J., 2013. Chemical Transformation of E.coli. *Methods Enzymol.,* Volume 529, pp. 329-336.

Gruenbaum, Y. & Medalia, O., 2015. Lamins: the structure and protein complexes. *Curr Opin Cell Biol,* Volume 32, pp. 7-12.

Gubbels, M.-J.et al., 2006. A MORN-repeat protein is a dynamic component of the Toxoplasma gondii cell division apparatus. *J Cell Sci.,* 119(Pt 11), pp. 2236-45.

Gundersen, G. G. & Worman, H. J., 2013. Nuclear positioning. *Cell,* 152(6), pp. 1376-89.

Gunderson, S. I., Polycarpou-Schwarz, M. & Mattaj, I. W., 1998. U1 snRNP inhibits pre-mRNA polyadenylation through a direct interaction between U1 70K and poly(A) polymerase. *Mol. Cell,* 1(2), pp. 255-64.

Hagan, I. & Yanagida, M., 1995. The product of the spindle formation gene sad1 associates with the fission yeast spindle pole body and is essential for viability. *J Cell Biol,* 129(4), pp. 1033-47.

Hakansson, S., Morisaki, H., Heuser, J. & Sibley, D. L., 1999. Time-laps video microscopy of gliding motility in Toxoplasma gondii reveals a novel, biphasic mechanism of cell locomotion. *Mol Biol Cell,* 10(11), pp. 3539-47.

Hao, H. & Starr, D. A., 2019. SUN/ KASH interactions facilitate force transmission across the nuclear envelope. *Nucleus,* 10(1), pp. 73-80.

Haque, F. et al., 2006. SUN1 interacts with nuclear lamin A and cytoplasmic nesprins to provide a physical connection between the nuclear lamina and tha cytoskeleton. *Mol Cell Biol.,* 26(10), pp. 3738-51.

Harding, C. R. & Meissner, M., 2014. The inner membrane complex through development of Toxoplasma gondii and Plasmodium. *Cell Microbiol,* 16(5), pp. 632-41.

Hartmann, J. et al., 2006. Golgi and centrosome cycles in Toxoplasma gondii. *Mol Biochem Parasitol,* 145(1), pp. 125-7.

Hassan, M. A. et al., 2017. Comparative ribosome profiling uncovers a dominant role for translational control in Toxoplasma gondii. *BMC Genomics,* 18(1), p. 961.

Heaslip, A. T., Dzierszinski, F., Stein, B. & Hu, K., 2010. TgMORN1 is a key organizer for the basal complex of Toxoplasma gondii. *PLoS Pathog,* 6(2), p. e1000754.

Hedgecock, E. M. & Thomson, J. N., 1982. A gene required for nuclear and mitochondrial attachment in the nematode Caenorhabditis elegans. *Cell,* 30(1), pp. 321-30.

Herm-Götz, A. et al., 2007. Rapid control of protein level in the apicomplexan Toxoplasma gondii. *Nat Methods,* 4(12), pp. 1003-5.

Hetzer, M. W., 2010. The nuclear envelope. *Cold Spring Harb Perspect Biol,* 2(3), p. a000539.

Hodzic, D. M. et al., 2004. Sun2 is a novel mammalian inner nuclear membrane protein. *J Biol Chem.,* 279(24), pp. 25805-12.

Horn, H. F., 2014. LINC complex proteins in development and disease. *Curr Top Dev Biol.,* Volume 109, pp. 287-321.

Hu , K. et al., 2006. Cytoskeletal components of an invasion machine - the apical complex of Toxoplasma gondii. *PLoS Pathog,* 2(2), p. e13.

Hu, K. et al., 2002a. Daughter Cell assembly in the protozoan parasite Toxoplasma gondii. *Mol Biol Cell,* 13(2), pp. 593-606.

Hu, K., Roos, D. S. & Murray, J. M., 2002b. A novel polymer of tubulin forms the conoid of Toxoplasma gondii. *J Cell Biol.,* 156(6), pp. 1039-50.

Hutchison, W. M., 1965. Experimental transmission of Toxoplasma gondii. *Nature,* 206(987), pp. 961-2.

Hutchison, W. M., Dunachie, J. F., Siim, J. C. & Work, K., 1969. Life cycle of toxoplasma gondii. *Br Med J,* 4(5686), p. 806.

Huynh, M.-H. & Carruthers, V. B., 2009. Tagging of endogenous genes in a Toxoplasma gondii strain lacking Ku80. *Eukaryot Cell.,* 8(4), pp. 530-9.

Jacobs, L., 1963. Toxoplasma and Toxoplasmosis. *Annu Rev Microbiol.,* Volume 17, pp. 429-50.

Jacot, D., Daher, W. & Soldati-Favre, D., 2013. Toxoplasma gondii myosin F, an essential motor for centrosomes positioning andn apicoplast inheritance. *EMBO J,* 32(12), pp. 1702-16.

Jaspersen , S. L. et al., 2006. The Sad1-UNC-84 homology domain in Mps3 interacts with Mps2 to connect the spindle pole body with the nuclear envelope. *J Cell Biol.,* 174(5), pp. 665-75.

Jaspersen, S. L., Giddings Jr., T. H. & Winey, M., 2002. Mps3p is a novel component of the yeast spindle pole body that interacts with the yeast centrin homologue Cdc31p. *J Cell Biol,* 159(6), pp. 945-56.

Jeffers, V., Tampaki, Z., Kim, K. & Sullivan, W. J. J., 2019. A latend ability to persist: differentiation in Toxoplasma gondii. *Cell Mol Life Sci,* 75(13), pp. 2355-73.

Jelenska, J. et al., 2001. Subcellular localization of acetly-CoA carboxylase in the apicomplexan parasite Toxoplasma gondii. *Proc Natl Acad Sci U S A.,* 98(5), pp. 2723-8.

Jiang, X.-Z.et al., 2011. SPAG4L, a novel nuclear envelope protein involved in the meiotic stage of spermatogenesis. *DNA Cell Biol,* 30(11), pp. 875-82.

Jiménez-Ruiz, E., Wong, E. H., Pall, G. S. & Meissner, M., 2014. Advantages and disadvantages of conditional systems for characterization of essential genes in Toxoplasma gondii. *Parasitology,* 141(11), pp. 1390-8.

Jinek, M. et al., 2012. A programmable dual-RNA-guided DNA endonuclease in adaptive bacterial immunity. *Science,* 337(6096), pp. 816-21.

Jinek, M. et al., 2013. RNA-programmed genome editing in human cells. *eLife,* Issue 2:e00471.

Jones, P. et al., 2014. InterProScan 5: genome-scale protein function classification. *Bioinformatics.,* 30(9), pp. 1236-40.

Jullien, N. et al., 2007. Conditional transgenesis using dimerizable Cre (DiCre). *PLoS One,* 2(12), p. e1355.

Jullien, N., Sampieri, F., Enjalbert, A. & Herman, J.-P., 2003. Regulation of Cre recombinase by ligand-induced complementation of inactive fragments. *Nucleic Acids Res,* 31(21), p. e131.

Kafsack, B. F. et al., 2009. Rapide membrane disruption by a perforin-like protein facilitates parasite exit from host cells. *Science,* 323(5913), pp. 530-3.

Katris, N. J. et al., 2014. The apical complex provides a regulated gateway for secretion of invasion factors in Toxoplasma. *PLoS Pathog,* 10(4), p. e1004074.

Katsumata, K. et al., 2017. Position matters: multiple functions of LINC-dependent chromosome positioning during mitosis. *Curr Genet.,* 63(6), pp. 1037-52.

Ketema, M. & Sonnenberg, A., 2011. Nesprin-3: a versatile connector between the nucleus and the cytoskeleton. *Biochem Soc Trans,* 39(6), pp. 1719-24.

Ketema, M. et al., 2007. Requirements for the localisation of nesprin-3 at the nuclear envelope and its interaction with plectin. *J Cell Sci,* 120(Pt 19), pp. 3384-94.

Kim, D. I., Birendra, K. C. & Roux, K. J., 2015. Making the LINC: SUN and KASH protein interactions. *Biol Chem,* 396(4), pp. 295-310.

Kim, K., Soldati, D. & Boothroyd, J. C., 1993. Gene replacement in Toxoplasma gondii with chloramphenicol acetyltransferase as selectable marker. *Science,* 262(5135), pp. 911-4.

Kite, G. L., 1913. The relative permeability of the surface and interior portions of the cytoplasm of animal and plant cells. *Biol Bull,* Volume 25, pp. 1-7.

Kozono, T. et al., 2018. Jaw1/LRMP has a role in maintaining nuclear shape via interaction with SUN proteins. *J Biochem,* 164(4), pp. 303-11.

Kracklauer, M. P. et al., 2010. The Drosophila SUN protein Spag4 cooperates with the coiled-coil protein Yuri Gagarin to maintain association of the basal body and spermatid nucleus. *J Cell Sci,* 123(Pt 16), pp. 2763-72.

Kreidenweiss, A., Hopkins, A. V. & Mordmüller, B., 2013. 2A and the auxin-based degron system facilitate control of protein levels in Plasmodium falciparum. *PLoS One,* 8(11), p. e:78661.

Laemmli, U. K., 1970. Cleavage of structural proteins during the assembly of the head of bacteriophage T4. *Nature,* 227(5259), pp. 680-5.

Lamarque, M. et al., 2011. The RON2-AMA1 interaction is a critical step in moving junction-dependent invasion by apicomplexan parasites. *PLoS Pathog,* 7(2), p. e1001276.

Lavy, M. & Estelle, M., 2016. Mechanisms of auxin signaling. *Development,* 143(18), pp. 3226-9.

Lee, K. K. et al., 2002. Lamin-dependent localisation of UNC-84, a protein required for nuclear migration in Caenorhabditis elegans. *Mol Biol Cell,* 13(3), pp. 892-901.

Lerner, M. R. et al., 1980. Are snRNPs involved in splicing?. *Nature,* 283(5743), pp. 220-4.

Leung, J. M. et al., 2014. Disruption of TgPHIL1 alters specific parameters of Toxoplasma gondii motility measured in a quantitative, three-dimensional live motility assay. *PLoS One,* 9(1), p. e85763.

Lewis, J. A. et al., 1987. The levamisole receptor, a cholinergic receptor of the nematode Caenorhabditis elegans. *Mol Pharmacol.,* 31(2), pp. 185-93.

Liu, J. et al., 2016. An ensemble of specifically targeted proteins stabilizes cortical microtubules in the human parasite Toxoplasma gondii. *Mol Biol Cell.,* 27(3), pp. 549-571.

Liu, W. et al., 2015. IBS: an illustrator for the presentation and visualization of biological sequences. *Bioinformatics,* 31(20), pp. 3359-61.

Li, W. et al., 2022. A splitCas9 phenotypic screen in Toxoplasma gondii identifies proteins involved in host cell egress and invasion. *Nature Microiology,* Issue https://doi.org/10.1038/s41564-022-01114-y.

Lorestani, A. et al., 2010. A Toxoplasma MORN1 null mutant undergoes repeated divisions but is defective in basal assembly, apicoplast division and cytokinesis. *PLoS One.,* 5(8), p. e12302.

Lourido, S., Tang, K. & Sibley, D., 2012. Distinct signalling pathways control Toxoplasma egress and host-cell invasion. *EMBO J,* 31(24), pp. 4524-34.

Mali, P. et al., 2013. RNA-guided human genome engineering via Cas9. *Science,* 339(6121), pp. 823-6.

Malone, C. J., Fixsen, W. D., Horvitz, H. R. & Han, M., 1999. UNC-84 localizes to the nuclear envelope and is required for nuclear migration and anchoring during C.elegans development. *Development,* 126(14), pp. 3171-81.

Malone, C. J. et al., 2003. The C.elegans hook protein, ZYG-12, mediates the essential attachment between the centrosome and nucleus. *Cell.,* 115(7), pp. 825-36.

Martorelli Di Genova, B., Wilson, S. K., Dubey, J. P. & Knoll, L. J., 2019. Intestinal delta-6-desaturase activity determines host range for Toxoplasma sexual reproduction. *PLoS Biol.,* 17(8), p. e3000364.

Matera, A. G. & Wang, Z., 2015. A day in the life of the spliceosome. *Nat. Rev. Mol. Cell. Biol.,* 15(2), pp. 108-21.

McCoy, J. M., Whitehead, L., van Dooren, G. G. & Tonkin, C. J., 2012. TgCDPK3 regulates calcium-dependent egress of Toxoplasma gondii from host cells. *PLoS Pathog,* 8(12), p. e1003066.

McDonald, V. & Shirley, M. W., 2009. Past and future: vaccination against Eimeria. *Parasitology,* 136(12), pp. 1477-89.

McGee, M. D., Stagljar, I. & Starr, D. A., 2009. KDP-1 is a nuclear envelope KASH protein required for cell-cycle progression. *J Cell Sci,* 122(Pt.16), pp. 2895-905.

McGregor, A. L., Hsia, C.-R. & Lammerding, J., 2016. Squish and squeeze - the nucleus as a physical barrier during migration in confined environments. *Curr Opin Cell Biol.,* Volume 40, pp. 32-40.

Meier, I., 2016. LINCing the eukaryotic tree of life - towards a broad evolutionary comparison of nucleocytoplasmic bridging complexes. *J Cell Sci.,* 129(19), pp. 3523-31.

Meissner, M., Brecht, S., Bujard, H. & Soldati, D., 2001. Modulation of mysin A expression by a newly established tetracycline repressor-based inducible system in Toxoplasma gondii. *Nucleic Acids Res,* 29(22), p. E115.

Meissner, M., Ferguson, D. J. & Frischknecht, F., 2013. Invasion factors of apicomplexan parasites: essential or redundant?. *Curr. Opin. Microbiol.,* 16(4), pp. 438-44.

Meissner, M., Schlüter, D. & Soldati, D., 2002. Role of Toxoplasma gondii myosin A in powering parasite gliding and host cell invasion. *Science,* 298(5594), pp. 837-40.

Mercier, C., Adjogble, K. D. Z., Däubener, W. & Cesbron-Delauw, M.-F., 2005. Dense granules: are they key organelles to help understand the parasitophorous vacuole of all apicomplexa parasites?. *Int J Parasitol,* 35(8), pp. 829-49.

Miki, F. et al., 2004. Two-hybrid search for proteins that interact with Sad1 and Kms1, two membrane-bound components of the spindle pole body in fission yeast. *Mol Genet Genomics,* 270(6), pp. 449-61.

Minn, I. L., Rolls, M. M., Hanna-Rose, W. & Malone, C. J., 2009. SUN-1 and ZYG-12, mediators of centrosome-nucleus attachement, are a functional SUN/KASH pair in Caenorhabditis elegans. *Mol Biol Cell,* 20(21), pp. 4586-95.

Mislow, J. M. K. et al., 2002. Nesprin-1alpha self-associates and binds directly to emerin and lamin A in vitro. *FEBS Lett.,* 525(1-3), pp. 135-40.

Mital, J., Meissner, M., Soldati, D. & Ward, G. E., 2005. Conditional expression of Toxoplasma gondii apical membrane antigen-1 (TgAMA1) demonstrates that TgAMA1 plays a critical role in host cell invasion. *Mol Biol Cell,* 16(9), pp. 4341-9.

Mojica, F. J. M., Villasenor-Díez, C., García-Martínez, J. & Soria, E., 2005. Intervening sequences of regularly spaced prokaryotic repeats derive from foreign genetic elements. *J Mol Evol.,* 60(2), pp. 174-82.

Mondragon, R. & Frixione, E., 1996. Ca(2+)-dependence of conoid extrusion in Toxoplasma gondii tachyzoites. *J Eukayot Microbiol,* 43(2), pp. 120-7.

Mordue, D. G., Hakansson, S., Niesman, I. & Sibley, L. D., 1999. Toxoplasma gondii resides in a vacuole that avoids fusion with host cell endocytic and exocytic vesicular trafficking pathways. *Exp Parasitol,* 92(2), pp. 87-99.

Morimoto, A. et al., 2012. A conserved KASH domain protein associates with telemores, SUN1, and dynactin during mammalian meiosis. *J Cell Biol,* 198(2), pp. 165-72.

Morrissette, N. S. & Sibley, D. L., 2002. Cytoskeleton of Apicomplexan Parasites. *Microbiol Mol Biol Rev,* 66(1), pp. 21-38.

Mosley-Bishop, K. L., Li, Q., Patterson, K. & Fischer , J. A., 1999. Molecular analysis of the klarsicht gene and its role in nuclear migration within differentiating cells of the Drosophila eye. *Curr Biol,* 4(21), pp. 1211-20.

Moudy, R., Manning, T. J. & Beckers, C. J., 2001. The loss of cytoplasmic potassium upon host cell breakdown triggers egress of Toxoplasma gondii. *J Biol Chem,* 276(44), pp. 41492-501.

Muniz-Hernández, S. et al., 2011. Contribution of the residual body in the spatial organization of Toxoplasma gondii tachyzoite within the parasitophorous vacuole. *J Biomed Biotechnol,* p. 473983.

Munoz-Centeno, M. C. et al., 1999. Saccharomyces cerevisiae MPS2 encodes a membrane protein localised at the spindle pole body and the nuclear envelope. *Mol Biol Cell,* 10(7), pp. 2393-406.

National Library of Medicine, N. c. f. B. I., 2023. *pubmed.ncbi.* [Online]
Available at: pubmed.ncbi.nlm.nih.gov
[Accessed 17 02 2023].

Nicolle, C. & Manceaux, L., 1908. Sur une infection à corps de Leishman (ou organismes voisins) du Gondi. *Comptes Rendus Hebdomadaires des Séances de l'Académie des Sciences,* 147(17), pp. 763-66.

Nishi, M., Hu, K., Muray, J. M. & Roos, D. S., 2008. Organellar dynamics during the cell cycle of Toxoplasma gondii. *J Cell Sci,* 121(Pt9), pp. 1559-68.

Nishimura, K. et al., 2009. An auxin-based degron system for the rapid depletion of proteins in nonplant cells. *Nat. Methods,* 6(12), pp. 917-22.

O'Leary , J. K., Sleator, R. D. & Lucey, B., 2021. Cryptosporidium spp. diagnosis and research in the 21st century. *Food Waterborne Parasitol,* p. e00131.

Opitz, C. & Soldati, D., 2002. "The glideosome": a dynamic complex powering gliding motion and host cell invasion by Toxoplasma gondii. *Mol Microbiol,* 45(3), pp. 597-604.

Oza, P. et al., 2009. Mechanisms that regulate localisation of a DNA double-strand break to the nuclear periphery. *Genes Dev.,* 23(8), pp. 912-927.

Padmakumar, V. C. et al., 2005. The inner nuclear membrane protein Sun1 mediates the anchorage of Nesprin-2 to the nuclear envelope. *J Cell Sci.,* 118(Pt 15), pp. 3419-30.

Patterson, K. et al., 2004. The functions of Klarsicht and nuclear lamin in developmentally regulated nuclear migrations of photoreceptor cells in the Drosophila eye. *Mol Biol Cell.,* 15(2), pp. 600-10.

Peng, D. & Tarleton, R., 2015. EuPaGDT: a web tool tailored to design CRISPR guide RNAs for eukaryotic pathogens. *Microb Genom.,* 1(4), p. e000033.

Periz, J. et al., 2019. A highly dynamic F-actin network regulates transport and recycling of micronemes in Toxoplasma gondii vacuoles. *Nat Commun,* 10(1), p. 4183.

Periz, J. et al., 2017. Toxoplasma gondii F-actin forms an extensive filamentous network required for material exchange and parasite maturation. *Elife.,* p. 6:e24119.

Pfluger, S. L. et al., 2005. Receptor for retrograde transport in the apicomplexan parasite Toxoplasma gondii. *Eukaryot Cell.,* 4(2), pp. 432-42.

Philip, N. & Waters, A. P., 2015. Conditional degradation of Plasmodium calcineurin reveals functions in parasite colonization of both host and vector. *Cell Host Microbe.,* 18(1), pp. 122-31.

Pieperhoff, M. S. et al., 2015. Conditional U1 gene silencing in Toxoplasma gondii. *PLoS One.,* 10(6), p. e0130356.

Pittman, K. J. & Knoll, L. J., 2015. Long-Term Relationships: the complicated interplay between the host and the developmental stages of toxoplasma gondii during acute and chronic infections. *Microbiol Mol Biol Rev,* 79(4), pp. 387-401.

Poupel, O. & Tardieux, I., 1999. Toxoplasma gondii motility and host cell invasiveness are drastically impaired by jasplakinolide, a cyclic peptide stabilizing F-actin. *Microbes Infect.,* 1(9), pp. 653-62.

Preston, C. C. & Faustino, R. S., 2018. Nuclear envelope regulation of oncogenic processes: roles in pancreatic cancer. *Epigenomes,* 2(3), p. 15.

Radke, J. R. et al., 2001. Defining the cell cycle for the tachyzoite stage of Toxoplasma gondii. *Mol Biochem Parasitoll,* 115(2), pp. 165-75.

Rajgor, D. et al., 2012. Multiple novel nesprin-1 and nesprin-2 variants at as versatile tissue-specific intracellular scaffolds. *PLoS One,* 7(7), p. e40098.

Rajgor, D. & Shanahan, C. M., 2013. Nesprins: from the nuclear envelope and beyond. *Expert Rev Mol Med.,* 15:e5(doi:10.1017/erm.2013.6).

Ramakrishnan, S. et al., 2012. Apicoplast and endoplasmic reticulum cooperate in fatty acid biosynthesis in apicomplexan parasite Toxoplasma gondii. *J Biol Chem,* 287(7), pp. 4957-71.

Ramos, J. A., Zenser, N., Leyser, O. & Callis, J., 2001. Rapid degradation of auxin/indoleacetic acid proteins requires conserved amino acids of domain II and is proteasome dependent. *Plant Cell,* 13(10), pp. 2349-60.

Renard, I. & Mamoun, C. B., 2021. Treatment of human babesiosis: then and now. *Pathogens,* 10(9), p. 1120.

Rey, A., Schaeffer, L., Durand, B. & Morel, V., 2021. Drosophila Nesprin-1 isoforms differentially contribute to muscle function. *Cells,* 10(11), p. 3061.

Rosenberg-Hasson, Y., Renert-Pasca, M. & Volk, T., 1996. A Drosophila dytrophin-related protein, MSP-300, is required for embryonic muscle morphogenesis. *Mech Dev,* 60(1), pp. 83-94.

Rothballer, A., Schwartz, T. U. & Kutay, U., 2013. LINCing complex functions at the nuclear envelope. *Nucleus,* 4(1), pp. 29-36.

Roux, K. J. et al., 2009. Nesprin 4 is an outer nuclear membrane protein that can induce kinesin-mediated cell polarization. *Proc Natl Acad Sci U S A,* 106(7), pp. 2194-9.

Russell, D. G. & Burns, R. G., 1984. The polar ring of coccidian sporozoites: a unique microtubule-organising centre. *J Cell Sci,* Volume 65, pp. 193-207.

Sabin, A. B. & Feldman, H. A., 1948. Dyes as microchemical indicators of a new immunity phenomen affecting a protozoon parasite (Toxoplasma).. *Science,* 108(2815), pp. 660-663.

Saeij, J. P., Boyle, J. P. & Boothryod, J. C., 2005. Differences among the three major strains of Toxoplasma gondii and their specific interactions with the infected host. *Trends Parasitol.,* 21(10), pp. 476-81.

Sanchez, S. G. & Besteiro, S., 2021. The pathogenicity and virulence of Toxoplasma gondii. *Virulence,* 12(1), pp. 3095-3114.

Sato, A. et al., 2009. Cytoskeletal forces span the nuclear envelope to coordinate meiotic chromosome pairing and synapsis. *Cell,* 139(5), pp. 907-19.

Sauer, B., 1987. Functional expression of the cre-lox site-specific recombination system in the yeast Saccharomyces cerevisiae. *Mol Cell Biol,* 7(6), pp. 2087-96.

Sauer, B. & Henderson, N., 1988. Site-specific DNA recombination in mammalian cells by the Cre recombinase of bacteriophage P1. *Proc Natl Acad Sci U S A,* 85(14), pp. 5166-70.

Schindelin, J. et al., 2012. Fiji: an open-source platform for biological-image analysis. *Nat Methods.,* 9(7), pp. 676-82.

Schmitt, J. et al., 2007. Transmembrane protein SUN2 is involved in tethering mammalian meiotic telomeres to the nuclear envelope. *Proc Natl Acad Sci U S A,* 104(18), pp. 7426-31.

Schultz, A. J. & Carruthers, V. B., 2018. Toxoplasma gondii LCAT primarily contributes to tachyzoite egress. *mSphere,* 3(1), pp. e00073-18.

Schwab, J. C., Beckers, C. J. & Joiner, K. A., 1994. The parasitophorous vacuole membrane surrounding intracellular toxoplasma gondii functions as a molecular sieve. *Proc Natl Acad Sci U S A,* 91(2), pp. 509-13.

Seeber, F. & Soldati-Favre, D., 2010. Metabolic pathways in the apicoplast of apicomplexa. *Int Rev Cell Mol Biol,* Volume 281, pp. 161-228.

Shao, X. et al., 1999. Spag4, a novel sperm protein, binds outer dense-fiber protein Odf1 and localizes to microtubules of manchette and axoneme. *Dev Biol,* 211(1), pp. 109-23.

Shapiro , K. et al., 2019. Environmental transmission of Toxoplasma gondii: Oocysts in water, soil and food. *Food Waterborne Parasitol.,* p. 15:e00049.

Sheffield, H. G. & Melton, M. L., 1968. The fine structure and reproduction of Toxoplasma gondii. *J Parasitol,* 54(2), pp. 209-26.

Sheffield, H. G. & Melton, M. L., 1970. Toxoplasma gondii: the oocyst, sporozoite, and infection of cultured cells. *Science,* 167(3919), pp. 892-3.

Shen, B., Brown, K. M., Lee, T. D. & Sibley, D. L., 2014a. Efficient gene disruption in diverse strains of Toxoplasma gondii using CRISPR/ Cas9. *mBio,* 5(3), pp. e01114-14.

Shen, B., Buguliskis, J. S., Lee, T. D. & Sibley, D. L., 2014b. Functional analysis of rhomboid proteases during Toxoplasma invasion. *mBio,* 5(5), p. e01795.

Sibley, D. L., 2003. Toxoplasma gondii: perfecting an intracellular life style. *Traffic,* 4(9), pp. 581-6.

Sibley, L. D., Messina, M. & Niesman, I. R., 1994. Stable DNA transformation in the obligate intracellular parasite Toxoplasma gondii by complementation of tryptophan auxotrophy. *Proc Natl Acad Sci U S A.,* 91(12), pp. 5508-12.

Sidik, S. M. et al., 2014. Efficient genome engineering of Toxoplasma gondii using CRISPR/Cas9. *PLoS One,* 9(6), p. e100450.

Sidik, S. M. et al., 2016. A genome-wide CRISPR screen in Toxoplasma identifies essential apicomplexan genes. *Cell.,* 166(6), pp. 1423-35.

Sidik, S. M., Huet, D. & Lourido, S., 2018. CRISPR-Cas9-based genome-wide screening of Toxoplasma gondii. *Nat Protoc.,* 13(1), pp. 307-323.

Simpson, J. G. & Roberts, R. G., 2008. Patterns of evolutionary conservation in the nesprin genes highlight probable functionally important protein domains and isoforms. *Biochem Soc Trans,* 36(6), pp. 1359-67.

Sohaskey, M. L. et al., 2010. Osteopotentia regulates osteoblast maturation, bone formation, and skeletal integrity in mice. *J Cell Biol,* 189(3), pp. 511-25.

Soldati, D. & Boothroyd, J. C., 1993. Transient transfection and expressin in the obligate intracellular parasite Toxoplasma gondii. *Science,* 260(5106), pp. 349-52.

Soldati, D. et al., 1995. Complementation of a Toxoplasma gondii ROP1 knock-out mutant using phleomycin selection. *Mol Biochem Parasitol.,* 74(1), pp. 87-97.

Sosa, B. A., Rothballer, A., Kutay, U. & Schwartz, T. U., 2012. LINC complexes form by binding of three KASH peptides to the interfaces of trimeric SUN proteins. *Cell,* 149(5), pp. 1035-47.

Speer, C. A. & Dubey, J. P., 2005. Ultrastructural differentiation of Toxoplasma gondii schizonts (types B-E) and gamonts in the intestines of cats fed bradyzoites. *Int J Parasitol.,* 35(2), pp. 193-206.

Starr, D. A. & Fridolfsson, H. N., 2014. Interactions between nuclei and the cytoskeleton are mediated by SUN-KASH nuclear-envelope bridges. *Annu Rev Cell Dev Biol,* Volume 26, pp. 421-44.

Starr, D. A. & Han, M., 2002. Role of ANC-1 in tethering nuclei to the actin cytoskeleton. *Science,* 298(5592), pp. 406-9.

Starr, D. A. & Han, M., 2003. ANChors away: an actin based mechanism of nuclear positioning. *J Cell Sci,* 116(Pt 2), pp. 211-6.

Starr, D. A. et al., 2001. unc-83 encodes a novel component of the nuclear envelope and is essential for proper nuclear migration. *Development,* 128(24), pp. 5039-50.

Stelzer, S. et al., 2019. Toxoplasma gondii infection and toxoplasmosis in farm animals: Risk factors and economic impact. *Food Waterborne Parasitol,* Issue 15, p. e00037.

Sternberg, N. & Hamilton, D., 1981. Bacteriophage P1 site-specific recombination. I. Recombination between loxP sites. *J Mol Biol,* 150(4), pp. 467-86.

Stortz, J. F. et al., 2019. Formin-2 drives polymerisation of actin filaments enabling segregation of apicoplast and cytokinesis in Plasmodium falciparum. *Elife,* Volume 8, p. e49030.

Striepen, B. et al., 2000. The plastid of Toxoplasma gondii is divided by association with the centrosomes. *J Cell Biol,* 151(7), pp. 1423-34.

Striepen, B., Jordan, C. N., Reiff, S. & van Dooren, G. G., 2007. Building the perfect parasite: cell division in apicomplexa. *PLoS Pathog,* 3(6), p. e78.

Su, C. et al., 2003. Recent expansion of Toxoplasma through enhanced oral transmission. *Science,* 299(5605), pp. 414-6.

Suss-Toby, E., Zimmerberg, J. & Ward, G. E., 1996. Toxoplasma invasion: the parasitophorous vacuole is formed from host cell plasma membrane and pinches off via a fission pore. *Proc Natl Acad Sci U S A,* 93(16), pp. 8413-8.

Suvorova , E. S., Francia, M., Striepen, B. & White , M. W., 2015. A novel bipartite centrosome coordinates the apicomplexan cell cycle. *PLoS Biol.,* 13(3), p. e1002093.

Tapley , E. C., Ly, N. & Starr, D. A., 2011. Multiple mechanisms actively target the SUN protein UNC-84 to the inner nuclear membrane. *Mol Biol Cell,* 22(10), pp. 1739-52.

Tapley, E. C. & Starr, D. A., 2013. Connecting the nucleus to the cytoskeleton by SUN-KASH bridges across the nuclear envelope. *Curr Opin Cell Biol.,* 25(1), pp. 57-62.

Tarnasky, H. et al., 1998. A novel testis-specific gene, SPAG4, whose product interacts specifically with outer dense fiber protein ODF27, maps to human chromosome 20q11.2. *Cytogenet Cell Genet,* 81(1), pp. 65-7.

Teale, W. D., Paponov, I. A. & Palme, K., 2006. Auxin in action: signalling, transport and the control of plant growth and development. *Nat. Rev. Mol. Cell. Biol.,* 7(11), pp. 847-59.

Tenter, A. M., Heckeroth, A. R. & Weiss, L. M., 2000. Toxoplasma gondii: from animals to humans. *Int J Parasitol,* 30(12-13), pp. 1217-58.

Tomasina, R. et al., 2022. Seperate to operate: the centriole-free inner core of the centrosome regulates the assemly of the intranuclear spindle in Toxoplasma gondii. *mBio,* 13(5), p. e0185922.

van Poppel, N. F. J. et al., 2006. Tight control of transcription in Toxoplasma gondii using an alternative tet repressor. *Int J Parasitol,* 36(4), pp. 443-52.

Votýpka, J. et al., 2016. Apicomplexa. In: *Handbook of the Protists.* s.l.:Springer, Cham., pp. 1-58.

Wälde, S. & King, M. C., 2014. The KASH protein Kms2 coordinates mitotic remodeling of the spindle pole body. *J Cell Sci,* 127(16), pp. 3625-40.

Waller, R. F. & McFadden, G. I., 2005. The Apicoplast: A review of the derived plastid of apicomplexan parasites. *Curr. Issues Mol. Biol.,* 7(1), pp. 57-80.

Wang, S. et al., 2018. Mechanotransduction via the LINC complex regulates DNA replication in myonuclei. *J Cell Biol.,* 217(6), pp. 2005-18.

Watson, M. L., 1955. The nuclear envelope; its structure and relation to cytoplasmic membranes. *J Biophys Biochem Cytol,* Volume 1, pp. 257-70.

Watson, M. L., 1959. Further observations on the nuclear envelope of the animal cell. *J Biophys Biochem Cytol,* 6(2), pp. 147-56.

Weinman, D. & Chandler, A. H., 1954. Toxoplasmosis in swine and rodents; reciprocal oral infection and potential human hazard. *Proc Soc Exp Biol Med.,* 87(1), pp. 211-6.

Weiss, L. M. & Dubey, J. P., 2009. Toxoplasmosis: a history of clinical observations. *Int J Parasitol,* 39(8), pp. 895-901.

Welte, M. A. et al., 1998. Developmental regulation of vesicle transport in Drosophila embryos: force and kinetics. *Cell,* 92(4), pp. 547-57.

Whitelaw, J. A. et al., 2017. Surface attachement, promoted by the actomyosin system of Toxoplasma gondii is important for efficient gliding motility and invasion. *BMC Biol,* 15(1).

Wilhelmsen, K. et al., 2005. Nesprin-3, a novel outer nuclear membrane protein associates with the cytoskeletal linker protein plectin. *J Cell Biol,* 171(5), pp. 799-810.

Witte , H. M. & Piekarski, G., 1970. Die Oocysten-Ausscheidung bei experimentall infizierten Katzen in Abhängigkeit von Toxoplasma-Stamm. *Z Parasitenk,* Volume 33, pp. 358-60.

Wolf, A., Cowen, D. & Paige, B., 1939. Human Toxoplasmosis: Occurence in infants as an encephalomyelitis verification by transmission to animals. *Science,* 89(2306), pp. 226-227.

Work, K. & Hutchison, W. M., 1969. The new cyst of Toxoplasma gondii. *Acta Pathol Microbiol Scand.,* 77(3), pp. 414-24.

World Health Organization, 2022. *World malaria report 2022,* Geneva: s.n.

Xia, J. et al., 2021. Third-generation sequencing revises the molecular karyotype for Toxoplasma gondii and identifies emerging copy number variants in sexual recombinants. *Genome Res,* 31(5), pp. 834-51.

Zhang , Q. et al., 2002. The nesprins are giant actin-binding proteins, orthologous to Drosophila melanogaster muscle protein MSP-300. *Genomics,* 80(5), pp. 473-81.

Zhang, Q. et al., 2001. Nesprins: a novel family of spectrin-repeat-containing proteins that localize to the nuclear membrane in multiple tissues. *J Cell Sci,* 114(Pt 24), pp. 4485-98.

Zhang, X. et al., 2009. SUN1/2 and Syne/Nesprin-1/2 complexes connect centrosome to the nucleus duing neurogenesis and neuronal migration in mice. *Neuron,* 64(2), pp. 173-87.

Zhang, X. et al., 2007. Syne-1 and Syne-2 play crucial roles in myonuclear anchorage and motor neuron innervation. *Development,* 134(5), pp. 901-8.

Zhao , Q., Brkljacic, J. & Meier, I., 2008. Two distinct interacting classes of nuclear-envelope associated coiled-coil proteins are required for the tissue-specific nuclear envelope targeting of Arabidopsis RanGAP. *Plant Cell,* 20(6), pp. 1639-51.

Zhen, Y.-Y.et al., 2002. NUANCE, a giant protein connecting the nucleus and actin cytoskeleton. *J Cell Sci,* 115(15), pp. 3207-22.

Zhou, L.-J.et al., 2021. Toxoplasma gondii SAG1 targeting host cell S100A6 for parasite invasion and host immunity. *iScience,* 24(12), p. 103514.

Zhou, X., Graumann, K., Evans, D. E. & Meier, I., 2012. Novel plant SUN-KASH bridges are involved in RanGAP anchoring and nuclear shape determination. *J Cell Biol.,* 196(2), pp. 203-11.

Zhou, X. et al., 2014. Identification of unique SUN-interacting nuclear envelope proteins with diverse functions in plants. *J Cell Biol.,* 205(5), pp. 677-92.

Zhou, X. & Meier, I., 2013. How plants LINC the SUN to KASH. *Nucleus,* 4(3), pp. 206-15.

Zhou, Z. et al., 2012. Structure of Sad1-UNC84 homology (SUN) domain defines features of molecular bridge in nuclear envelope. *J Biol Chem,* 287(8), pp. 5317-26.

Zuther, E. et al., 1999. Growth of Toxoplasma gondii is inhibited by aryloxyphenoxypropionate herbicides targeting acetyl-CoA carboxylase. *Proc Natl Acad Sci U S A.,* 96(23), pp. 13387-92.

Acknowledgements

I am very grateful to finally be able to write this acknowledgement and would like to take this opportunity to thank all the people who supported me during my PhD and always believed in me when I wasn't sure if I could do it.

Many thanks to Prof. Dr. Markus Meissner for the opportunity to carry out the work in his research group, for the scientific guidance, the support and supervision, for the constructive discussions. Thank you for the patience and the encouragement to complete my PhD with two kids, I really appreciate that.

Many thanks to Dr. Elena Jiménez-Ruiz, Dr. Mirko Singer, Dr. Simon Gras, Dr. Sujaan Das and Dr. Javier Periz for supervising me and teaching me all the important techniques in the lab with *Toxoplasma*. Thank you for helpful discussions, constructive suggestions, and patient explanations. Special thanks to Simon who always reminded us to have lunch on time.

Special thanks to Marzena Broniszewska and Kathrin Simon for providing host cells, organising the lab, and helping with *Toxoplasma* experiments when I wasn't allowed to.

I am very grateful to my PhD buddies Janessa Grech, Wei Li, Matthew Gow, Julia von Knoerzer-Suckow , Dr. Miriam Rafajlovic and - for a short but beautiful time - Frea Mehta. Thank you for the good times in Leopoldstraße and later in Martinsried with countless coffees and for sharing the anger when the experiment (again…) didn't work - shared pain is half pain.

Many thanks to Yuan Song for taking over the experiments for the revision of our paper.

Thanks to Adelheid Ackermann and Angelika Derschum for help with administrative and IT issues.

Many, many special thanks to my family: my sister Danie for the emotional support, my parents, Dorothea and Ottmar, my mother-in-law Renate and Hans for the emotional support and especially the support with the children. Without your help, this work would never have been finished!

Many thanks to my dearest friends, Ronny, Marlene, Pauline and Fritzi, who always have an open ear for me. I am very thankful to have you.

Finally, I would like to thank my beloved husband Günni, for always believing in me and for giving me emotional support and security. You are my source of repose. Thank you for all the love you give me and our wonderful daughters Magdalena and Antonia. I dedicate this work to you three!